# Solid-Core Heat-Pipe Nuclear Battery Type Reactor

Award Number: DE-FC07-05ID14706

Summary Report

September 30, 2008

University of California
Department of Nuclear Engineering
Berkeley, CA 94720
Congressional District 9

Ehud Greenspan
(510) 643-9983
gehud@nuc.berkeley.edu

## TABLE OF CONTENTS


| | | |
|---|---|---|
| ABSTRACT | | 1 |
| 1. | INTRODUCTION | 3 |
| 2. | CONCEPT OUTLINE | 5 |
| 3. | MATERIAL SCREENING | 8 |
| 3.1 | Introduction | 8 |
| 3.2 | Core Mechanical Analysis | 9 |
| 3.3 | Cladding-Fuel Mechanical Interaction, Some Considerations | 12 |
| 3.4 | Corrosion of Core Internals | 14 |
| 3.5 | Reactor Vessel | 15 |
| 3.6 | Proposed Materials and Design Guidelines | 15 |
| 4. | HEAT PIPE PERFORMANCE | 17 |
| 4.1 | Introduction | 17 |
| 4.2 | Heat Pipe Description | 17 |
| 4.3 | Heat Pipe Performance Review | 18 |
| 4.4 | Design Considerations | 21 |
| 4.5 | Analysis | 21 |
| 4.6 | Heat Pipe Lifetime | 25 |
| 4.7 | Summary | 26 |
| 5. | NEUTRONIC ANALYSIS | 27 |
| 5.1 | Introduction | 27 |
| 5.2 | Results | 28 |
| 5.3 | Minimizing Reactivity Swing | 29 |
| 5.4 | More Realistic Core Design | 32 |
| | 5.4.1 Optimal Reflectors | 32 |
| | 5.4.2 Reactivity Control | 34 |
| 5.5 | Reference Core Design | 42 |
| 6. | THERMAL HYDRAULIC ANALYSIS | 45 |
| 6.1 | Introduction | 45 |
| 6.2 | Candidate Fluids for Intermediate Coolant | 46 |

6.3 Design Optimization With Water as the Thermodynamic Working Fluid 47
6.3.1 Hydraulic Analysis 48
6.3.2 Flow Rate Optimization 49
6.3.3 Thermal Analysis 49
6.3.4 System Volume Optimization 50
6.3.5 Preferred Design 51
6.4 Design Optimization With S-$CO_2$ as the Thermodynamic Working Fluid 52
6.5 Decay Heat Removal Capability 52
7. ADVANCED ENERGY CONVERSION SYSTEM 53
7.1 Introduction 53
7.2 Recompression Cycle 54
7.3 Indirect Cycle 55
7.4 Power Control Scheme for Recompression Cycle 57
7.5 Drawbacks of the S-$CO_2$ Cycle 61
8. PRELIMINARY SAFETY ANALYSIS 62
8.1 Introduction 62
8.2 Advanced Reactor Policy 62
8.3 Containment/Confinement 65
8.4 Site Characterization 68
8.5 General design Criteria 69
8.6 Design Basis Accidents 72
8.6.1 Class A 72
8.6.2 Class B 75
8.6.3 Class C 75
8.7 Heat Pipes Failure 75
8.8 Reactor Site Criteria 79
8.9 Severe Accidents 80
8.10 Beyond Design Basis Accidents 81
8.11 Risk Assessment, Risk Management and Safety Goals 84
8.11.1 Risk Assessment of Inherently Safe Feature 84
8.11.2 Probabilistic Risk Assessment of Heat Pipes 85
8.11.3 Loss Of Offsite Power (LOOP) 88
8.12 Seismic Safety 88

8.12.1 Seismic Isolators 91
8.12.2 Seismically Induced Component Failure 93
8.13 Summary 94
9. CONCLUSIONS 96
ACKNOWLEDGEMENT 97
REFERENCES 98

## LIST OF TABLES


Table 1 Recommended Design Variables 16

Table 2 Selected Core Temperatures 23

Table 3 Summary of Heat Pipe Performance 26

Table 4 Actinide Composition of LWR Spent Fuel after 50 GWd/MTHM and Different Cooling Periods 29

Table 5 Atom Densities of Non-Fuel Materials Used for MCNP Computations 36

Table 6 Actinides Atom Densities Used for MCNP Computations 37

Table 7 Selected Thermo-Physical Properties of Reactor Coolants 47

Table 8 Summary of Design Features of the HP-ENHS 70

Table 9 Reference Heat Pipe Specifications 76

Table 10 Temperature and Heat Load Increases Due to Heat Pipe Failure 78

Table 11 Failure Fraction of Key Structures (LTSP) 93

## LIST OF FIGURES


| | | |
|---|---|---|
| Figure 1 | Schematic heat pipe and fuel arrangement; cross-sectional cut | 6 |
| Figure 2a | Schematic heat pipe and core arrangement; axial cut. | 6 |
| Figure 2b | Alignment of heat pipes and fuel elements in the HP-ENHS (not to scale) | 6 |
| Figure 3 | Schematic layout of the HP-ENHS module | 7 |
| Figure 4 | Cladding equivalent stress, after 20 years of reactor operation, as a function of fission gas plenum length and cladding thickness, at: a) LHR of 150W/cm; cladding inner wall temperature of 1300K; fuel average temperature of 1525K; b)LHR of 240W/cm; cladding inner wall temperature of 1350K; fuel average temperature of 1830K. Note: 400μm of cladding thickness are not considered to contribute to the mechanical strength due to corrosion and chemical interaction between cladding and fuel. | 11 |
| Figure 5 | HP equivalent stress and allowable stress for: a) Mo TZM alloy; b) ODS ferritic martensitic steels. Allowable stress due to irradiation creep is determined for a fast neutron fluence corresponding to a LHR of 240W/cm for Mo TZM alloy and to 75W/cm for ODS ferritic martensitic steels. The equivalent stress is determined assuming HP inner pressure of 3.5 atm and outer pressure of 1 atm at operating temperature. Note: 400μm of wall thickness are not considered to contribute to the mechanical strength due to corrosion between HP wall and primary coolant. | 13 |
| Figure 6 | Average fuel radius variation due to fuel swelling [33] for an initial fuel radius of 0.65cm and fuel theoretical density of 95%. Fuel is assumed to be free to expand. | 14 |
| Figure 7 | Outer vessel equivalent stress and Hastelloy XR allowable stress. | 15 |
| Figure 8 | Schematic layout of a heat pipe | 18 |
| Figure 9 | Wick parameters | 22 |
| Figure 10 | Temperature profile in the HP-ENHS core calculated using the finite element heat transfer code | 22 |
| Figure 11 | Calculated Na heat pipe operating limits (top) and LANL high performance heat pipe data (left) | 24 |
| Figure 12 | Capillary pumping force | 25 |
| Figure 13 | Multiplication factor as a function of exposure time for different structural material with P/D of 1.0 | 28 |
| Figure 14 | Multiplication factor as a function of exposure time for different Pu-to-HM initial load | 29 |
| Figure 15 | Effect of reactivity of LWR spent fuel composition after long cooling time and effect of only Pu initial load vs. all TRU recycling | 30 |

Figure 16 Effect of using natural nitrogen fuel vs 100% $^{15}N$ when using only Pu initial load 31

Figure 17 Effect on reactivity swing when of natural nitrogen fuel vs 100% $^{15}N$ when using all TRU initial load 31

Figure 18 Schematic view of the bare (left) and reflected (right) HP-ENHS core 33

Figure 19 Comparison between MoTZM and BeO reflectors (20cm thick reflector, 22.5% TRU) 33

Figure 20 Effect of the BeO reflector thickness on $k_{eff.}$ 22.45% TRU, 50 years cooling 34

Figure 21 Peripheral control system schematics 35

Figure 22 Upward moving peripheral control system schematics 35

Figure 23 Effect of control slabs – downwards 38

Figure 24 Effect of control slabs – upwards 38

Figure 25 Schematic view of the HP-ENHS core having a perpendicular split 39

Figure 26 $k_{eff}$ time evolution (in years) of the HP-ENHS perpendicularly split core having a 40cm thick BeO blade 40

Figure 27 Effect of BeO reflector blade thickness on the BOL $k_{eff}$ of a perpendicularly split core 40

Figure 28 Relative fission rate distribution for a central horizontal section of the core – 40cm thick BeO reflector blade in a perpendicularly split core 41

Figure 29 Relative fission rate distribution for a central horizontal section of the core – 20 cm thick BeO reflector blade in a perpendicularly split core 41

Figure 30 Relative fission rate distribution for a central horizontal section of the core – 10cm thick BeO reflector blade in a perpendicularly split core 42

Figure 31 Evolution of $k_{eff}$ of a split HP-ENHS core with a 10 cm voided blade; 22.87% TRU 43

Figure 32 $k_{eff}$ evolution with and without 10 cm thick central control blade inserted into the split core. 22.87% TRU 43

Figure 33 $k_{eff}$ evolution with and without 10 cm thick central $B_4C$ control blade inserted into the split core. 40 cm thick $B_4C$ absorbers replace the BeO side reflectors simultaneously. 22.87% TRU 43

Figure 34 Neutronically preferred reference core design schematics 44

Figure 35 Schematics of the safety preferred reference design 44

Figure 36 Evolution of $k_{eff}$ of a split HP-ENHS core with a two 10 cm voided blade; 22.9% TRU 45

Figure 37 Multiplication factor in normal and shutdown configurations 45

Figure 38 Relative flow resistance vs. riser area 49
Figure 39 Dimensions of the HP-ENHS reactor 51
Figure 40 S-$CO_2$ recompression cycle layout [50] 54
Figure 41 Temperature vs. entropy diagram of recompression Brayton cycle [49] 55
Figure 42 Recompression cycle with one stage of reheat [50] 56
Figure 43 S-$CO_2$ cycle efficiency for different number of reheaters [49] 57
Figure 44 Possible locations of bypass and throttling valves [50] 59
Figure 45 Bypass control performance [49] 60
Figure 46 Recompress fraction and bypass flow [49] 60
Figure 47 Diablo Canyon location and surrounding major faults 69
Figure 48 Overflow cooling of the Flibe 74
Figure 49 Component bathtub curve 76
Figure 50 Performance limit curves for the reference case in Table 9 77
Figure 51 New operating point caused by neighboring heat pipe failure 78
Figure 52 New operating points caused by cascading heat pipe failure 79
Figure 53 Heat transfer in LOCA 82
Figure 54 LOCA heat transfer model 82
Figure 55 Heat distribution on reactor pressure vessel 83
Figure 56 Heat pipe failure event tree 86
Figure 57 Probability tree of control slab (per hour) 87
Figure 58 Maximum magnitude distribution for Hosgri fault zone 90
Figure 59 Maximum magnitude distribution for Hosgri fault zone as a function of the sense of slip 91
Figure 60 Location of seismic isolators, represented on an ENHS [20] 92
Figure 61 Lead rubber isolator diagram [22] 93

## ABSTRACT

This project was devoted to a preliminary assessment of the feasibility of designing an Encapsulated Nuclear Heat Source (ENHS) reactor to have a solid core from which heat is removed by liquid-metal heat pipes (HP). Like the SAFE 400 space nuclear reactor core, the HP-ENHS core is comprised of fuel rods and HPs embedded in a solid structure arranged in a hexagonal lattice in a 3:1 ratio. The core is oriented horizontally and has a square rather cylindrical cross section for effective heat transfer. The HPs extend from the two axial reflectors in which the fission gas plena are embedded and transfer heat to an intermediate coolant that flows by natural-circulation.

The HP-ENHS is designed to preserve many features of the ENHS including 20-year operation without refueling, very small excess reactivity throughout life, natural circulation cooling, walk-away passive safety, and robust proliferation resistance. The target power level and specific power of the HP-ENHS reactor are those of the reference ENHS reactor. Compared to previous ENHS reactor designs utilizing a lead or lead-bismuth alloy natural circulation cooling system, the HP-ENHS reactor offers a number of advantageous features including: (1) significantly enhanced passive decay heat removal capability; (2) no positive void reactivity coefficients; (3) relatively lower corrosion of the cladding (4) a core that is more robust for transportation; (5) higher temperature potentially offering higher efficiency and hydrogen production capability.

This preliminary study focuses on five areas: material compatibility analysis, HP performance analysis, neutronic analysis, thermal-hydraulic analysis and safety analysis. Of the four high-temperature structural materials evaluated, Mo TZM alloy is the preferred choice; its upper estimated feasible operating temperature is 1350 K. HP performance is evaluated as a function of working fluid type, operating temperature, wick design and HP diameter and length. Sodium is the preferred working fluid and the HP working temperature can be as high as 1300 K. It is feasible to achieve criticality and to maintain a nearly zero burn-up reactivity swing for at least 20 EFPY with an average linear heat generation rate (LHR) of 90W/cm. The preferred design utilizes nitride fuel made of natural nitrogen and loaded with depleted uranium and TRU from LWR spent fuel cooled for approximately 30 years. The preferred intermediate coolant is LiF-

$BeF_2$; its average outlet temperature is ~ 1040K. Effective heat transfer to the intermediate coolant is obtained with HPs extending out of the core less than 50 cm. The required reactor vessel height is significantly smaller than that of the reference ENHS: 9 vs. ~20 m. The vessel diameter is slightly larger: 4 vs. ~ 3.5 m.

In conclusion, it appears feasible to design a HP-ENHS reactor to achieve its primary design objectives. The resulting HP-ENHS reactor concept is unique in offering sustainable proliferation-resistant nuclear energy that can be delivered at very high temperatures. A number of outstanding issues need be addressed, though, before the practicality of the HP design concept could be asserted. Included among these issues are:

- More thorough reactor safety analysis, including transient analysis
- Fuel-cladding chemical compatibility
- Manufacturability and welding of Mo TZM alloy
- Maximization of the specific power by optimization of fuel/HP diameter and core length
- Economic analysis

# 1. INTRODUCTION

This project is devoted to a preliminary assessment of the feasibility of designing an Encapsulated Nuclear Heat Source (ENHS) reactor to have a solid core from which heat is removed by liquid-metal heat pipes (HP). The HP-ENHS design is intended to preserve many features of the original ENHS reactor [1] including:

- At least 20 full power years without refueling
- Small excess reactivity throughout the lifetime of the core
- Natural circulation cooling; no pumps or valves in the primary and intermediate loops
- Walk-away passive safety
- Autonomous load following capability
- Simple to construct, operate, and maintain
- Reactor module is factory manufactured and fueled
- No onsite refueling equipment required
- Reactor can be shipped to and from the site as a single sealed module
- Specific power and total power.

The HP-ENHS is expected to offer a number of advantages as compared to the original ENHS reactor, including:

- High heat delivery temperature
- Higher energy conversion efficiency as it is not subjected to the conventional coolant outlet temperature limitations. The alkaline HP working fluid is relatively less corrosive and the HPs can safely and reliably operate for the core lifetime at temperatures significantly higher than ~550$^{o}$C, limit of lead alloy primary coolants.
- Higher efficiency for converting the fission energy to hydrogen.
- Enhanced safety:
  - No positive void coefficient of reactivity
  - No positive coolant temperature coefficient of reactivity
  - The solid core precludes fuel rod bowing or other abnormal changes in core geometry that could interfere with core heat removal

  - The HPs provide for very effective decay heat removal from the core to the intermediate coolant or, in case of loss of intermediate coolant to the reactor vessel that provides an effective heat sink.
  - Low probability for the release of fission products due to low fission gas pressure buildup, the solid core structure and the lack of contact between the fuel clad and coolant.
- Smaller and simpler module
- No need for a reactor pool
- Smaller friction of intermediate coolant through IHX resulting in shorter riser for natural circulation cooling.
- No need to embed the fuel in solidified Pb-Bi for transportation, and handling of decay heat at EOL is considerably simpler.
- Module weight is significantly smaller.
- Robust proliferation resistance:
  Decay heat can be more effectively removed compared to other nuclear battery concepts. This may allow the core module to be removed from the host country immediately at EOL.

This feasibility assessment examined five areas: material compatibility, HP performance, neutronic performance, thermal-hydraulic performance along with overall HP-ENHS module layout and dimensions and safety analysis. The studies performed in these five disciplines are summarized in Sections 3 through 7, following a brief description of the HP-ENHS module concept (Section 2).

## 2. CONCEPT OUTLINE

The HP-ENHS core design, illustrated in Figures 1 and 2, adopted elements from the SAFE-400 space reactor core concept [2]. The HP-ENHS core is comprised of fuel rods and HPs embedded in a solid structure arranged in a hexagonal lattice in a 3:1 ratio. The HPs extend beyond the core length and transfer heat to an intermediate coolant that flows by natural-circulation. Two heat pipes are used for every three fuel rods; one extends from the core axial center to one direction and the other to the other direction; that is each HP serves one half of the core. The space between fuel rods and HPs is filled by the metallic structure to form a solid core.

Each fuel element consists of an active fuel region and a fission gas plenum region that also serves as an axial reflector, as illustrated in Figures 2a and 2b. The heat generated in the active fuel region is deposited along the evaporator section of the HP. The fission gas plenum of the fuel element accommodates gaseous fission products and corresponds to the adiabatic section of the heat pipe. The condenser section of the heat pipe extends past the axial reflector region and makes the intermediate heat exchanger (IHX) region that transfers the core generated heat to the intermediate coolant. The ends of each heat pipe are embedded in the vessel structure (not shown in the figures) that provides a heat sink in case of loss of the intermediate coolant accident.

The core and heat pipe assembly is square in cross section in order to minimize the peak-to-average intermediate coolant temperature at the outlet from the IHX. The layout of the HP-ENHS module is shown in Figure 3.

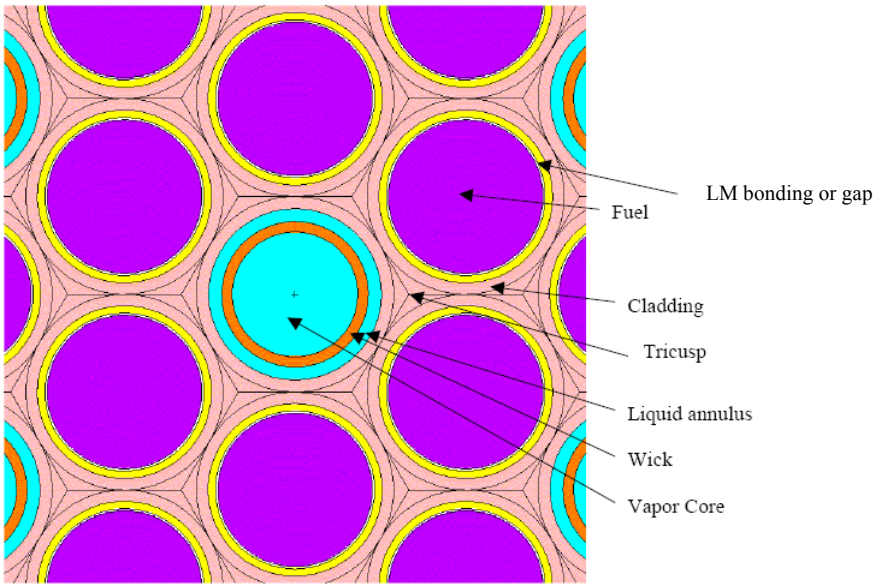


Figure 1 Schematic heat pipe and fuel arrangement; cross-sectional cut.

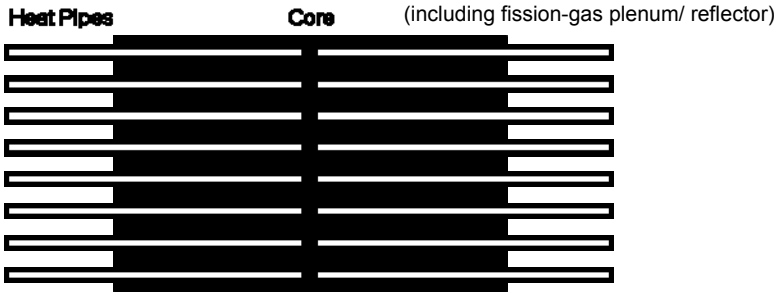


Figure 2a Schematic heat pipe and core arrangement; axial cut.

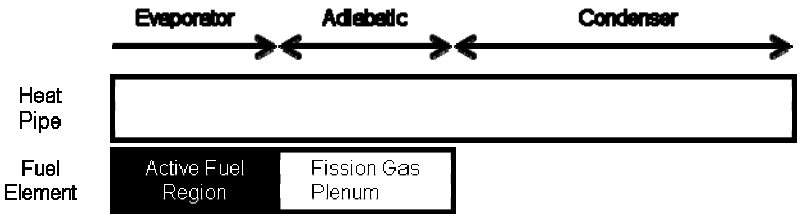


Figure 2b Alignment of heat pipes and fuel elements in the HP-ENHS (not to scale)

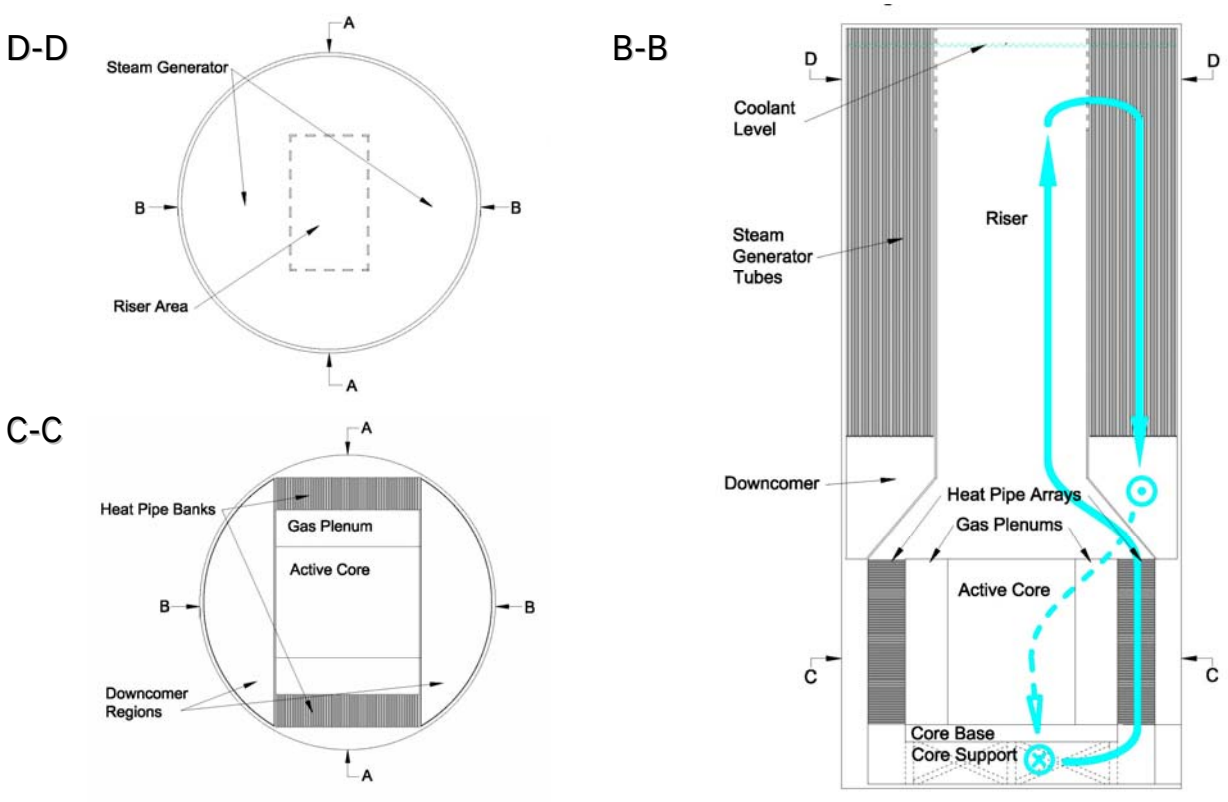


Figure 3 Schematic layout of the HP-ENHS module

The cold intermediate coolant gets from the cavity below the core into the two IHX regions, one in each axial side of the core, heats as it flows up through the IHX and gets into the rectangular riser above the core. At the top of this riser are slots through which the hot intermediate coolant enters the heat exchangers (HX) with the thermodynamic working fluid that are located in the space between the rectangular riser and the module outer structural wall that is cylindrical. After getting out through the bottom of these HX, the intermediate coolant enters two downcomers; one in each side of the core that is not occupied by the HP IHX. At the bottom of the downcomers, openings in the core support structure allow the cold intermediate coolant to get to a cavity below the core from which it reenters the HP IHXs. The preferred thermodynamic working fluid is supercritical $CO_2$ although water has been examined for the initial design.

# 3. MATERIAL SCREENING

## *3.1 Introduction*

The primary issues addressed in this part of the work are:

- Selection of the preferred fuel material
- Defining the upper permissible temperature of candidate structural materials for the core
- Selection of the preferred material for the intermediate coolant
- Selection of the preferred structural material for the reactor vessel and other components in contact with the hot intermediate coolant

Selection of the preferred working fluid for the heat pipes was based, primarily, on the HP performance analysis. This is because the leading candidates for HP coolant at the temperature range of interest are all alkaline elements.

Three materials were considered for the intermediate coolant – Na, lead or Pb-Bi eutectic and a number of molten salts. Drawbacks of sodium are strong chemical reactivity with air and water as well as relatively low vapor pressure; at the HP-ENHS operating temperatures the reactor vessel will have to be pressurized in order to eliminate Na boiling. The primary drawback of lead and its alloy is high corrosion rate with structural materials at the operating temperatures of interest. Based on the above considerations and on the results from the thermal-hydraulic analysis (Section 6), the molten salt LiF-$BeF_2$ was selected for the preferred intermediate coolant.

Three material types were considered for the fuel: metallic alloy with 10% zirconium, oxide and nitride. Nitride was selected as the preferred fuel material due to its high operating temperature, relatively high heavy metal (HM) density and relatively low fraction of fission gas release. Uranium nitride is also the fuel of choice for space nuclear reactors that are designed to operate at comparable temperatures [2].

Four candidate alloys – HT9, Mo-TZM refractory alloy, Nb-1Zr, and oxide dispersion strengthened (ODS) ferritic martensitic steels, were evaluated for the core structural material.

Operating temperature limits were established for each of these candidate materials by considering the materials mechanical properties and corrosion behavior in the operating environment of the HP-ENHS reactor core. In general, the lower temperature limit is determined by radiation hardening while the upper temperature limit is determined by corrosion effects and/or by thermal and irradiation creep. The permissible operating temperature of the structural material depends on a number of core design variables including the clad thickness, ratio of fission gas plenum length to fuel length, specific power or linear heat generation rate and discharge burnup. As the preferred value of some of these design variables was not known at the initiation of the project, part of the material analyses was done parametrically with some of the design variables.

The properties of the candidate structural materials were obtained from the open literature [3-18], in particular from databases on materials proposed for high-temperature fusion applications. Following is a summary of the structural materials analysis.

### *3.2 Core Mechanical Analysis*

According to the available databases [3-10], Mo TZM alloy offers higher mechanical strength than Nb-1Zr, ODS ferritic martensitic steels, and HT9, particularly at high temperatures. This material is not thermal creep limited up to 1350K [5]; it retains the highest absolute ultimate tensile strength (UTS) at temperatures above 1000K; and presents a relatively lower UTS degradation with increasing temperature [9]. The allowable stress in the structure (cladding and HPs) is established, at a given displacement per atom (dpa) and temperature, based on the mechanical properties of the structural material. For this analysis, the maximum allowable stress is determined as: 1/3 of the UTS; the stress which determines 1% of creep strain; 2/3 of the creep rupture stress. Having established the temperature dependent allowable stress, a quantitative analysis is performed to evaluate the dependence of the stress on the design variables. Fission gas plenum length, cladding thickness, and temperature are treated as design variables. The analysis is performed at three different Linear Heat Generation Rate (LHR): 75W/cm, 150W/cm and 240W/cm; the LHR being measured per cm of fuel rod.

Given the fission gas production rate and release in nitride fuel [19-25], the time dependent pressure inside the cladding is evaluated assuming thermal equilibrium between the fission gas plenum and cladding. For this analysis, the gas release is calculated as a function of burn up and fuel temperature according to the semi-empirical relation proposed by Storms [22]; the fuel theoretical density is assumed to be 95%. The mechanical stress analysis assumes a core design with free standing fuel rods. The inner and outer pressure acting on the cladding at the BOL at reactor operating temperatures is assumed to be 0.1 MPa. Stress is conservatively evaluated by approximating the clad as a thin wall tube rather than evaluating the solid core structure.

Figure 4 shows the EOL equivalent stress in the cladding as a function of plenum length and cladding thickness at: LHR of 150 W/cm and 240W/cm; cladding temperature of 1300K and 1350K; and fuel average temperature of 1525K and 1830K, respectively. The fuel temperature is established based on reasonable values published in the open literature [19-25]; the optimization of this analysis with respect to the design parameters which determine the thermal resistance between fuel and cladding is considered to be the subject for future design studies.

A creep analysis was also performed as a function of the design variables and time dependent applied stress. After evaluating several irradiation creep models [26-29], we adopted a model which assumes the irradiation creep rate to depend linearly on stress and dpa rate at a given temperature. Irradiation creep coefficients were obtained from the open literature [9, 30]. Information on the effects of irradiation on the mechanical properties of the structural candidate materials is relatively poor, nevertheless, some preliminary data on the irradiation creep coefficient exist up to 900K for ODS ferritic martensitic steels [30] and, at relatively higher temperature, for Mo TZM alloy [9]. Although, the irradiation creep coefficient for both materials appears to be relatively low at high temperature, as compared to more conventional steels such as HT-9 [30], and although the stress levels in the ENHS can be relatively low, irradiation creep could be an issue. This is mainly due to the high dpa levels at EOL in the reactor core. A preliminary analysis based on the fast neutron flux in the core indicates that the displacements per atom exceed by far the 100 dpa level.

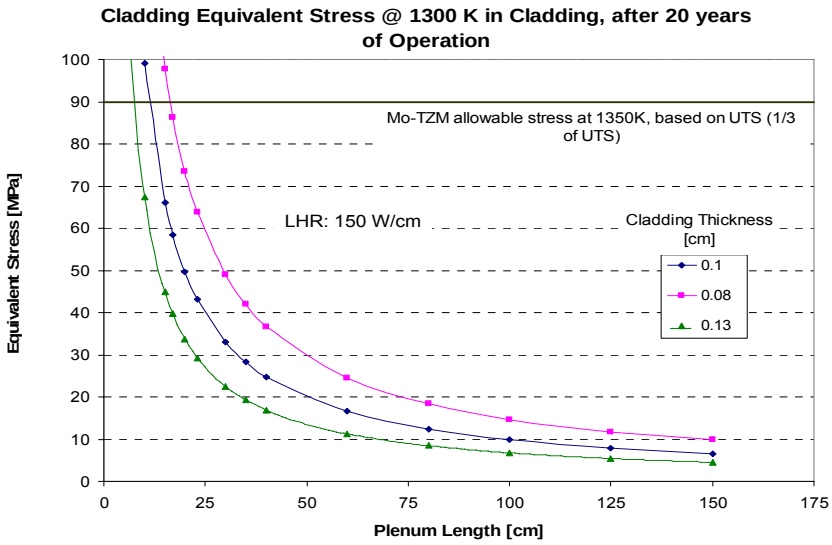


**a)**

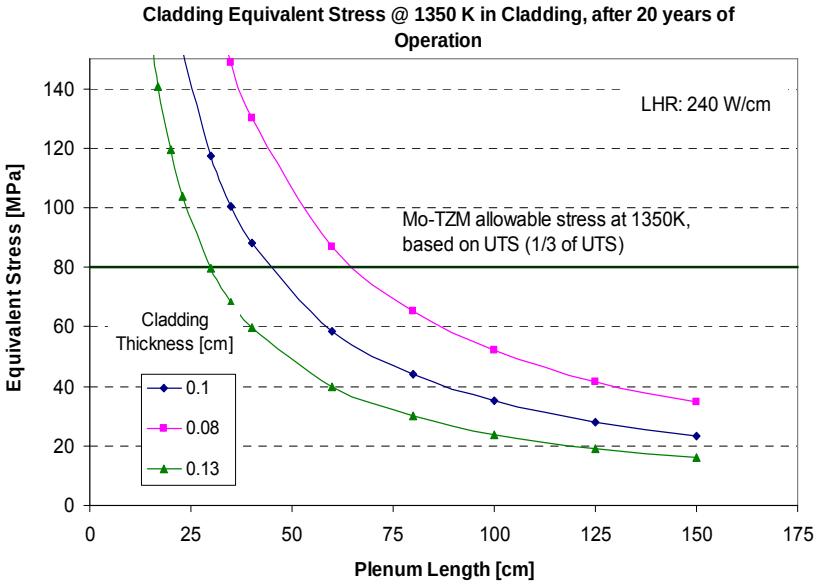


**b)**

Figure 4 Cladding equivalent stress, after 20 years of reactor operation, as a function of fission gas plenum length and cladding thickness, at: a) LHR of 150W/cm; cladding inner wall temperature of 1300K; fuel average temperature of 1525K; b)LHR of 240W/cm; cladding inner wall temperature of 1350K; fuel average temperature of 1830K. Note: 400μm of cladding thickness are not considered to contribute to the mechanical strength due to corrosion and chemical interaction between cladding and fuel.

The dpa rate was calculated given the average fast neutron flux in the ENHS core [31] and the displacement cross section of a typical steel [26, 32] and of molybdenum [32] for a typical fast reactor neutron energy spectrum. Based on this preliminary dpa estimate, irradiation creep could

be a significant issue when employing ODS ferritic martensitic steels; this does not seem to be the case for a core featuring Mo TZM as structural material. This result is due mainly to the following aspects: 1) the displacement cross section of Mo is lower than the displacement cross section of Fe [31]; 2) the irradiation creep coefficient of Mo seems to be lower than the irradiation creep coefficient of ODS ferritic martensitic steels [9, 30]; 3) the fast neutron flux seems to be higher in the core featuring an ODS steel structure rather than a Mo TZM structure [31].

Based on the preliminary estimate of the fast neutron flux and dpa levels, the EOL irradiation creep strain in the ODS ferritic martensitic cladding exceeds 1% at a LHR of 150 W/cm and fission gas plenum length of 100cm. A EOL creep strain lower than 1% is achieved for the Mo TZM cladding at a LHR of 240W/cm, by providing for adequate fission gas plenum length in excess of 70cm. A similar irradiation creep analysis performed on the HP, illustrated in Figure 5, shows that a detailed design optimization study needs to be performed in order to avoid reaching the 1% irradiation creep strain at EOL when employing ODS ferritic martensitic steels (even at a relatively low LHR).

### *3.3 Cladding-Fuel Mechanical Interaction, Some Considerations*

Although Mo TZM alloy can be generally employed at elevated temperatures, this result is coupled with the stress levels in the cladding and HPs. The stress analysis performed for this feasibility study does not assume fuel-cladding mechanical interaction due to fuel swelling. This assumption implies: relatively low fuel temperature (i.e. low LHR and thermal resistance between fuel and cladding, for a given cladding temperature); and/or large gap between fuel and cladding. If these conditions are not verified, fuel swelling could be an issue. Swelling of the fuel depends on burn up, fuel temperature and fuel theoretical density. In turn, LHR and thermal resistance between cladding and fuel affect fuel swelling (for a given cladding temperature).

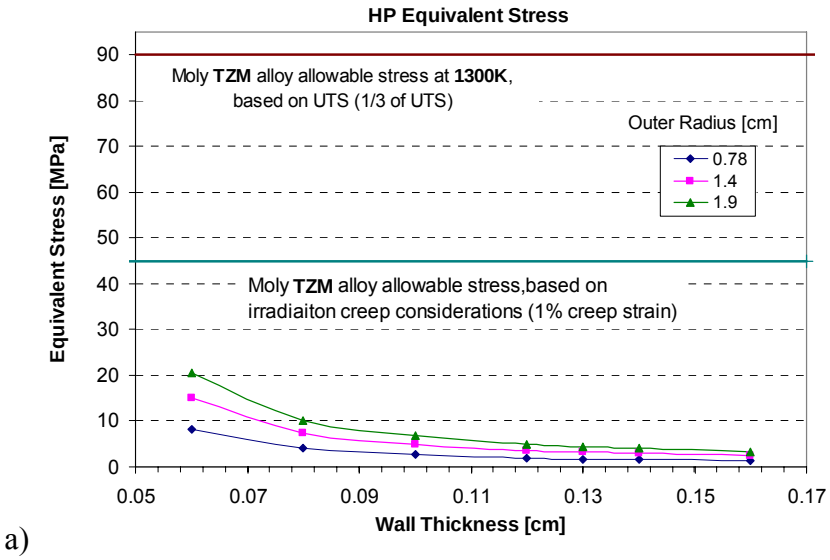


a)

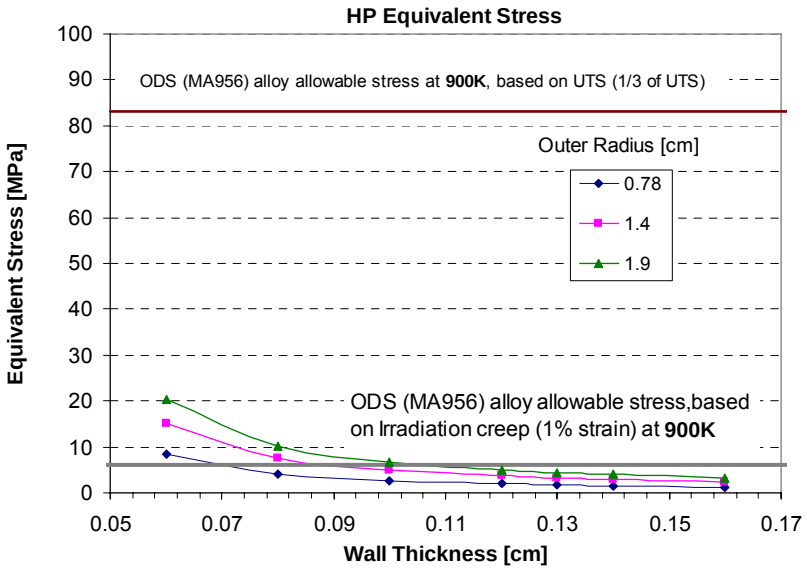


**b)**

Figure 5. HP equivalent stress and allowable stress for: a) Mo TZM alloy; b) ODS ferritic martensitic steels. Allowable stress due to irradiation creep is determined for a fast neutron fluence corresponding to a LHR of 240W/cm for Mo TZM alloy and to 75W/cm for ODS ferritic martensitic steels. The equivalent stress is determined assuming HP inner pressure of 3.5 atm and outer pressure of 1 atm at operating temperature. Note: 400μm of wall thickness are not considered to contribute to the mechanical strength due to corrosion between HP wall and primary coolant.

Figure 6 shows the fuel radius variation due to swelling of nitride fuel [34]; swelling is assumed to be isotropic. In order to avoid significant cladding-fuel mechanical interaction, we recommend considering design options which limit the thermal resistance between fuel and cladding,

particularly at relatively high LHR and cladding temperature. Liquid metal bonding between fuel and cladding could be a viable option, topic for further design optimization studies.

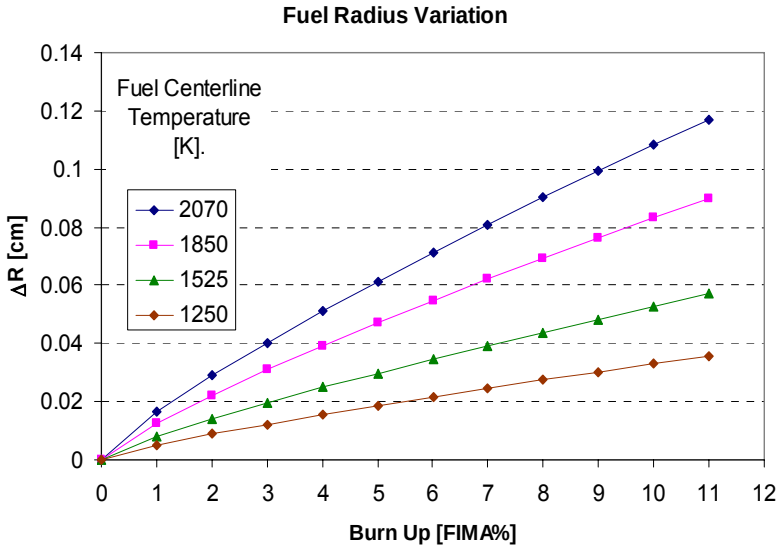


Figure 6 Average fuel radius variation due to fuel swelling [33] for an initial fuel radius of 0.65cm and fuel theoretical density of 95%. Fuel is assumed to be free to expand.

### *3.4 Corrosion of Core Internals*

Data on wet corrosion of the candidate structural materials were obtained from the open literature [12-19]. As a general outcome of this study, alkali metals, such as Na, are found to be less corrosive than lead-bismuth alloys. In particular, Mo TZM alloy seems to be compatible with liquid Na based on a corrosion rate of 5μm/years [3] at temperature higher than 1350K. This result however assumes oxygen partial pressure lower than $10^{-10}$ Torr. At relatively high temperature, Molybdenum forms volatile oxides and erosion of the base metal is an issue if the oxygen partial pressure is not controlled. Based on the same corrosion rate of 5μm/year, a temperature limit of 900K is identified for ODS ferritic martensitic steels. This value was obtained from the corrosion data[33] related to HT9 in contact with flowing liquid Na. No data were found in the open literature on wet corrosion of ODS materials at relatively high temperature.

### *3.5 Reactor Vessel*

Hastelloy is proposed as the preferred structural material to be employed for the outer vessel and other reactor components that are in contact with the hot intermediate coolant. An advantage of this material with respect to Mo-TZM and ODS ferritic martensitic steels is its relatively more mature manufacturing technology. Chemical compatibility of this material with the intermediate coolant, LiF-$BeF_2$**,** was evaluated based on data from the open literature [18]. A corrosion rate of ~20μm/year is estimated at 1100K. The results of the mechanical preliminary stress analysis are shown in Figure 7; the materials properties have been obtained from the open literature [35, 36]. The analysis was performed assuming negligible dpa levels in the vessel.

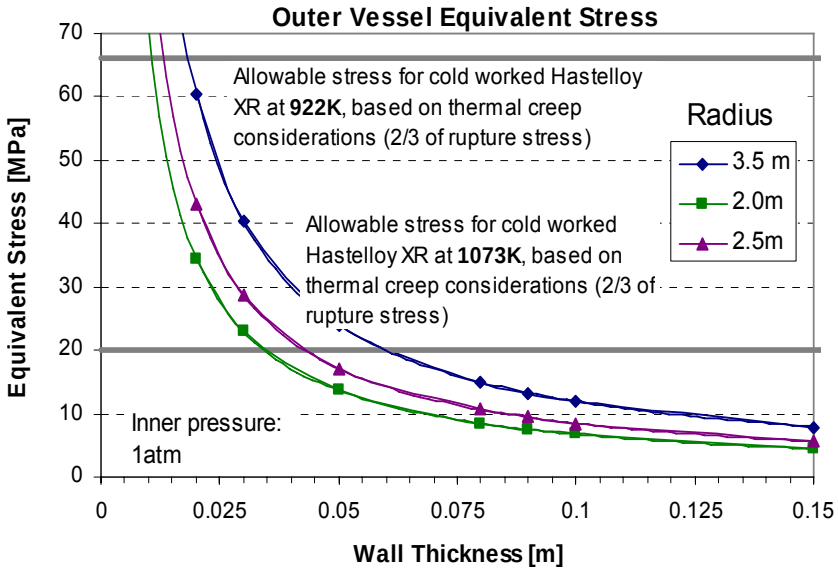


Figure 7 Outer vessel equivalent stress and Hastelloy XR allowable stress.

### *3.6 Proposed Materials and Design Guidelines*

Based on the above analysis it is proposed to pursue two HP-ENHS reactor designs: a high temperature design that is based on Mo-TZM structural material and a lower temperature design that is based on ODS steel. The former presents more challenging neutronic design due to the relatively high neutron capture cross section of Mo and might require significant engineering efforts to control the oxygen partial pressure in the core. The latter poses fewer technological

challenges but is expected to have degraded performance. Table 1 summarizes recommended design variables for the core of the two designs.

Table 5 Recommended Design Variables

| Design variable | Mo-TZM | ODS |
|---|---|---|
| Operating temperature | 1000K* to 1350K | 600K* to 1100K |
| Hot rod/core average LHR | 240/150 W/cm | 120/75 W/cm |
| Clad thickness | 0.1cm | 0.1cm |
| HP wall thickness | 0.1cm | > 0.1cm |
| Fission gas plenum length | > 70cm | 100cm |
| Outer vessel radius | 2.5m | 2.5m |
| Vessel wall thickness | > 5cm | ~5cm |
| Fuel centerline temperature** | < 1830K | < 1525K |
| Fuel/Clad Gap** (BOL; room T) | > 700μm | >200μm |

* Lower temperature limit is due to embrittlement and radiation hardening.

** Values refer to fuel-clad gap closure. The gap closure analysis is based on fuel swelling, cladding creep and thermal differential contraction. Swelling of cladding is not considered in the analysis due to lack of data at dpa level of interest. Fuel centerline temperature and BOL gap thickness are coupled. The higher the fuel temperature, the larger the initial gap needs to be in order to avoid gap closure.

While from the mechanical point of view, Mo-TZM alloy seems to be the preferable high temperature material, some engineering issues emerge. Oxidation of this alloy at high temperature is a concern [4, 16] as well as manufacturability and welding. While oxidation of ODS steels does not seem to be a particular issue [13], manufacturability and welding presents similar issues to Mo-TZM alloy. Moreover, ODS steels are to be preferred to Molybdenum due to the lower absorption cross section which favors neutron economy [31].

There are significant uncertainties in the above recommendations due to the lack of experimental data. Feasibility issues recommended for further research and development include: manufacturability and welding of Mo TZM alloy; oxygen partial pressure control in the core (due to oxidation of Mo at high temperature); characterization and proof-of-principle tests of irradiation creep properties and swelling of Mo TZM alloy at relatively high displacement per atom; and fuel-cladding chemical compatibility.

# 4. HEAT PIPE PERFORMANCE

## *4.1 Introduction*

The primary feasibility issue addressed in this part of the study is whether or not heat pipes can be designed to transfer to the intermediate coolant the fission power generated when the core is designed to operate at a specific power that is comparable to that of the reference ENHS design in which the fuel is cooled by flowing lead-bismuth coolant. Another objective of this study was to optimize the HP design and define their performance characteristics while abiding by the structural material and fuel temperature constraints.

Heat pipes offer a passive mechanism to transport heat from one area to another via the evaporation and condensation of a working fluid. The key design goal of the heat pipes in this reactor is to remove the power generated by the core at the highest possible temperature. This study evaluates the range of power levels that can be removed by heat pipes as a function of various design variables including working fluid, operating temperature, wick design, diameter, and length. Based on a rough materials temperature limits, Cs, K, Na, and Li are candidate working fluids and this study focuses on the use of Na and K Fuel elements dimensions are fixed at 1.56cm in diameter and 1.5m in length with target linear heat rates (core averaged) of 75W/cm and 150W/cm. The radial power peaking factor is assumed to be 1.6 based on the design of the ENHS. For the following analysis, the length of the evaporator and condenser sections of the heat pipe are set at half the active length of the fuel (75cm), the adiabatic length is set at 50 cm to accommodate fission product gases.

## *4.2 Heat Pipe Description*

The heat input from the core into a heat pipe causes some of the liquid sodium to evaporate, while at the other end the pipe is being cooled by the Flibe, causing the vapor to condense. The higher vapor density in the hot end causes a net flow of vapor to the cool end, and at the same time, the higher concentration of liquid in the cool end forces flow into the hot end as shown in Figure 8 [37]. The liquid is contained on the outside of the heat pipe by a wick.

The ability of a heat pipe to axially transfer heat is limited by five mechanisms: the viscous limit, the sonic limit, the entrapment limit, the capillary limit, and the boiling limit; all of which will be examined in the section on heat pipe performance.

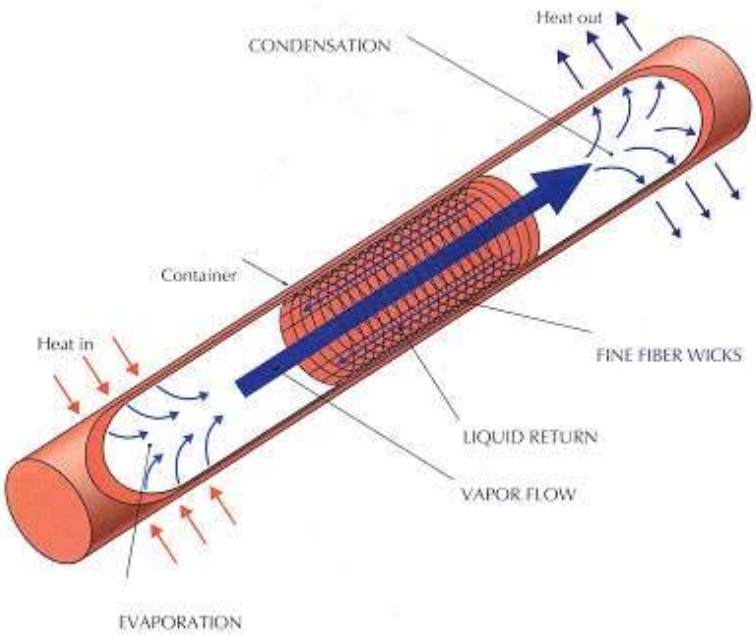


Figure 8 Schematic layout of a heat pipe

### *4.3 Heat Pipe Performance Review*

Heat pipe performance is a critical area because sufficient test data is not currently available to formally evaluate the reliability of the heat pipe. A design studies report from Los Alamos National Laboratory [37] summarizes heat pipe performance and failure mechanisms described below. The modes of performance of the heat pipes are fairly well understood, as discussed subsequently. They are of critical importance because the associated limits could lead to heat pipe failure.

*Viscous Limit*

Normally the pressure in the heated zone is the primary driving force. At low temperatures (startup) the vapor pressure difference between the condenser and evaporator may be low enough that the pressure gradients imposed by the temperature field are insufficient to overcome the

viscous resistance in the vapor flow region. The viscous limit rarely leads to serious problems and can be avoided by increasing the evaporator temperature during startup (increasing the vapor pressure). The viscous limit can be described by the following equation

$$Q_v = \frac{A_v \, r_o^2 \, h_{fg} \, \rho_v \, P_v}{16 \, \mu_v \, L}$$

where $\rho_v$ is the vapor density, $P_v$ is the vapor pressure, and $A_v$ is the flow area of the vapor (determined from the inner radius of the wick structure). This equation shows that the viscous limit is determined primarily by the operating temperature of the heat pipe and the vapor flow area.

*Sonic Limi*

Mass addition in the evaporator and mass removal in the condenser will cause variations in the vapor velocity along the length of the heat pipe. Vapor velocity at the evaporator exit can reach the speed of sound. In this case further increases in the heat load will not result in increases in the mass flow rate. The sonic limit rarely leads to problems as the heat pipes are not asked to transfer heat as such a high rate during normal operation. It can be described by the following equation

$$Q_s = \frac{A_v \, \rho_v \, V_s \, h_{fg}}{\sqrt{2 \, (k+1)}}$$

where $V_s$ is the sonic velocity, $\rho_v$ the vapor density, and k is the specific heat ratio. Increasing the internal area will significantly increase the sonic limit margin.

*Entrainment Limit*

Since the liquid and vapor flow in opposite directions in the heat pipe, shear stresses that occur at the liquid-vapor interface may be strong enough to inhibit the return of the liquid to the evaporator. Operation under these conditions could lead to evaporator dry out and heat pipe failure. A limited amount of work has been done in this area for alkali-metal heat pipes. The main parameters of interest for the entrainment limit are the surface tension of the liquid, the

vapor density, and the hydraulic radius of the wick. There is a relatively incomplete knowledge of the mechanisms involved in this limit. Thus, a high uncertainty is associated with entrainment limit data.

*Capillary Limit*

The difference in the capillary pressure across the liquid-vapor interfaces in the evaporator and condenser regions governs the operation of heat pipes. Net capillary pressure difference must be greater than the sum of the friction and inertial pressure drops in the vapor and liquid phases as shown in the following equation

$$(\Delta P_c)_{\max} \geq (\Delta P_f)_v + (\Delta P_i)_v + (\Delta P_f)_l + (\Delta P_i)_l$$

where f and i represent the friction and inertial pressure drops and v and l represent the vapor and liquid phases. If not, the evaporator could dry out. The net capillary difference is approximated as

$$(\Delta P_c)_{\max} = \frac{2\sigma}{r_{c,e}}$$

where $\sigma$ is the surface tension and $r_{c,e}$ is the local capillary radius in the evaporator (related to the wick pore radius). If the maximum pore size is used, a conservative estimate is obtained. Smaller pore sizes will yield higher capillary limit margins of safety.

*Boiling Limit*

When the radial heat flux is too high, incipient boiling may occur in the evaporator, trapping vapor bubbles in the wick. Unlike other performance limits, the boiling limit depends on the local wall heat flux rather than the axial heat transport. Uncertainties in the boiling limit arise from the limited knowledge of the size and number of nucleation sites, as well as the theory explaining the precise mechanics behind bubble formation. Smaller nucleation sites and fewer sites will delay the occurrence of the boiling limit and increase heat pipe performance. Finishing techniques for the curved pipe surfaces should be developed to reduce the number of nucleation sites as much as possible.

### *4.4 Design Considerations*

As with all nuclear reactors, heat must be removed from the core to prevent the core from overheating. Though heat pipes passively remove heat from the core, they remain susceptible to failure due to materials degradation, thermal transients, etc. Should a heat pipe fail, neighboring heat pipes must be able to transport the power that was removed by the failed heat pipe. Based on the work of Barnes, Kapica, and Wongsawaeng in a previous student design project, a single isolated heat pipe failure is expected to increase the heat load on surrounding heat pipes by 17-33% depending on the location of the failure.[38] Our study assumed that a power safety factor of two (a power increase of 100%) was sufficient to deal with heat pipe failures i.e. each heat pipe is designed to remove twice the normal operating power. However, more detailed analysis is required to establish a stronger basis for this safety factor. While the 17-33% additional heat load values may be adequate for high reliability heat pipes, a high heat pipe failure rate could invalidate the assumption of isolated heat pipe failures. The possibility of cascading heat pipe failures also requires further evaluation. In the event of a single heat pipe failure, the resulting temperature and power transient on surrounding heat pipes may cause additional heat pipe failures. For instance, a temperature transient caused by one heat pipe may accelerate materials degradation in neighboring heat pipe and initiate a cascading failure. The current analysis has not considered the effects of transient behavior.

### *4.5 Analysis*

Heat pipe performance is conservatively quantified using the iterative process specified by Silverstein that calculates various heat transport limits (e.g. sonic limit, capillary pumping limit, entrainment limit, and boiling limit) [39]. The target heat pipe power is based on the configuration of the core, the target linear heat rates, the power peaking factor, and a power safety margin. The target heat pipe power is at least 54.4kW per heat pipe corresponding to a LHR of 75W/cm, a radial power peaking factor of 1.6, and a power safety margin of 2. An annular wick was selected due to its low frictional resistance to liquid flow. However, this design is sensitive to disruptions by non-condensable gas that could block the fluid flow channel. Initial

wick parameters were adopted from the work of Barnes, Kapica, and Wongsawaeng [38] as specified in Figure 9. Mo TZM was selected for the wick material to limit corrosion by a sodium working fluid.

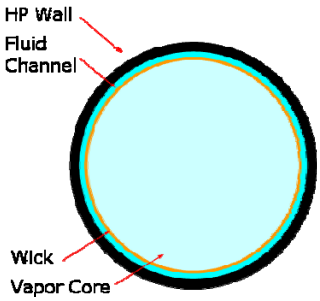


HP parameters:

Wall thickness – 0.6 mm
Fluid channel thickness – 0.7 mm
Wick thickness – 0.6 mm

Figure 9 Wick parameters

Heat pipe performance is a strong function of operating temperature and is constrained by the maximum allowable temperature of the structural material (to control corrosion and mechanical properties) and by fuel temperature (to maintain a temperature margin to melting, control fuel expansion, and control gaseous fission product release). Based on these temperature limits, a finite element heat transfer code was used to determine the temperature profile for an infinite core to establish the maximum heat pipe operating temperature as specified in Table 2. A typical temperature profile is shown in Figure 9.

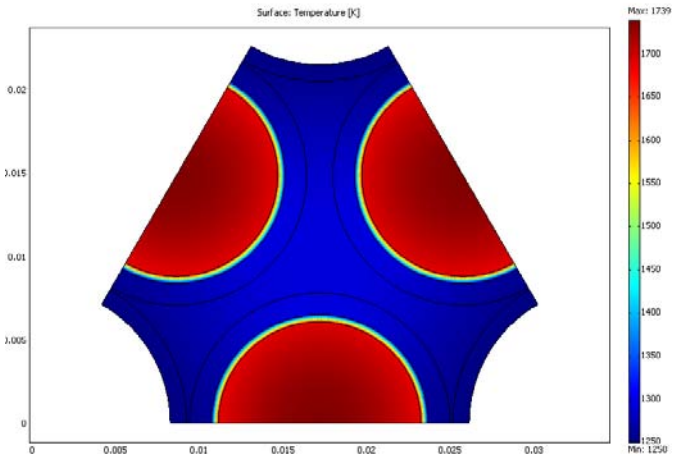


Figure 10 Temperature profile in the HP-ENHS core calculated using the finite element heat transfer code

Table 6 Selected Core Temperatures

| | *Mo TZM* | | | *ODS* | | |
|---|---|---|---|---|---|---|
| | *75 W/cm* | *150 W/cm* | *240 W/cm* | *75 W/cm* | *150 W/cm* | *240 W/cm* |
| Max HP Temp (K) | 1320 | 1290 | 1255 | 900 | 850 | 670 |
| Max Structure Temp (K) | 1350 | 1350 | 1350 | 1100 | 1100 | 1100 |
| Max Fuel Temp (K) | 1569 | 1816 | 2047 | 1216 | 1480 | 1702 |

Filling the gap between the fuel and the fuel cladding with a liquid metal could be used to reduce the peak fuel temperature to maintain a higher safety margin and reduce fission gas release. However, a sodium gap filler reduces the maximum allowable temperature in ODS due to corrosion. A sodium gap filler is feasible for a Mo structure since Mo-TZM is not corrosion limited. Nevertheless, the horizontal orientation of the core complicates the use of a liquid gap filler since the liquid would pool at the bottom of the fuel element unless a mechanism could be developed to retain the gap filler around the fuel while allowing gaseous fission products to escape the active fuel region into the fission gas plenum. The horizontal orientation of the core also requires accounting for persistent fuel-cladding interaction and for asymmetric heat flux from the fuel elements.

Bob Reid at Los Alamos National Laboratory cautions that the approach outlined by Silverstein is overly conservative [40]. These conservatisms include:

- Sonic limit: Heat transport should not exceed 30-50% of the sonic limit to avoid excessive temperature and pressure drops
- Wick design: This analysis uses the pore diameter of LANL's high performance laser screen wick. The 5 micron pore diameter of the LANL high performance wick is fabricated with pulses from a femtosecond laser.
- Capillary Pumping: Silverstein's method limits the vapor pressure drop to 3% to maintain a nearly isothermal heat pipe. A larger vapor pressure drop might be possible to increase heat transfer if non-isothermal heat pipe operation can be tolerated. This analysis assumed a 10% vapor pressure drop along the evaporator which corresponds to a 11K temperature drop. The vapor pressure drop for the LANL data is unknown.
- Entrainment: the vapor flow is conservatively assumed to be turbulent

- Boiling: Nucleation site radius is assumed to be 3 μm. This should be better characterized for the structural material and working fluid used in the heat pipe. Interface heat transfer coefficient

Figure 10 gives the expected power that can be removed by high performance heat pipe designs proposed by LANL as a function of the HP working fluid temperature. Sodium offers greater heat transport capability for operating temperatures above approximately 1150K while potassium is a better choice for below 1150K [40]. The figure also shows that the heat transport capability of the HP strongly depends on the HP radius.

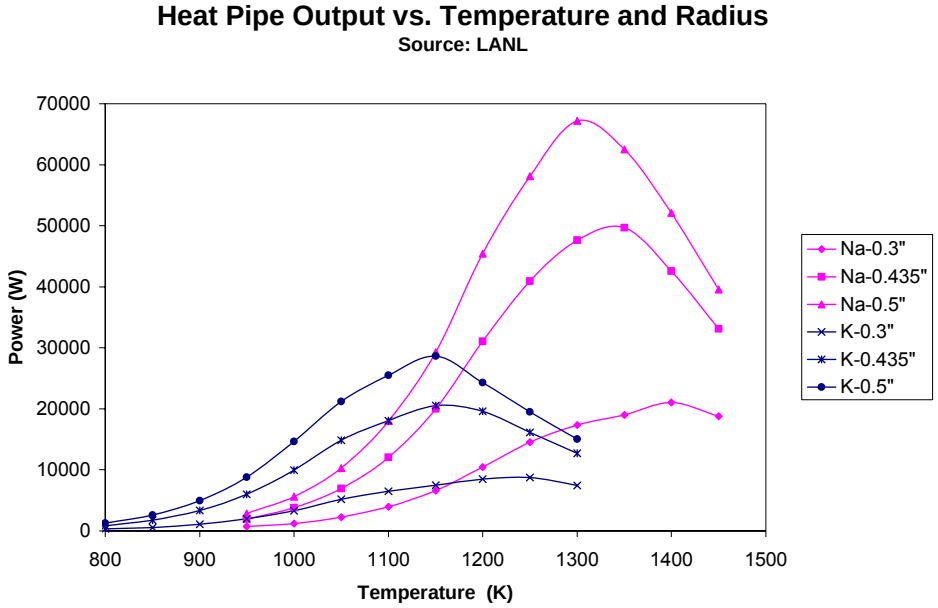


Figure 11 Calculated Na heat pipe operating limits (top) and LANL high performance heat pipe data (left)

The capillary pumping force in the wick must overcome pressure losses in the heat pipe to circulate the HP working fluid. The largest resistance to flow comes from the vaporized working fluid in the central vapor core of the HP. Increasing the radius of the vapor core reduces frictional losses and increases heat transport capability. Figure 12 gives the power output of a sodium heat pipe using the conservative assumptions in Silverstein (though with a less conservative 10% vapor pressure drop) and data supplied by Los Alamos for their high performance heat pipes.

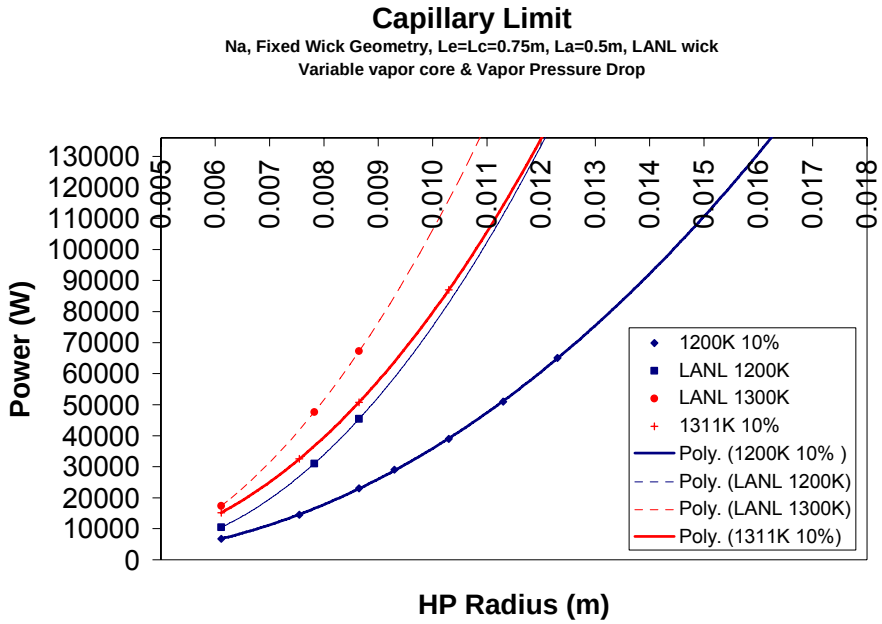


Figure 12 Capillary pumping force

Varying the length of heat pipe segments (evaporator, adiabatic, condenser) has relatively small effect on the heat pipe output. This provides little incentive to change the initial length of the heat pipe and offers some flexibility should other aspects of the design require shorter or longer heat pipe sections.

### *4.6 Heat Pipe Lifetime*

Corrosion due to the presence of impurities in the heat pipe may limit the heat-pipe lifetime. Soluble impurities present in the system (including material dissolved from the structure of the heat pipe) concentrate along the evaporator where they can clog the wick pores, form low melting point eutectics, or form ternary compounds. Reducing these impurities during heat pipe fabrication can enable longer lifetimes. According to Reid, alkali metal heat pipes have successfully operated for longer than $10^4$ hours and 12 year operation appear possible with proper heat pipe fabrication methods. A Mo HP with a Na working fluid operated for 45,039hours at 24 W/cm$^2$ and 1391K. The test ended due to the lack of support and not due to heat pipe failure [41].

### *4.7 Summary*

Table 3 summarizes the expected heat pipe performance based on the high performance heat pipe data provided by Los Alamos.

Table 7 Summary of Heat Pipe Performance

| Structural material | LHR (W/cm) | Working Fluid | HP Temp (K) | HP Outer Diameter (cm) |
|---|---|---|---|---|
| Mo | 300 | Na | ~1200 | ~2.4 |
| | 240 | Na | ~1200 | ~2.2 |
| | 150 | Na | ~1300 | ~1.8 |
| | 120 | Na | ~1300 | ~1.65 |
| | 75 | Na | ~1300 | ~1.5 |
| ODS | 300 | K | ~550 | N/A |
| | 150 | K | ~850 | > 5 |
| | 75 | K | ~900 | ~2.8 |

# 5. NEUTRONIC ANALYSIS

## *5.1 Introduction*

The primary feasibility issue addressed by the neutronic analysis is whether or not it is possible to design a solid core reactor with relatively leaky (neutronically) heat pipes and with relatively strongly absorbing Mo-TZM alloy to be critical and to have a conversion ratio of approximately 1.0 so as to maintain a nearly constant $k_{eff}$ over the 20 EFPY of core life.

The core of the HP-ENHS maintains many of the characteristics of the previously designed ENHS core. Fuel rods external diameter is kept the same (1.56 cm) while the fuel clad is reduced from 1.3 mm to 1 mm as found permissible from the stress analysis[1]. Nitride is selected for the fuel because of its high operating temperature, high HM density, high thermal conductivity and low fission gas release; it is also the fuel type preferred for high temperature space nuclear reactors. The HM is composed of depleted uranium (0.2% $^{235}U$), typically more than 80%, and Pu or TRU of the isotopic composition in which it is found in the spent fuel (SF) from Light Water Reactors (LWR) after 50 GWd/t burn-up and 10 or more years of cooling. The smear density of the fuel is 87%. Nitrogen is initially assumed enriched in $^{15}N$ at 100% so as to minimize the parasitic neutron capture in the fuel; i.e., to maximize the fuel $\eta$. The core is assumed to have an hexagonal lattice with pitch-to-diameter ratio (P/D) of 1.0. The HPs are assumed to have the same outer diameter as of the fuel rods. This implies that the outer surface of the fuel rods and HPs are touching. The gap between the rods is filled with the structural material.

The core is modeled as a homogeneous mixture of all the components obtained conserving their mass and core volume. The weight percent of Pu (TRU) initially loaded is determined so as to obtain $k_{eff} = 1+\beta$ at BOL. The 1 dollar excess reactivity is a margin assumed to compensate for uncertainties in the nuclear data and computational model. The primary and intermediate coolants are assumed to be sodium, although the preferred intermediate coolant was later selected to be molten salt.

[1] The reference ENHS clad thickness of 1.3 mm is a significant overdesign

### *5.2 Results*

The initial results of the neutronic analysis are presented in Figure 13. They pertain to initial loading of Pu that was cooled for 10 years. It is found that the materials tested can be divided, in terms of their neutronic behavior, into two groups: HT-9 and ODS; Mo and Nb1Zr. HT9 and ODS are less absorbing and are neutronically preferred. A core constructed of these two materials requires a smaller initial loading of Pu and a higher conversion ratio to guarantee criticality for the entire core lifetime. These two materials can accommodate a larger P/D (i.e. larger volume of structural material) since the excess reactivity at EOL is too large. While Mo-TZM and Nb1Zr are much stronger absorbers; they require about 4% more Pu at BOL and the conversion ratio is insufficient to maintain criticality. These materials require a smaller P/D.

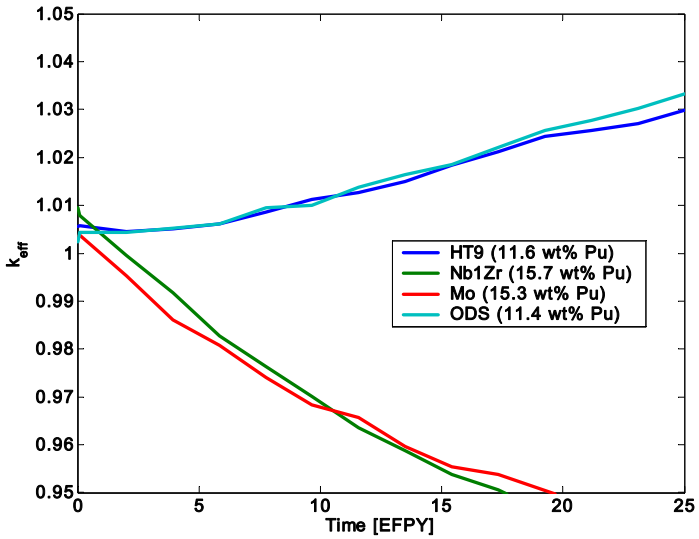


Figure 13 Multiplication factor as a function of exposure time for different structural material with P/D of 1.0

For a high temperature design, Mo-TZM was found to be the most suitable structural material (See Section 3). Its peak operating temperature is as high as 1350 K and the HP's working temperature is 1300 K. At such temperature the working fluid to use into the heat pipes to maximize the heat removal is sodium (See Section 4) and the required diameter is on the order of the diameter of the fuel rods. Since Mo-TZM is a relatively strong absorber, the volume fraction of the structure must be minimized (P/D 1.0). The LHR is set at 75 W/cm for this study. This makes the total diameter of the core about 2 m for a total of 11,111 fuel rods and 5,556 heat pipes.

Figure 14 shows that despite of the small P/D, nearly zero reactivity swing can not be obtained for 20 years of full power operation initially loading fuel with only Pu from SF. Criticality can be guaranteed if the core is started with an excess of reactivity of about 5%, increasing the initial load of Pu from 14% (required to get $k_{eff} = 1+\beta$) up to 15.2%. In this case burnable poisons should be added to the start up core.

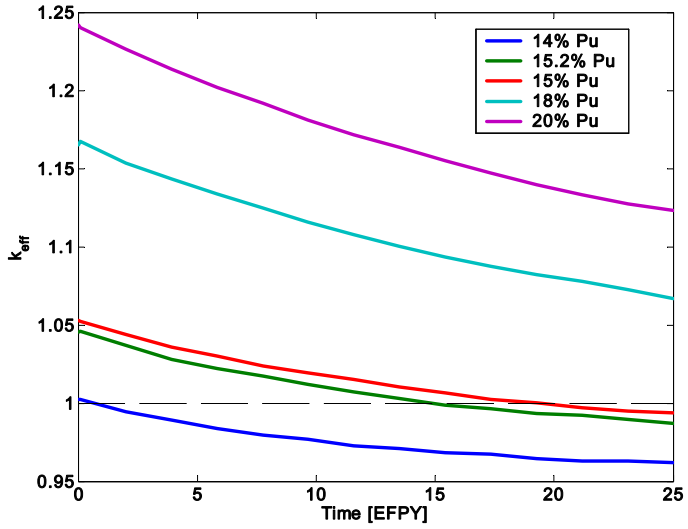


Figure 14 Multiplication factor as a function of exposure time for different Pu-to-HM initial load

### *5.3 Minimizing Reactivity Swing*

Alternative solutions to the use of initial excess of reactivity and burnable poisons have been investigated. One option is to increase the cooling time of spent fuel to allow $^{241}$Pu to decay. The resulting isotopic composition of the fed fuel is given in Table 8. The $^{241}$Pu has a fairly high fission cross section and relative short half life. At the relatively low power density of the ENHS core the loss of $^{241}$Pu via radioactive decay is relatively high and this is a major contributor to the decline of $k_{eff}$ with burnup. By allowing $^{241}$Pu to decay before entering the reactor, the amount of Pu that needs to be loaded to achieve BOL criticality increases but the initial conversion ratio is larger and $k_{eff}$ evolution is flatter. This trend is confirmed by comparing, in Figure 15, the results obtained using 30 years versus 10 years cooled Pu: the initial fraction increases from 14% for 10 years cooling to 17.2% and the $k_{eff}$ evolution is flatter.

Table 8 Actinide Composition of LWR Spent Fuel after 50 GWd/MTHM and Different Cooling Periods

| Isotope | Cooling period (years) | | |
|---|---|---|---|
| | 10 | 30 | 50 |
| $^{237}$Np | 6.66% | 6.93% | 7.28% |
| $^{238}$Pu | 2.76% | 3.63% | 3.12% |
| $^{239}$Pu | 48.81% | 49.14% | 49.42% |
| $^{240}$Pu | 23.06% | 23.43% | 23.65% |
| $^{241}$Pu | 6.95% | 2.67% | 1.03% |
| $^{242}$Pu | 5.05% | 5.09% | 5.12% |
| $^{241}$Am | 4.67% | 8.80% | 10.21% |
| $^{242m}$Am | 0.02% | 0.02% | 0.02% |
| $^{242}$Cm | 1.48% | 0.00004% | 0.00004% |
| $^{243}$Cm | 0.01% | 0.003% | 0.002% |
| $^{244}$Cm | 0.50% | 0.23% | 0.11% |
| $^{245}$Cm | 0.04% | 0.04% | 0.04% |
| $^{246}$Cm | 0.01% | 0.006% | 0.006% |

An alternative solution tried is to load the minor actinides (MA) from the spent fuel along with the Pu. While the addition of MAs initially absorbs more neutrons and increases the initial loading of TRU, it increases the conversion ratio. Figure 15 shows that combining a 50 years cooling periods with loading of all TRU (17.9%) allows reaching nearly zero reactivity swing.

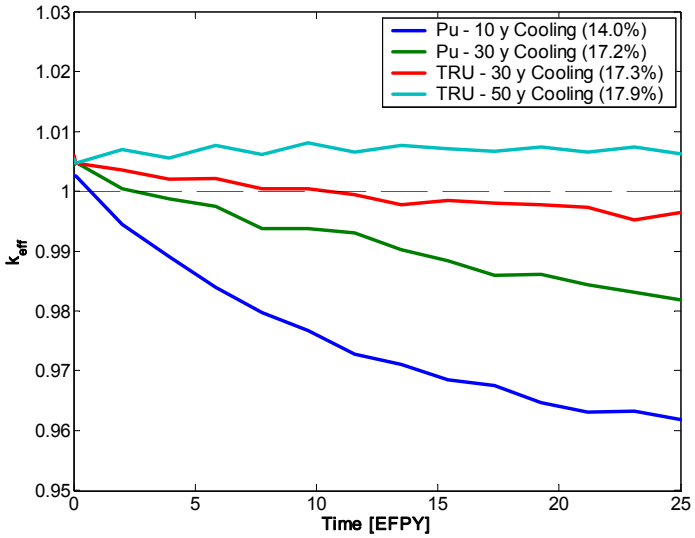


Figure 15 Effect of reactivity of LWR spent fuel composition after long cooling time and effect of only Pu initial load vs. all TRU recycling

An alternative approach explored for minimizing the burnup reactivity swing is use of natural nitrogen in the nitride fuel; it was initially assumed that the nitrogen used is enriched to 100% $^{15}N$ so as to minimize neutron absorption in $^{14}N$. It was found, as shown in Figures 16 and 17, that natural nitrogen (99.632 at% $^{14}N$, 0.368 at% $^{15}N$) could, indeed, help flattening the $k_{eff}$ evolution with burnup. This is probably due to relatively high absorption cross section of $^{14}N$ for high energy neutrons that causes spectrum softening that results in a conversion ratio increase. A drawback of using natural nitrogen is the production of the long-life $^{14}C$ isotope.

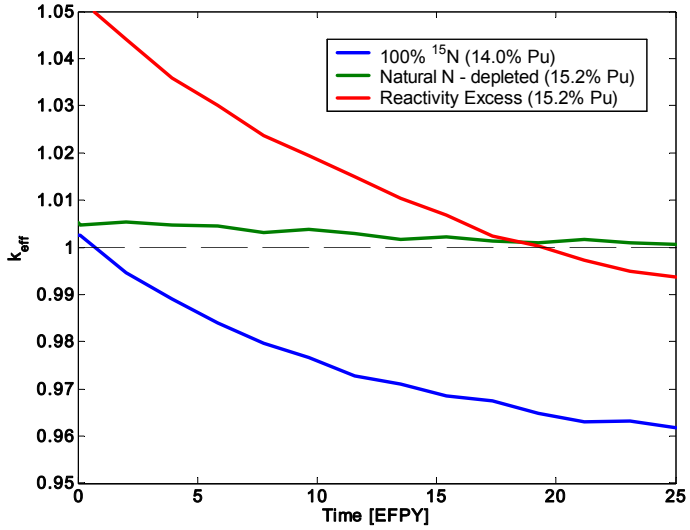


Figure 16 Effect of using natural nitrogen fuel vs 100% $^{15}N$ when using only Pu initial load

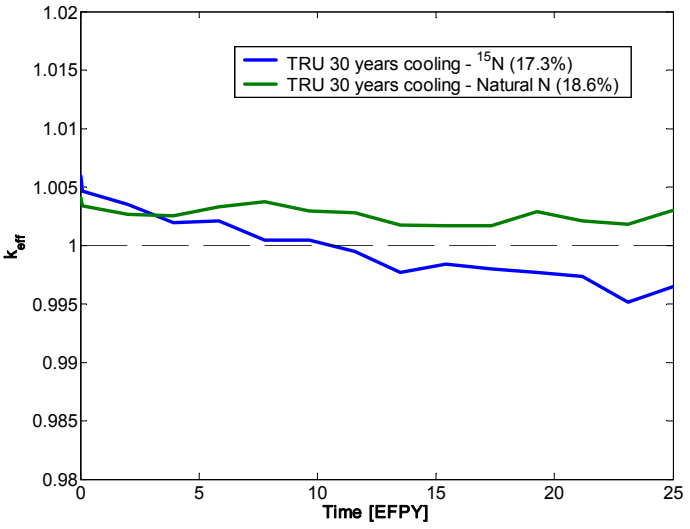


Figure 17 Effect on reactivity swing when of natural nitrogen fuel vs 100% $^{15}N$ when using all TRU initial load

### *5.4 More Realistic Core Design*

The preliminary neutronic analysis summarized in the preceding sections considered cores having a circular cross section and sodium reflector. No control elements were taken into account. A preliminary design of an alternative, more realistic core is undertaken in this and the following sub-sections. It features the following new ingredients relative to the preliminary design:

- A square rather than a circular cross-section area so as to provide an IHX design that has the same number of tubes – the condenser section of the heat pipes, in all the rows. A disadvantage of this design is increased neutron leakage from the core – by up to 12.21% in case of a bare core.
- A solid reflector is now used instead of the intermediate coolant.
- Control elements are introduced.
- LiF-$BeF_2$ (Flibe) is used rather than sodium as the secondary coolant.

All the results reported in the following subsections are calculated assuming nitride fuel having natural nitrogen and TRU from LWR that was cooled for 50 years.

#### 5.4.1 Optimal Reflectors

Figure 18 shows a schematic view of the bare and reflected parallelepiped core examined. Two materials were examined for the reflector: MoTZM and BeO. Both can operate at the elevated temperature of the Flibe.

Figure 19 compares the $k_{eff}$ evolution with burnup of the reference bare core and the two reflected cores; both reflectors are 20 cm in thickness and all cores are loaded with the same amount of TRU of identical composition. It is found that the BeO is, neutronically, a better reflector; it reduces the neutron leakage probability more than the MoTZM reflector and, hence, enables getting criticality using a lesser amount of TRU. The lower the critical TRU loading is the larger will be the conversion ratio and the flatter will be the effective multiplication factor.

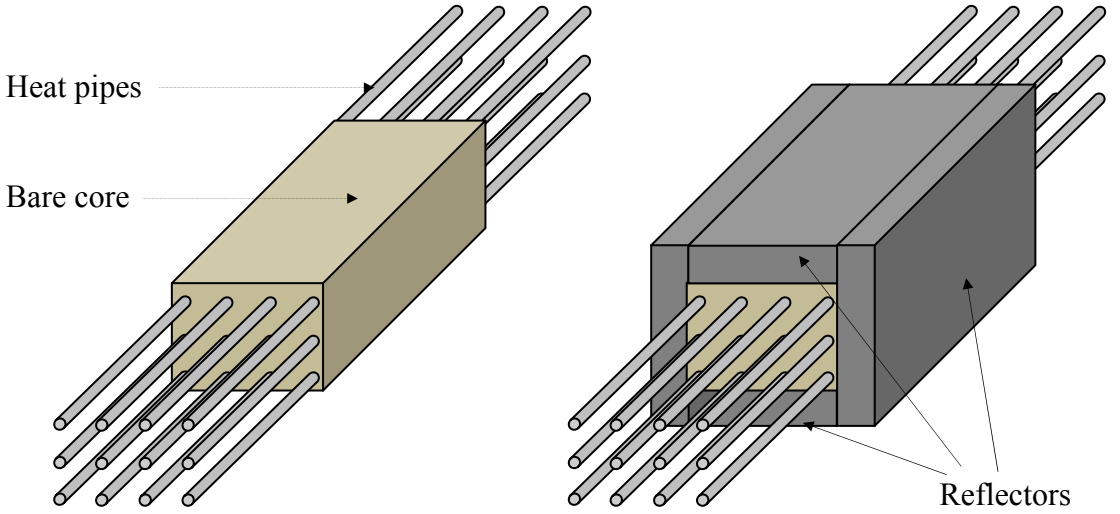


Figure 18 Schematic view of the bare (left) and reflected (right) HP-ENHS core

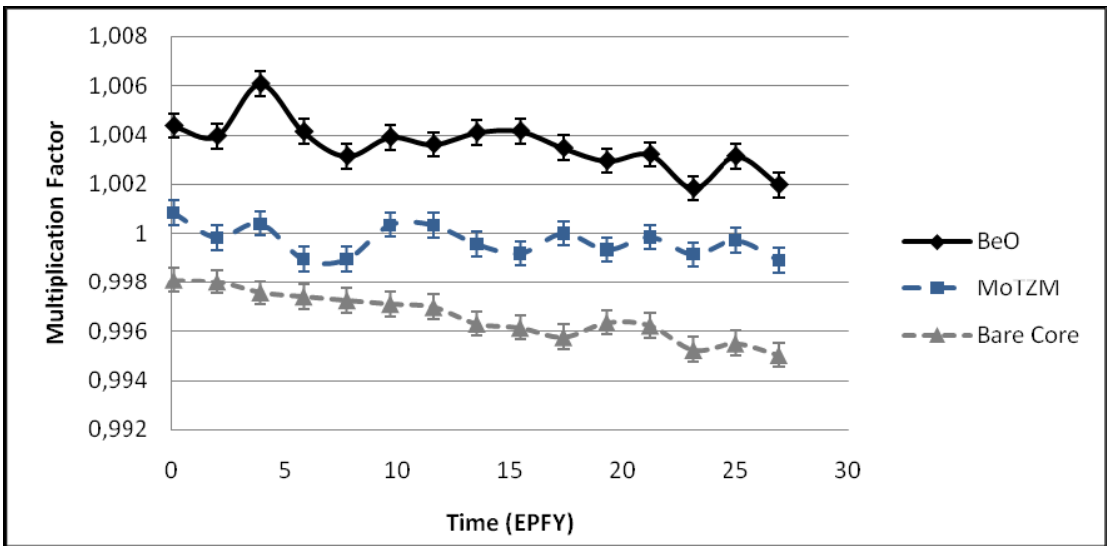


Figure 19 Comparison between MoTZM and BeO reflectors
(20cm thick reflector, 22.5% TRU)

Figure 20 shows the effect of the BeO reflector thickness on $k_{eff}$. A 40cm thick reflector is chosen for the final design. The required TRU weight percent is 22.45%.

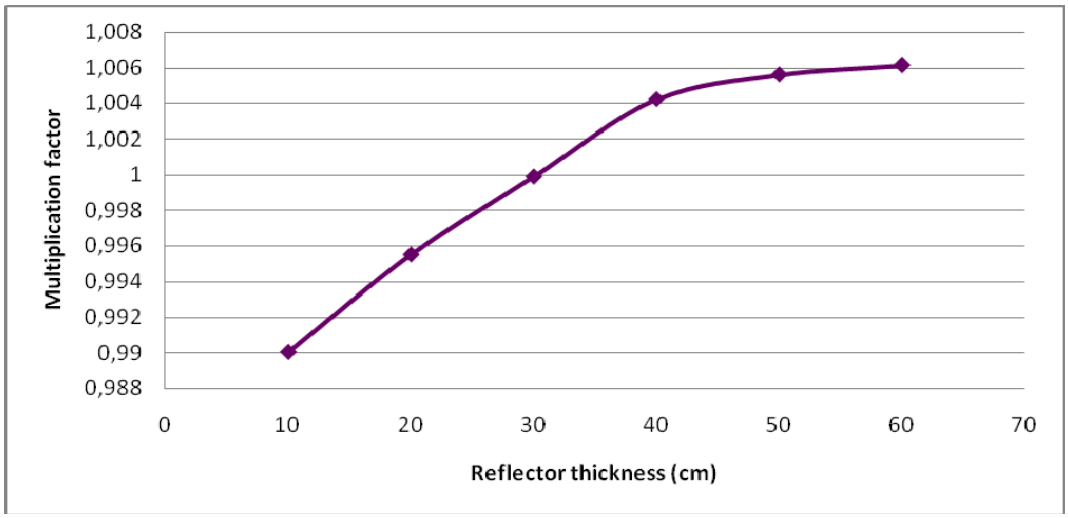


Figure 20 Effect of the BeO reflector thickness on $k_{eff.}$ 22.45% TRU, 50 years cooling

5.4.2 Reactivity Control

The original ENHS reactor uses peripheral control elements for the reactivity control and a central safety element for scramming the reactor and keeping it sub-critical under any possible circumstances. Two approaches for shutting the reactor down were investigated – using a peripheral control and using a central control. The design goal is to be able to shut down the HP-ENHS core and bring $k_{eff}$ to 0.95 or below; that is, to have a shut-down safety margin of at least 5%.

A schematic illustration of the approach to peripheral control is given in Figure 21. It involves lowering the vertically oriented side reflectors to replace their lower reflective section by the upper absorbing section. The advantage of this design is lack of the need to "split" the solid heat-pipe core to provide access to insertion of control elements.

An alternative design considered is illustrated in Figure 22; it involves lifting up the upper reflector of the core, letting its location be filled with secondary coolant (LiF-$BeF_2$). The advantage of this design is the larger drop in the multiplication factor due to the removal of the upper reflector. It is not possible to do a similar design for the downwards configuration since movement of the lower reflector is constrained by the core support structure.

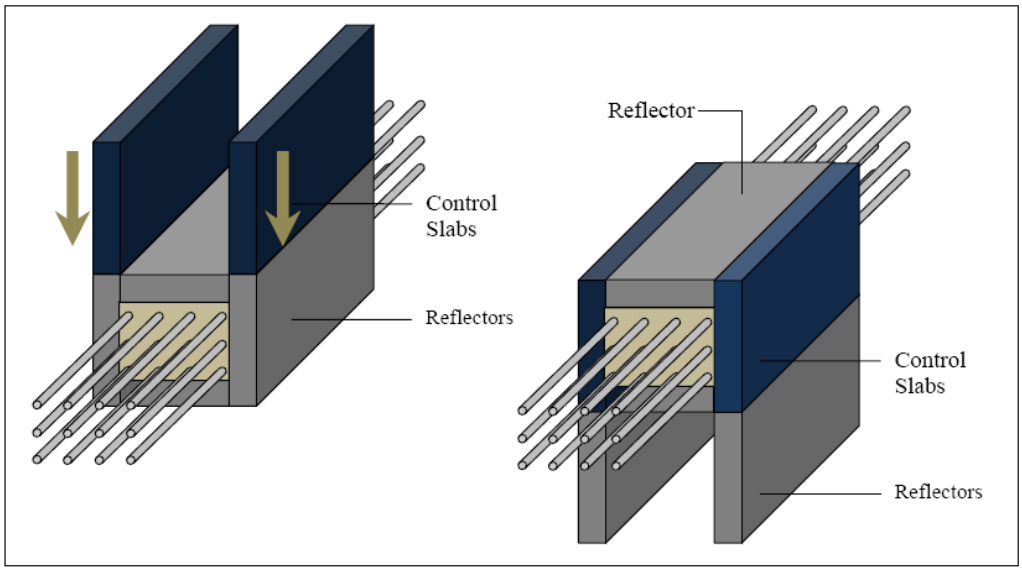


Figure 21 Peripheral control system schematics

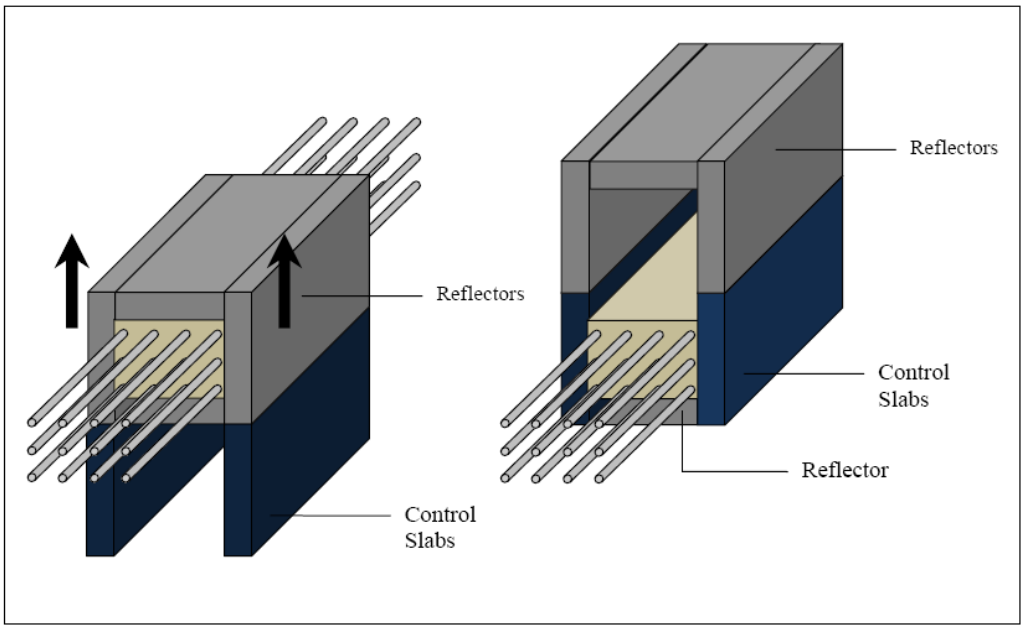


Figure 22 Upward moving peripheral control system schematics

Three materials are considered for the control section: $B_4C$, Rhenium, and Flibe. $B_4C$ is the control material used in many reactor designs, including the SAFE-400 space heat-pipe reactor, whereas using Flibe is the simplest approach – just letting the secondary coolant take the place of the BeO reflector. The material compositions used are summarized in Tables 5 and 6.

Table 5 Atom Densities of Non-Fuel Materials Used for MCNP Computations

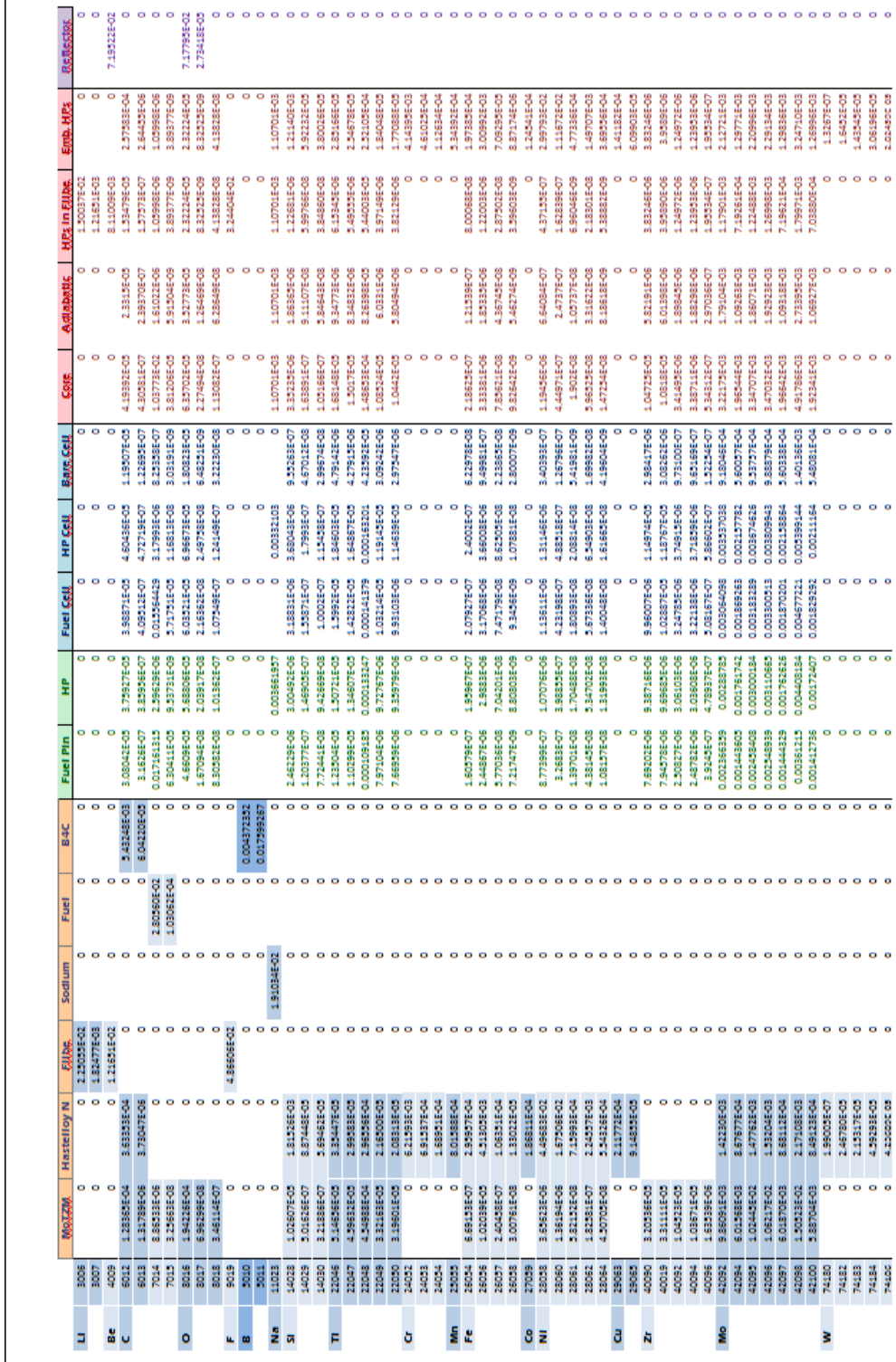

Table 6 Actinides Atom Densities Used for MCNP Computations

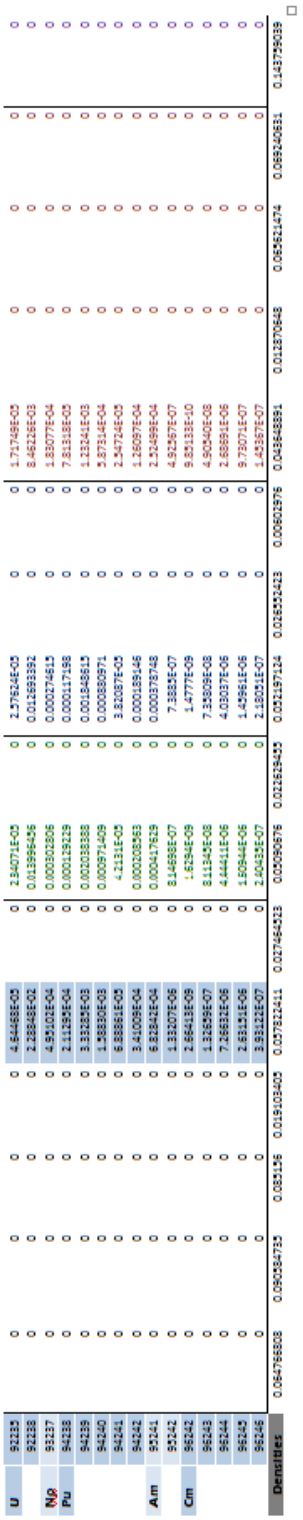

Figures 23 and 24 show the results obtained for, respectively, the Downwards and the Upwards configurations.

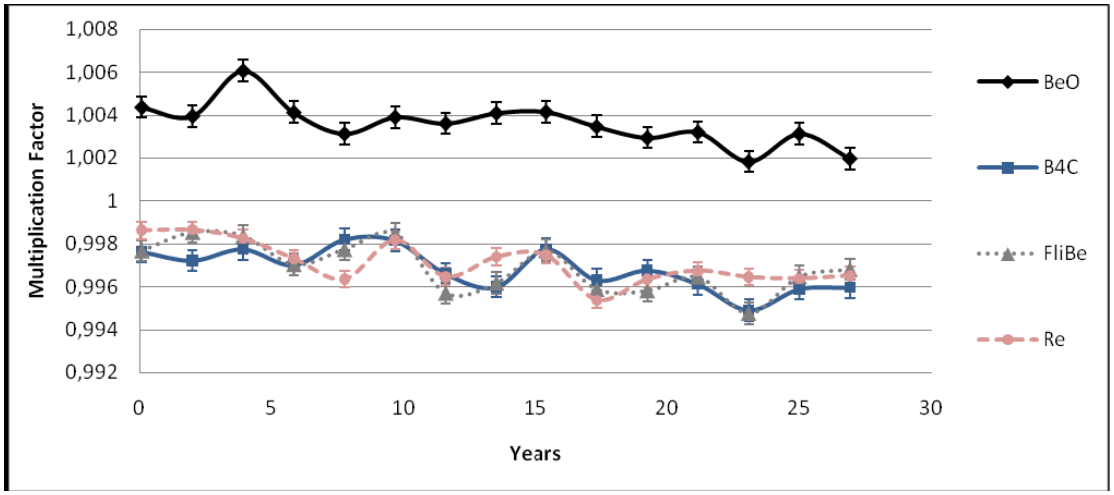


Figure 23 Effect of control slabs – downwards

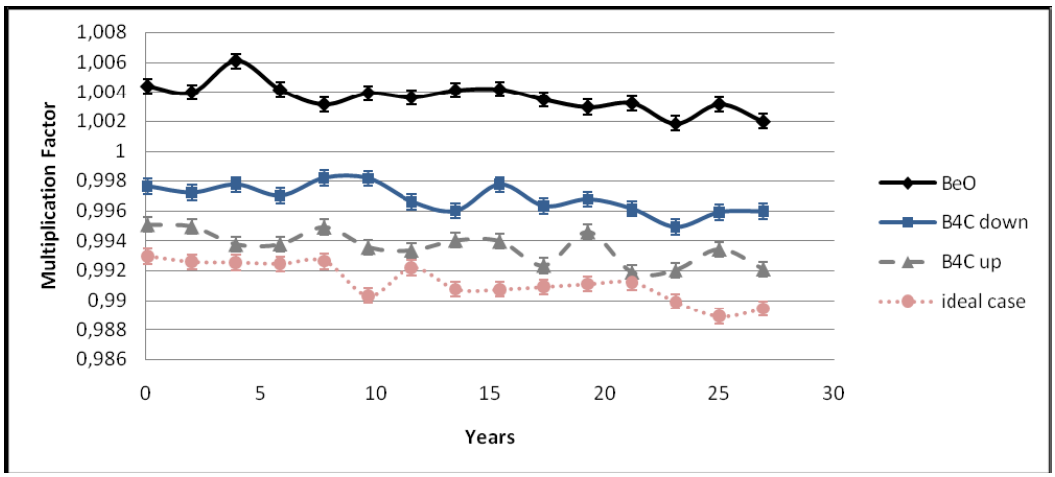


Figure 24 Effect of control slabs – upwards

These results show that the upper reflector removal is worth a notable fraction of the reactivity drop (0.003/0.010 = 30%). The maximum reactivity drop to $k_{eff}$ = 0.993 gives, however, an insufficient safety margin of less than 0.8%. The peripheral control approach is therefore not good enough to guarantee a safe reactor shutdown. Hence, control elements need be introduced inside the core.

The heat-pipe core configuration prevents installation of control rods parallel to the fuel rods, as is commonly done in most of the reactors; it is not possible to install mechanisms for horizontal insertion of control rods without major interference with the HP heat-exchangers and without

significant increase in the reactor vessel diameter. An alternative approach examined is splitting the core into two halves and insertion of one or two control elements in the space provided between the two halves of the core.

Figure 25 shows one of the split core design approach examined. The gap provided is perpendicular to the heat pipes and fuel rods; its introduction requires splitting the fuel rods into two, as the heat-pipes are split. To minimize the reactivity loss due to the introduction of a gap at the core center a slab of BeO, a good reflecting material, is introduced at normal operating conditions. The control material was taken to be $B_4C$. Figure 26 shows the multiplication factor obtainable for a central control blade that is 40cm thick. The multiplication factor flatness is impaired by the greater amount of TRU necessary to attain criticality (22.4%) of the split core. $k_{eff}$ does not stay sufficiently flat.

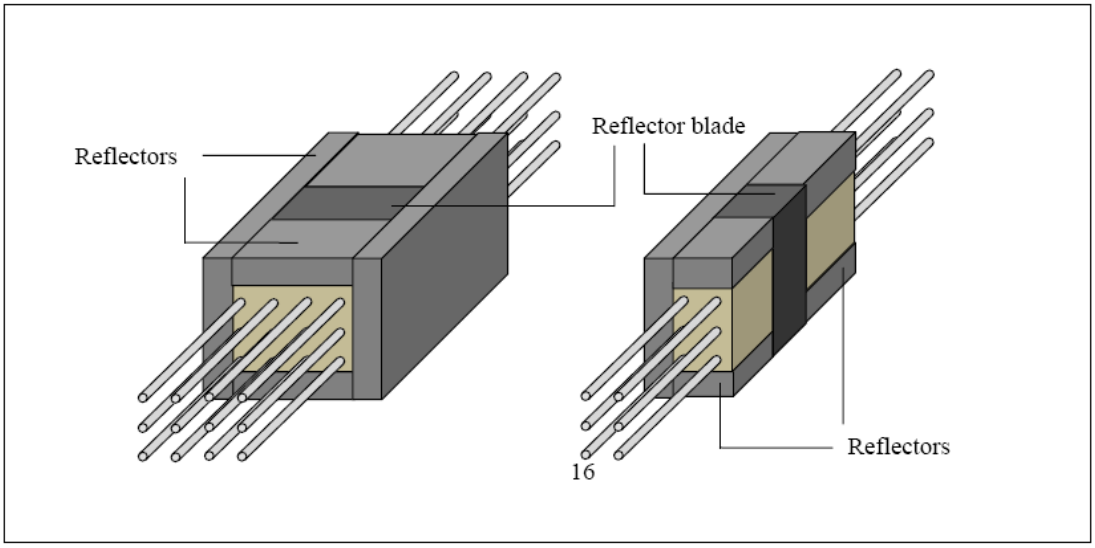


Figure 25 Schematic view of the HP-ENHS core having a perpendicular split

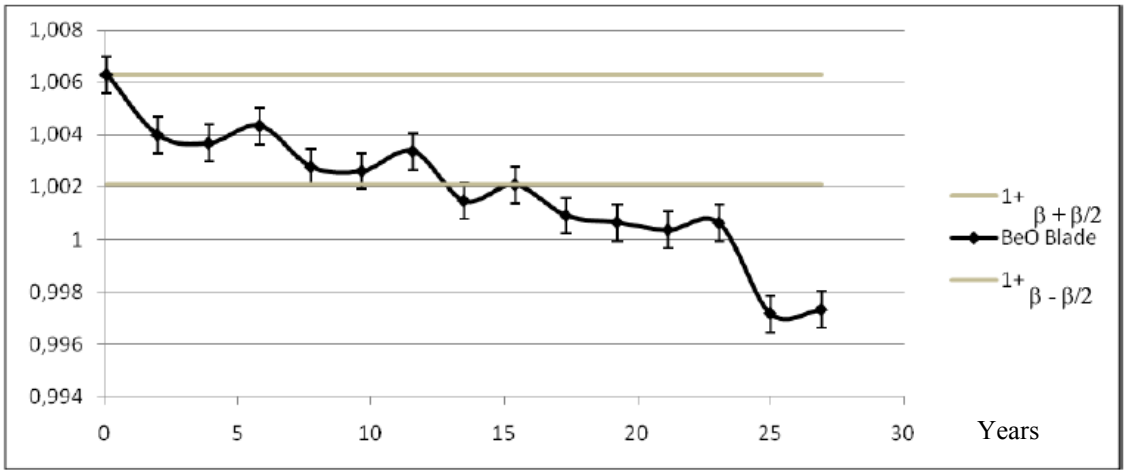


Figure 26 $k_{eff}$ time evolution (in years) of the HP-ENHS perpendicularly split core having a 40cm thick BeO blade

Figure 27 describes the impact of the reflector blade thickness on the multiplication factor at beginning of life, for an initial TRU concentration of 22.5%. The steep drop in $k_{eff}$ at low reflector thicknesses is probably due to spectrum softening to the below the fast fission threshold of, primarily, $^{238}U$ and to the upper resonance energy range where η of $^{239}Pu$ and other fissile isotopes is relatively low. The increase in $k_{eff}$ when the BeO reflector thickness increases beyond approximately 5 cm is probably due to the buildup of a thermal flux component that is characterized by a higher $^{239}Pu$ η value than in the epithermal energy range. Beyond 50 cm the enhanced leakage probability reduces $k_{eff}$.

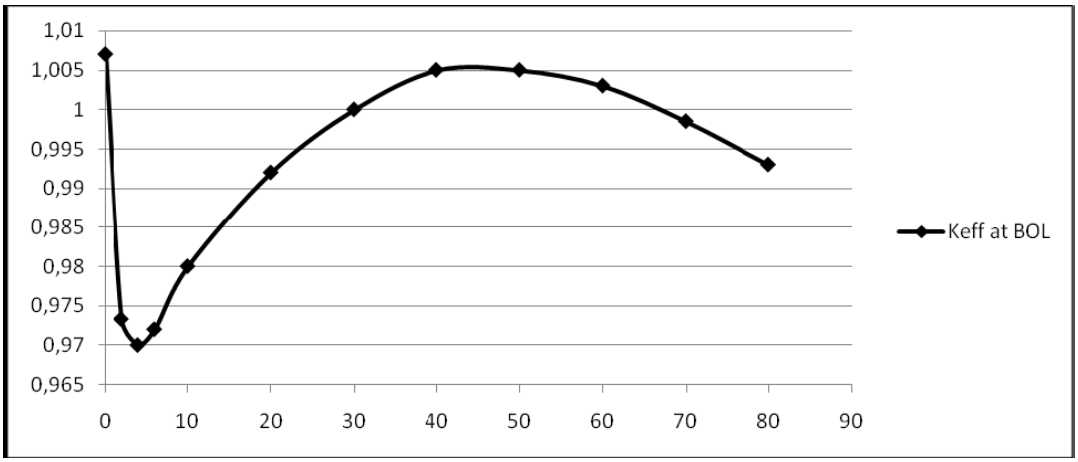


Figure 27 Effect of BeO reflector blade thickness on the BOL $k_{eff}$ of a perpendicularly split core

Figures 28 to 30 show the effect of the BeO reflector blade on the fission rate probability distribution. The position of the blade is clearly visible at the core center, where the fission

probability equals zero. The effect of the reflector blade thickness can be deduced from the contrast between distributions of the 40 cm versus 10 cm thick designs. Whereas for the thick blade the fission probability goes up sharply to 8.3 E-07 near the blade at x = -20 cm and x = +20 cm and drops steeply beyond the peak, the thin blade design features a relatively flat fission probability of 5.2 E-07 in at the central part of the core. These differences are due to the effect of the blade on the neutron spectrum as discussed above.

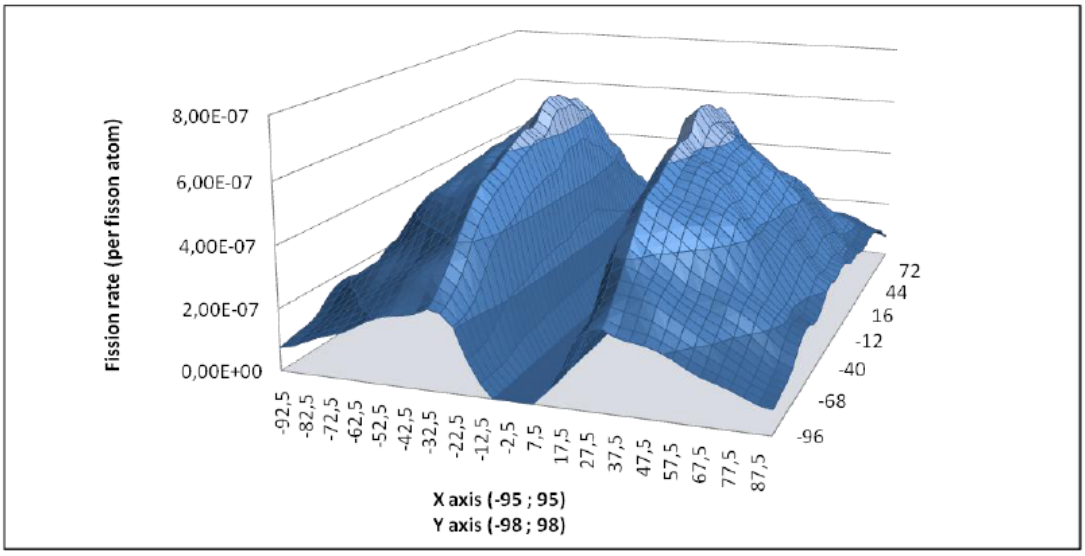


Figure 28 Relative fission rate distribution for a central horizontal section of the core – 40cm thick BeO reflector blade in a perpendicularly split core

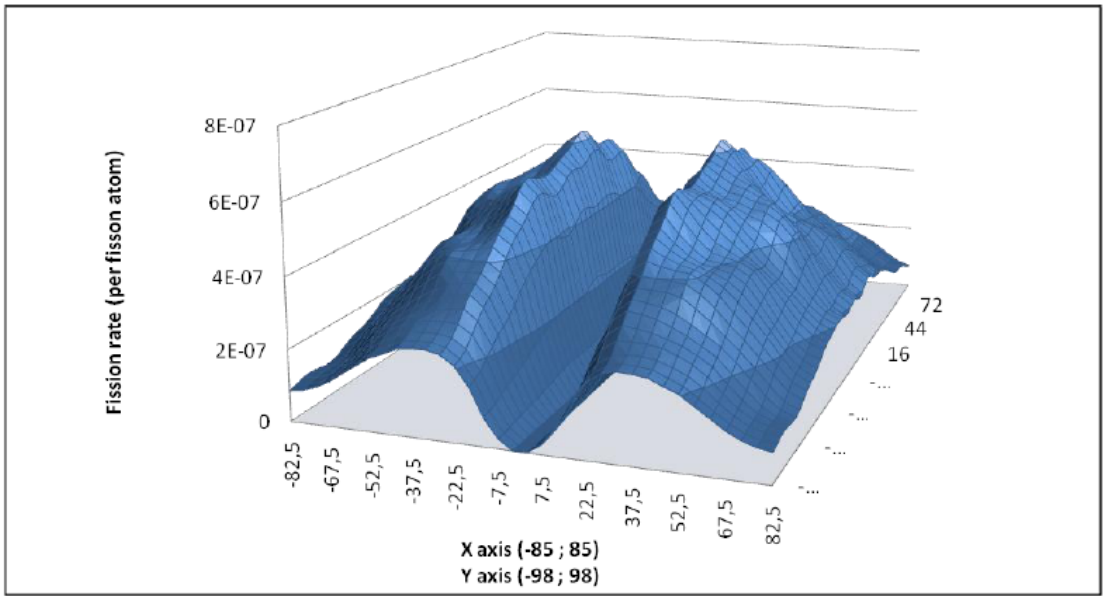


Figure 29 Relative fission rate distribution for a central horizontal section of the core – 20 cm thick BeO reflector blade in a perpendicularly split core

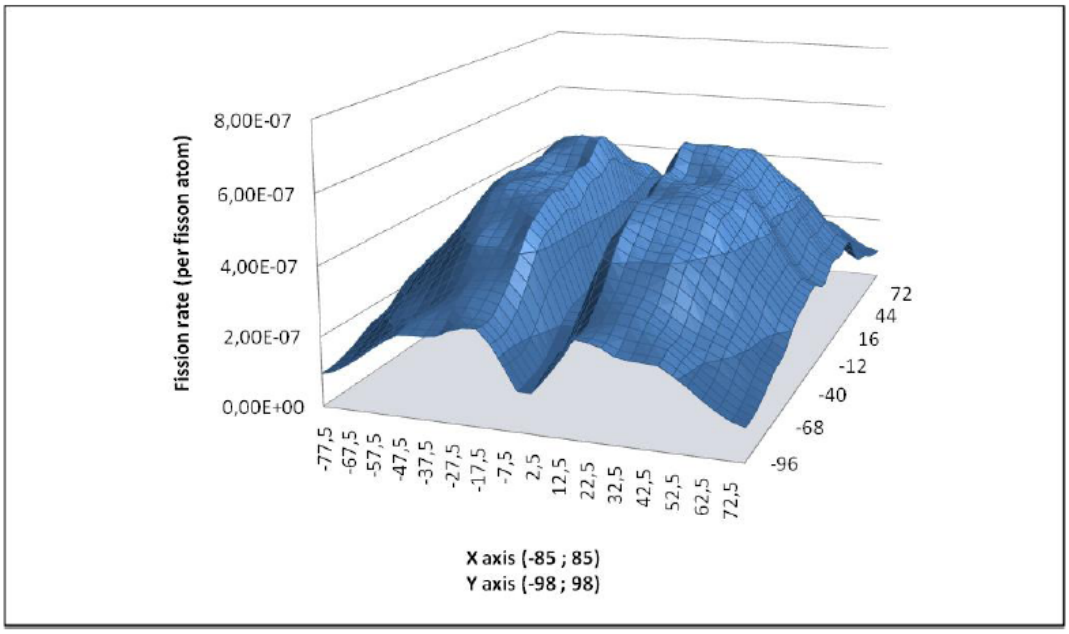


Figure 30 Relative fission rate distribution for a central horizontal section of the core – 10cm thick BeO reflector blade in a perpendicularly split core

It is concluded that a BeO reflector slab at the center of the split core is undesirable on two counts. First it softens the neutron spectrum and thereby reduces the conversion ratio to the point that makes it impossible to attain a flat enough $k_{eff}$ over the core life. In addition, it can increase the power peaking factor in the core, depending on its thickness.

### *5.5 Reference Core Design*

An alternative design approach investigated is use of a voided container made of thin MoTZM walls in the space between the two halves of the core. When lowered, a $B_4C$ follower of the same cross section area is inserted into the core. Figure 31 shows the time evolution of $k_{eff}$ of the split HP-ENHS core with a 10 cm voided blade. The TRU weight percent is 22.87%. $k_{eff}$ is not as flat as in the case without a split. Nevertheless, it is flatter than when using BeO reflector in-between the core halves and enables 20 years of core life with acceptably small reactivity swing.

Figure 32 compares $k_{eff}$ of the scrammed core in which a $B_4C$ control blade replaces the voided container. The shutdown margin obtained is slightly more than 4%; little short of the 5% constraint. However, by simultaneously scramming also the 40 cm thick side reflectors a shutdown margin exceeding 5% is achieved, as illustrated in Figure 33. This design, a schematic view of which is shown in Figure 34, is adopted for the neutronically preferred reference design.

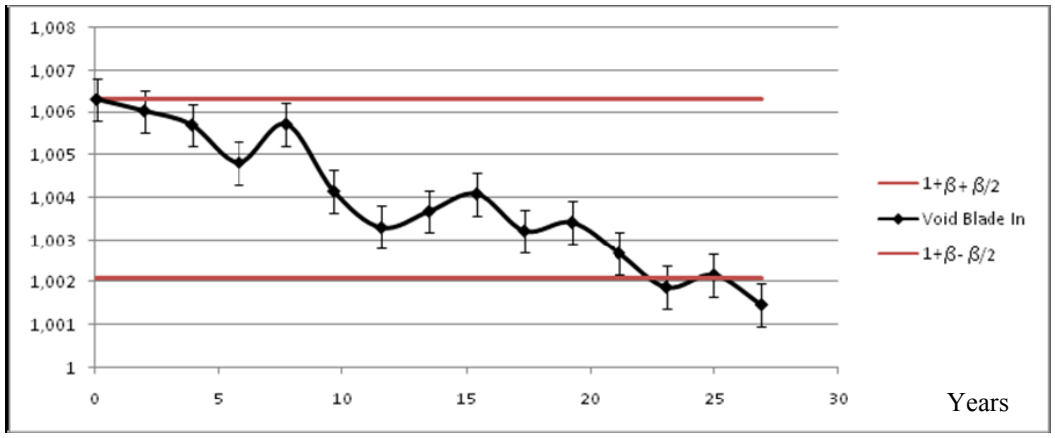


Figure 31 Evolution of $k_{eff}$ of a split HP-ENHS core with a 10 cm voided blade; 22.87% TRU

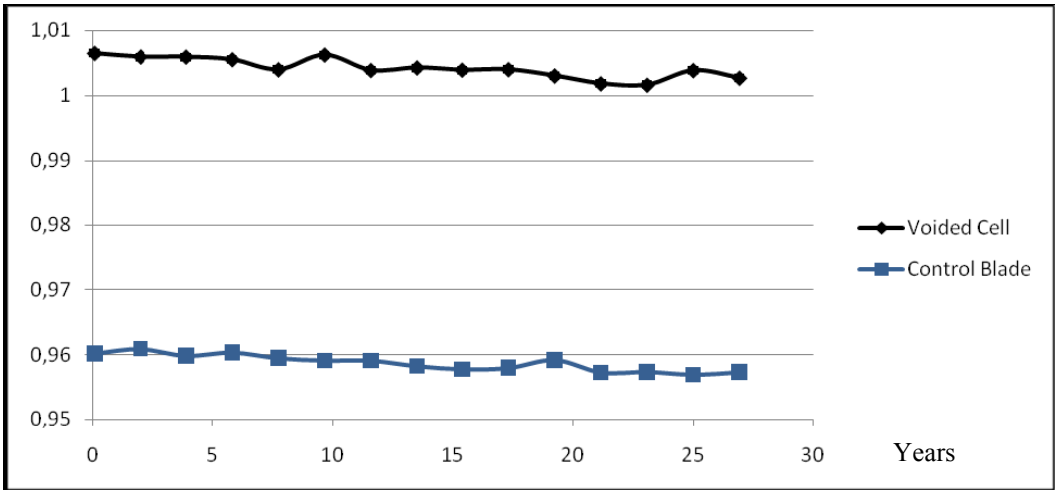


Figure 32 $k_{eff}$ evolution with and without 10 cm thick central control blade inserted into the split core. 22.87% TRU

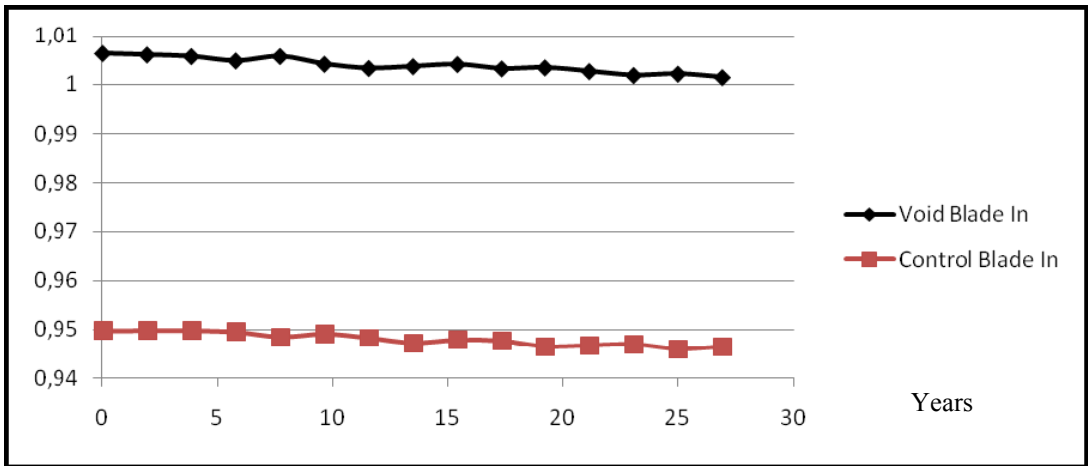


Figure 33 $k_{eff}$ evolution with and without 10 cm thick central $B_4C$ control blade inserted into the split core. 40 cm thick $B_4C$ absorbers replace the BeO side reflectors simultaneously. 22.87% TRU

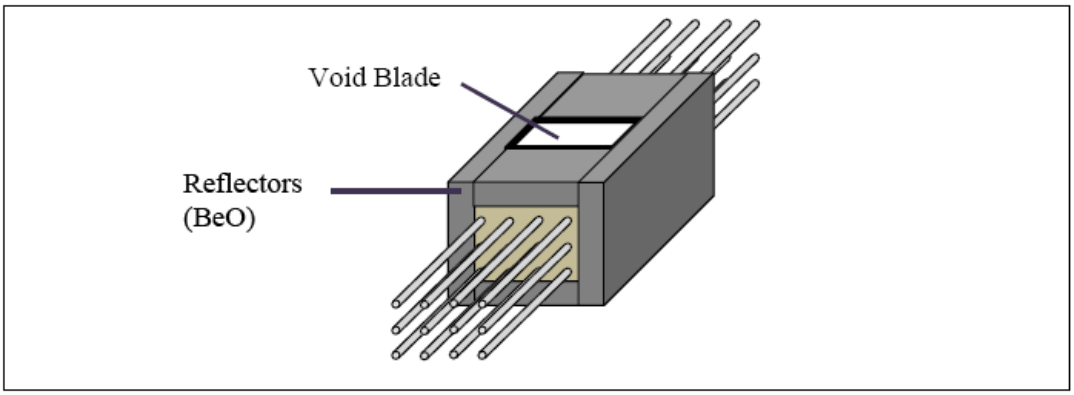


Figure 34 Neutronically preferred reference core design schematics

A drawback of the above design is that it does not have redundant systems for scramming the reactor. An alternative design is schematically illustrated in Figure 35; it has two central void blades 10 cm thick, each having a $B_4C$ absorber plate on top. The TRU initial concentration required for establishing criticality is 22.9% and its conversion ratio is slightly smaller. As a result the variation of $k_{eff}$ with burnup, shown in Figure 36, is somewhat steeper than in case of the neutronically preferred design (Figure 31). This design is referred to as the safety preferred reference design.

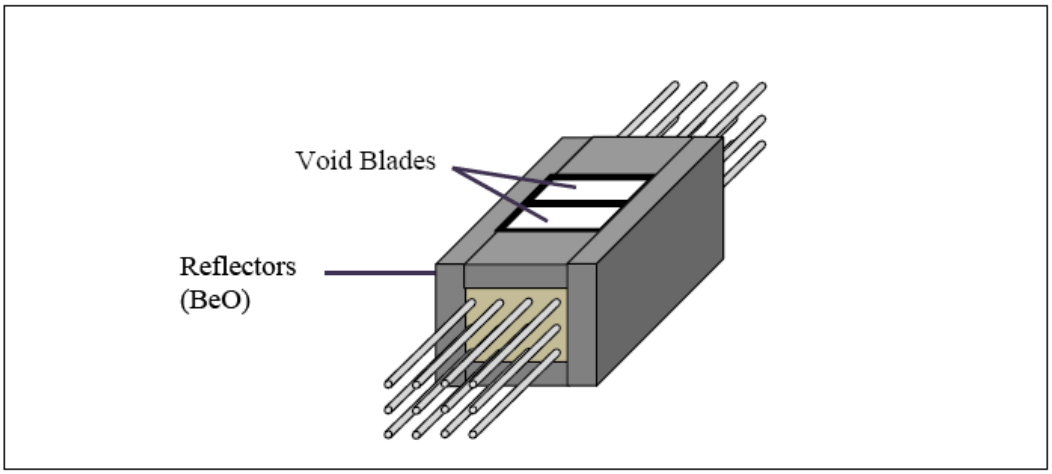


Figure 35 Schematics of the safety preferred reference design

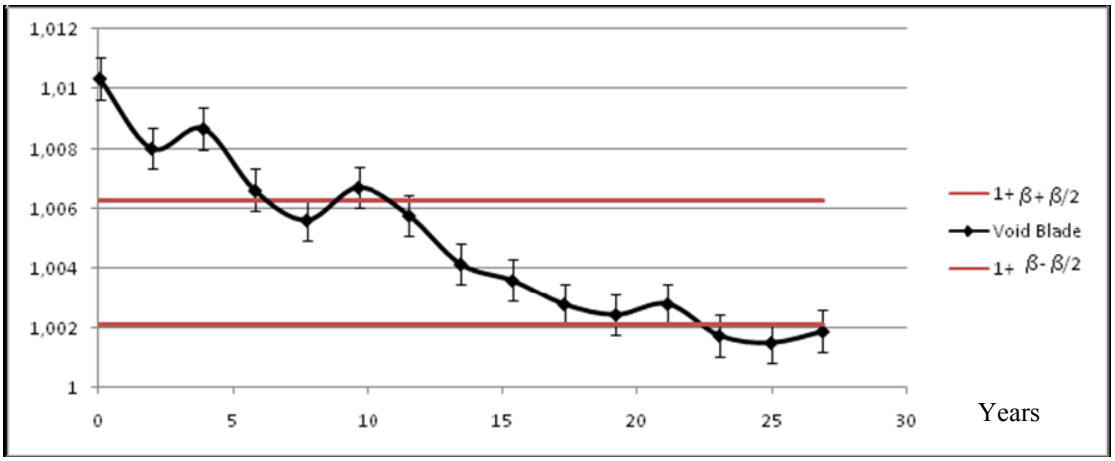


Figure 36 Evolution of $k_{eff}$ of a split HP-ENHS core with a two 10 cm voided blade; 22.9% TRU

One central blade along with the two side reflector slabs replaced by $B_4C$ slabs are sufficient to bring the multiplication factor down to 0.95, as illustrated in Figure 37.

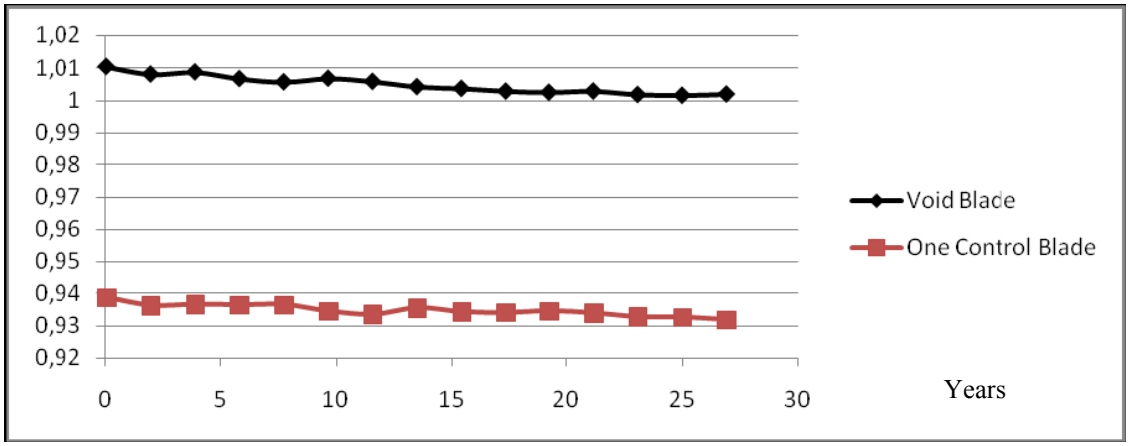


Figure 37 Multiplication factor in Normal and Shutdown configurations

# 6. THERMAL HYDRAULIC ANALYSIS

## *6.1 Introduction*

The first feasibility issue addressed in this part of the work is whether or not it is possible to remove the core power carried out by the heat-pipes by naturally circulating intermediate coolant using heat exchanger of reasonable dimensions and riser of reasonable height. The heat exchanger dimensions of primary interest in the maximum required length of the condenser part of the heat-pipes (See Figure 2). Additional objectives of this part of the study are to select the optimal fluid for the intermediate coolant, to minimize the total reactor vessel height, and come up with an overall HP-ENHS module layout and dimensions when using water that drives a Rankine cycle for the energy conversion system. This first-round of thermal-hydraulic design study is summarized in Section 6.3, following a brief review, in Section 6.2, of the candidate fluids considered for the intermediate coolant. Section 6.4 performs a design optimization of the intermediate cooling system, including the heat exchanger dimensions, using Flibe for the intermediate coolant and supercritical carbon dioxide (S-$CO_2$) for the thermodynamic working fluid. The feasibility for passively removing decay-heat from the HP-ENHS core is addressed in Section 6.5. The latter two studies are on-going beyond the termination of this NEER project and will be reported upon separately.

## *6.2 Candidate Fluids for Intermediate Coolant*

Three fluids were considered for the intermediate coolant: lead-bismuth, sodium and the molten-salt LiF-$BeF_2$ (also referred to as Flibe). Table 7 compares selected thermo-physical properties of the three coolants (the properties of Pb-Bi are very similar to those of Pb) as well as of two other fluids commonly used or considered as reactor coolants – water and helium. Of these, the Flibe was preferred because it can operate at significantly higher temperatures than either Na or Pb-Bi and enables designing a more compact natural circulation system and, hence, the most compact reactor vessel. The Na maximum acceptable operating temperature is limited by the relatively low boiling temperature, as we did not want to pressurize the vessel in order to avoid boiling. The Pb-Bi operating temperature is limited by corrosion of structural materials to around 600$^{o}$C.

The water and helium coolants are included in the table for comparison purpose only; they were not considered as candidate coolants for the HP-ENHS.

Table 7 Selected Thermo-Physical Properties of Reactor Coolants

| Material | $T_{melt}$ °C | $T_{boil}$ °C | $\rho$ kg/m$^3$ | $\rho c_p$ kJ/m$^3$C | K W/m$^2$C |
|---|---|---|---|---|---|
| $^7Li_2BeF_4$ (Flibe) | 459 | 1,430 | 1,940 | 4,540 | 1.0 |
| Sodium | 97.8 | 883 | 790 | 1,000 | 62. |
| Lead | 328 | 1,750 | 10,540 | 1,700 | 16. |
| Helium (7.5 MPa) | — | — | 3.8 | 20 | 0.29 |
| Water (7.5 MPa) | 0 | 100 | 732 | 4,040 | 0.56 |

Particularly large is the high volumetric heat capacity of Flibe that allows for a more compact equipment design than is possible with either sodium or Pb. The boiling point of Flibe is greater than 1300ºC allowing operation at very high temperatures leading to high system efficiencies. Optical inspection is possible with Flibe that is transparent. The heat transfer capabilities of Flibe make it an excellent coolant as well. Flibe also has a low vapor pressure and offers the possibility of using redox buffers to maintain a highly reducing environment in the salt leading to a very low corrosivity of structural materials [9]. Another advantage of Flibe that makes it particularly useful for the HP-ENHS is its large change in density with temperature allowing for good natural circulation.

Molten salts usage was first attempted in the United States with the Aircraft Nuclear Propulsion Program and the Molten Salt Breeder Reactor Program in the 1950s and 1960s. Later, the Aircraft Reactor Experiment (ARE) showed that the use of Inconel with molten salts was not viable because of corrosion problems. Hastelloy N is a much better choice for molten salts [9]. The fluorine molten salts such as Flibe are a combination of very electropositive metals and a very electronegative element (F). Thus, corrosion is not an issue as long as a compatible alloy such as Hastelloy N is used for the container material.

### *6.3 Design Optimization With Water as the Thermodynamic Working Fluid*

The goal in designing the intermediate coolant loop was to create a system that can: (a) remove all heat from the core, (b) operate via natural circulation, (c) maximize average coolant outlet

temperature, and (d) minimize system size. Since coolant temperature and system size depend on one another there is a tradeoff between satisfying goals (c) and (d).

6.3.1 Hydraulic Analysis

By first assuming that the intermediate coolant is able to remove all heat from the heat pipe heat exchanger, it is possible to uniquely determine the coolant flow rate in the system. This is done by balancing the head losses in the system due to flow resistance with the buoyant head available [42-48]:

$$\Delta P = gH\left(\rho(T_1) - \rho(T_2)\right) = K_L \frac{\rho_{\text{ave}} V_{\max}^{\ 2}}{2}$$

$\Delta P$: total head gain/loss

$g$: acceleration due to gravity (9.81 m/s$^2$)

$H$: Thermal separation distance (m)

$\rho(T_1)$, $\rho(T_2)$: coolant densities at the inlet (cold) and outlet (hot) temperatures (kg/m$^3$)

$K_L$: Loss coefficient for the flow path (unit less)

$\rho_{\text{ave}}$: coolant density at the average temperature (kg/m$^3$)

$V_{\max}$: maximum coolant flow rate in the flow path (m/s)

The coolant temperature change and the coolant flow rate are also related to the core thermal power by conservation of energy:

$$\Delta T = \frac{Q}{\rho_{ave} c_p G}$$

$\Delta T$: coolant temperature change (K)

$Q$: System thermal power (125 MW)

$\rho_{\text{ave}}$: coolant density at the average temperature (kg/m$^3$)

$c_p$: coolant heat capacity (J/kg-K)

$G$: coolant volumetric flow rate (m$^3$/s)

By simultaneously solving the above two equations, one can determine the coolant temperature change and flow rate for a given flow geometry and set of coolant properties. The loss coefficient $K_L$ is estimated by treating the coolant flow path as a series of simpler components. For our proposed 125 MWt design using a LiF-$BeF_2$ coolant, the loss coefficient $K_L$ is

conservatively calculated as 33.1, yielding a coolant flow rate of 0.25 m³/s. This corresponds to a maximum coolant velocity through the heat pipe heat exchanger of 0.29 m/s.

### 6.3.2 Flow Rate Optimization

According to the pressure drop equation above, minimizing the system loss coefficient maximizes the coolant flow rate. This is desirable because it improves heat transfer to the coolant and reduces the change in coolant temperature. A way to minimize the loss coefficient is to vary the area available to the riser and steam generator at the top of the module. Having too small a riser or steam generator area increases the flow velocity and flow resistance in that component, as illustrated in Figure 38. The optimal flow resistance is achieved for a riser area corresponding to approximately 14% of the total vessel cross section.

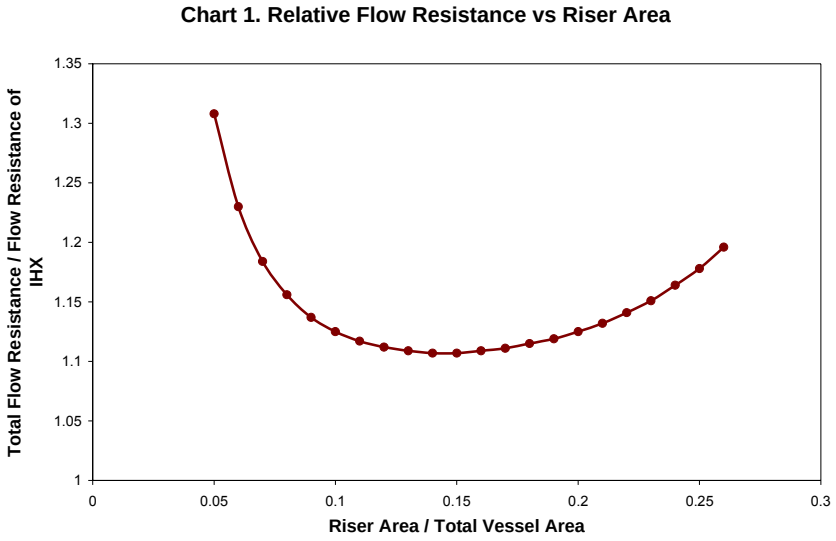


Figure 38 Relative flow resistance vs. riser area

### 6.3.3 Thermal Analysis

Given a coolant flow rate it is possible to determine the Nusselt number and heat transfer coefficient for the coolant in the heat pipe heat exchanger. This is done using the following correlation, given in Incropera & Dewitt [42]:

$$\mathrm{Nu} = C * \mathrm{Re}_{D,\max}^{m} * \mathrm{Pr}^{0.36} \left( \frac{\mathrm{Pr}}{\mathrm{Pr}_s} \right)^{1/4}$$

The Nusselt number is converted into the heat transfer coefficient using the hydraulic diameter of the heat exchanger. This coefficient can be combined with the conductive thermal resistance in the heat pipe wall to yield a total heat transfer coefficient *h*. With this heat transfer coefficient, it is possible to determine that maximum coolant temperature that allows full removal of heat from a heat pipe, via the relation:

$Q_{HP} = h\pi DL_{Eff}\left(T_{HP} - T_c\right)$, in which

$Q_{HP}$: Heat pipe power
$D$: Heat pipe diameter (1.56 cm)
$L_{eff}$: Heat pipe effective length (must be less than actual heat pipe length)
$T_{HP}$: Heat pipe operating temperature (1300K)
$T_C$: Coolant temperature

The maximum coolant temperature can be found by substituting the heat pipe effective length with its maximum value; the actual length of the heat pipe. This can be taken to be the coolant exit temperature. Effects due to non-uniform heat transfer along the heat pipe are determined to increase this maximum temperature, so the result obtained with this method is conservative. Together with the coolant temperature change determined via ΔT equation above, this determines the average temperature of the intermediate coolant. The non-uniform power distribution of the core introduces some uncertainty that is conservatively treated by adjusting these temperatures downward by 0.3 times the coolant temperature change. For the proposed design the average coolant temperature is calculated to be 1040 K and the maximum coolant temperature is 1096K.

### 6.3.4 System Volume Optimization

The results of the above calculations depend on the specific geometry assumed, and therefore depend on the length of the riser and length of the heat pipes. Because the average coolant temperature is a stronger function of heat pipe length, it turns out that system volume can be optimized by using the shortest riser possible then adjusting the heat pipe length to produce a desired coolant temperature or size. Our proposed design uses a thermal separation distance (distance between the mid-plane of the core and the mid-plane of the active steam generator

region) of 4.89 meters, and the heat pipes extend 52.5 cm from the core. This heat pipe length was selected to make the module radius 2 meters, similar to that of the ENHS.

### 6.3.5 Preferred Design

It was found feasible to effectively transfer the core power from the heat-pipes to the energy conversion system by natural circulation. The required length of the condenser part of the heat-pipes is approximately 50 cm and the required riser height is only approximately 5 m. As a result, the required HP-ENHS reactor vessel height is significantly smaller than that of the reference ENHS: 9 vs. ~20 m. The vessel diameter is slightly larger: 4 vs. ~ 3.5 m. Figure 40 gives the dimensions of the resulting HP-ENHS design.

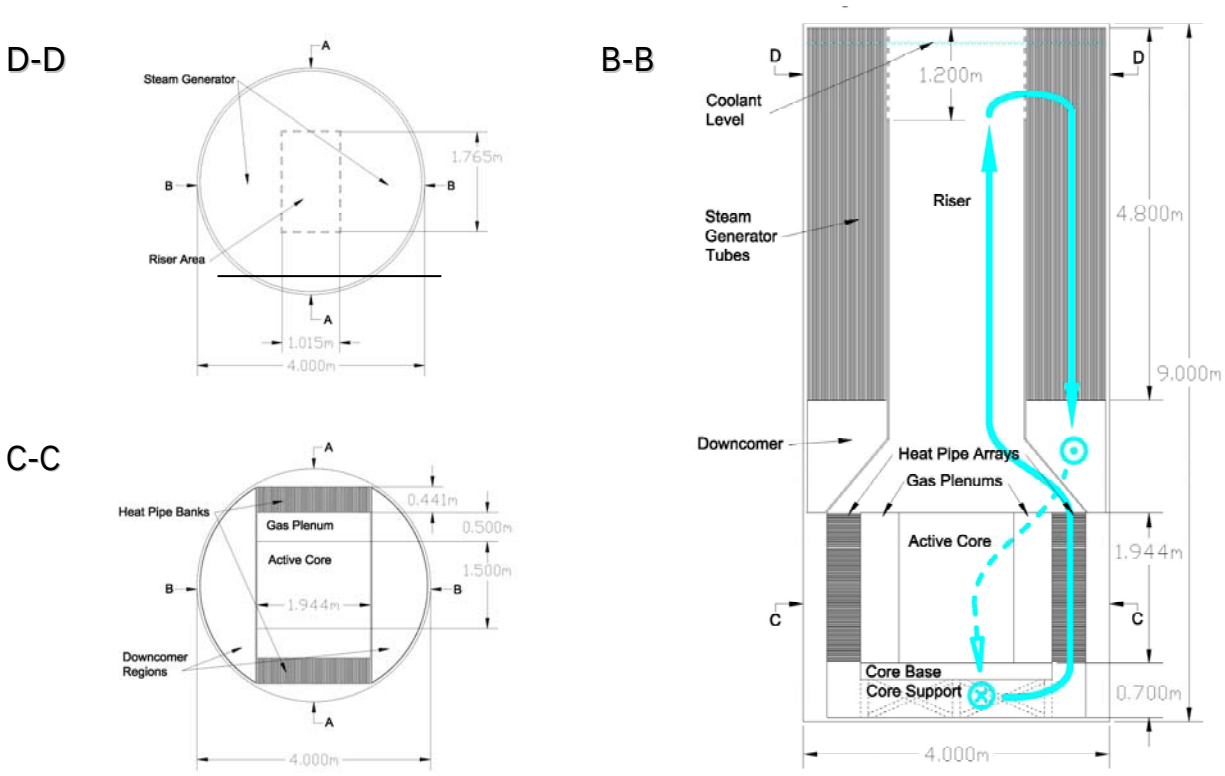


Figure 39 Dimensions of the HP-ENHS reactor

Molten salt, such as LiF-$BeF_2$, was found the preferred intermediate coolant. Using conservative assumptions it was found that the average intermediate coolant outlet temperature is 1040K. This is a significantly higher than ~775K intermediate coolant outlet temperature of the reference

ENHS design, and is achieved using a significantly more compact ENHS module and smaller reactor volume.

### *6.4 Design Optimization With S-$CO_2$ as the Thermodynamic Working Fluid*

This design study is still on-going by graduate student Steven Mullet. It is not funded by the NEER contract. The summary of this study will be published by the end of 2008.

### *6.5 Decay Heat Removal Capability*

This design study is still on-going by graduate student Steven Mullet. It is not funded by the NEER contract. The summary of this study will be published by the end of 2008.

# 7. ADVANCED ENERGY CONVERSION SYSTEM[2]

## *7.1 Introduction*

A conventional Rankine steam cycle was assumed (Section 6.3) for the energy conversion system in the preliminary feasibility assessment of the HP-ENHS reactor concept. A Rankine steam cycle is, however, not a good fit for a high temperature heat source. A supercritical $CO_2$ (S-$CO_2$) cycle is recently being advocated [49, 50] for GENERATION-IV reactors that can deliver their fission heat at above 500ºC. The HP-ENHS has a high outlet temperature, approximately 770 ºC, which makes it more than sufficient to be coupled with the S-$CO_2$ cycle. The primary advantages of the S-$CO_2$ over a Rankine steam cycle are higher energy conversion efficiency and greatly more compact hardware. The primary disadvantage of the S-$CO_2$ technology is the relatively high pressure it requires – exceeding 20 MPa.

The main advantage of the S-$CO_2$ cycle relative to a He Brayton cycle is that it has a reduced compression work since S-$CO_2$ operates near the critical point of $CO_2$, which has lower compressibility. However, the non-ideality of $CO_2$ also brings disadvantages as well – the specific heat, which affects the recuperator, varies widely. For certain cycle operating conditions a pinch-point exists in the recuperator. The pinch-point is the location in the recuperator with the lowest temperature difference between the hot and cold $CO_2$ streams, with the limit being zero [50]. The temperature difference between the hot and cold fluid in the recuperator varies greatly because of the temperature and pressure dependence of the specific heat. So the minimum difference in temperature does not always occur at the recuperator inlet or outlet, but sometimes within the recuperator. The irreversibility of the recuperator, resulting from the pitch-point phenomenon, causes the largest reduction in the efficiency of the S-$CO_2$ cycle [49].

However, the use of a combined cycle improves efficiency greatly. The combined cycle incorporates either recompression or pre-compression. The most efficient and simple of these cycles is the recompression cycle. This cycle is now briefly described.

[2] The work reported in this section was performed by an HP-ENHS design team consisting of Michael Levy, Steve Mullet, Thien-An Nguyen and David Simon as an NE-167 Nuclear Safety Project taught by Prof. Kastenberg. The team was co-advised by Prof. Greenspan.

### *7.2 Recompression Cycle*

Figure 40 is a layout of the recompression cycle and Figure 41 is a T-S diagram of this cycle. This cycle improves efficiency by decreasing the amount of heat rejected by using a recompressing compressor before the precooler. The mass flow is split before entering the precooler, with only part of the heat rejected with the flow. The outlet of the recompressing compressor is between the high and low temperature recuperator. The working fluid is first compressed in the main compressor (points 1-2). Then it is preheated in the low temperature recuperator (point 2-3) to reach the outlet temperature of the recompressing compressor. The working fluid is then merged with the outlet fluid from the recompressing compressor (point 3). The merged fluid is heated in the high temperature recuperator (point 3-4), which then enters the reactor. The fluid emerging from the reactor enters the turbine (points 5-6) at the highest temperature in the cycle. Fluid expansion in the turbine is doing the work that generates electricity. The fluid emerges from the turbine and transfers heat to the cooler high pressure fluid first in the high temperature recuperator (point 6-7) and then in the low temperature recuperator (point 7-8). The fluid is split before going into the precooler. One part of the fluid is compressed in the recompressing compressor (point 8-3) and the other part is cooled in the precooler (point 8-1), which then flows into the main compressor [49].

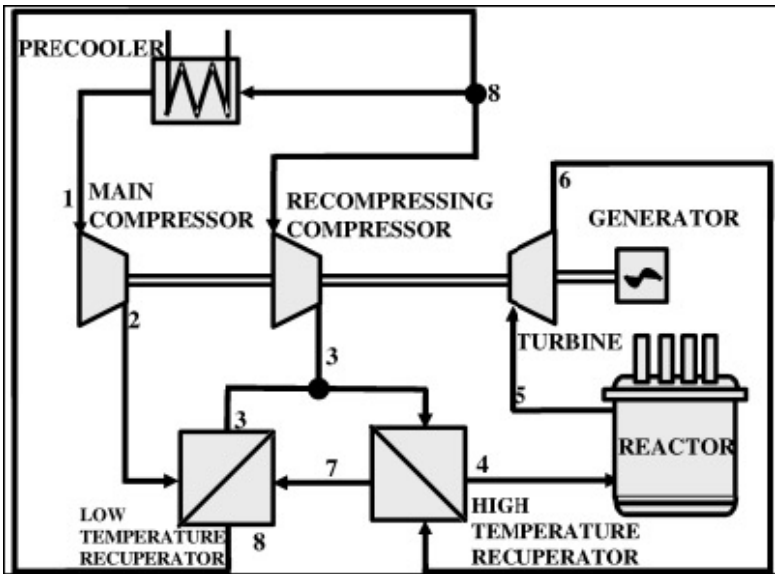


Figure 40 S-$CO_2$ recompression cycle layout [50]

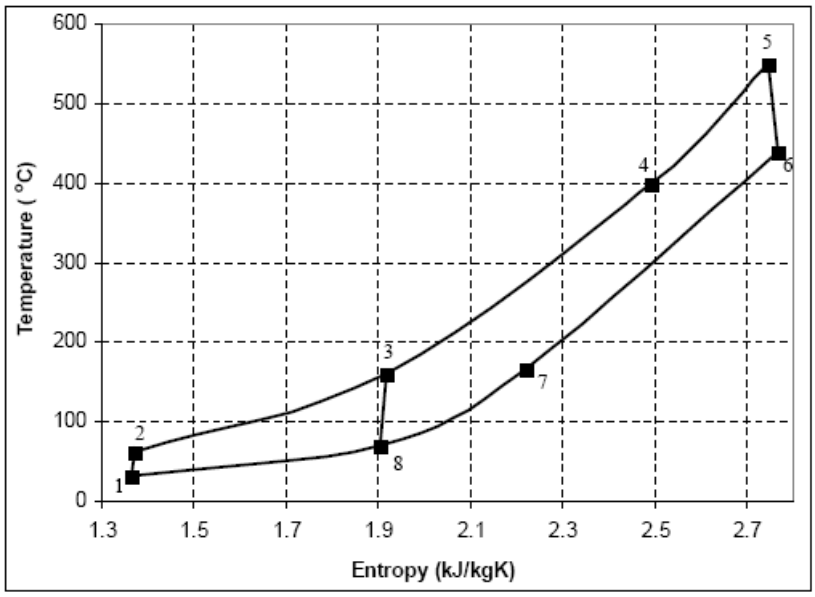


Figure 41 Temperature vs. entropy diagram of recompression Brayton cycle [49]

Care has to be taken in the layout design such that the minimum cycle operating temperature is not below 30.98 ºC, which is the critical temperature of $CO_2$. Below this temperature, condensation will occur. In ideal Brayton cycles, decreasing the turbine inlet temperature will increase the cycle efficiency. However, this is not the case in S-$CO_2$ cycle because it operates near the critical point.

### *7.3 Indirect Cycle*

The cycle shown in Figure 49 and discussed in Section 7.2 is a direct cycle. A direct cycle is the most efficient from an electricity generation point of view, since there is no enthalpy loss associated with the transfer of heat from the intermediate to the secondary loop. Indirect cycles also increase the complexity of the plant layout and the plant's cost. Nevertheless, an indirect cycle is selected for the HP-ENHS reactor as it offers several important advantages: (1) The intermediate Flibe coolant can deliver the high temperature heat at, practically, atmospheric pressure and by natural circulation, thus greatly simplifying the reactor vessel design and enhancing the reactor safety. LOCA initiators for reactor vessel depressurization are far less frequent and severe. (2) Indirect cycle greatly reduces radiological hazards. The turbine plant is not contaminated by failed fuel or the transport of corrosion products. There are no $^{16}N$ contaminations due to $^{16}O(n,p)^{16}N$ reactions from $CO_2$. (3) Reheat can be used to enhance the

indirect cycle efficiency [49]. This option does not exist for a direct cycle because it is impractical to reheat inside the core. Figure 42 is a layout of the indirect cycle with one stage of reheat.

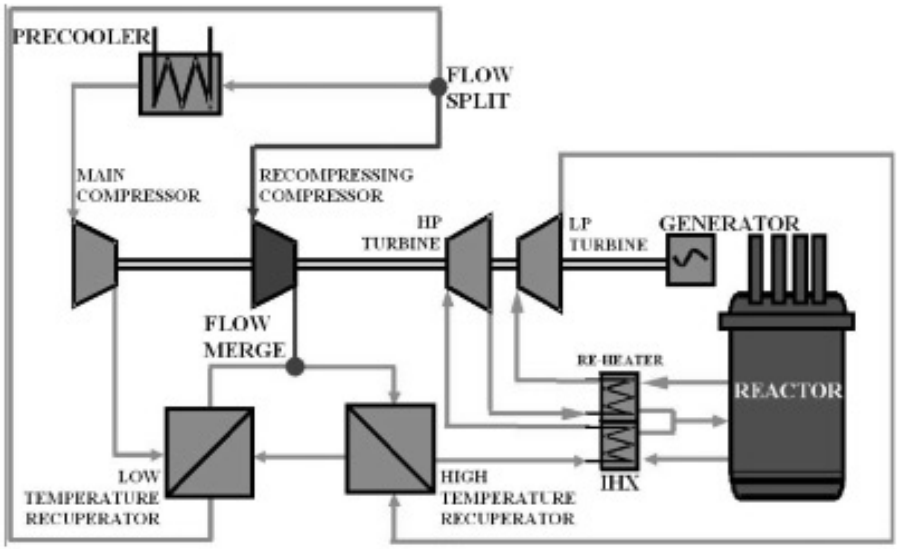


Figure 42 Recompression cycle with one stage of reheat [50]

The S-$CO_2$ indirect cycle was studied by Dostal using lead alloy as the primary coolant [49]. The results from Dostal's study can be applied to the HP-ENHS reactor that uses molten salt rather than lead for the intermediate coolant. Reheating was found [49] to be uneconomical because the efficiency increase it offered, shown in Figure 43, did not compensate the extra costs associated with the additional required heat exchanger (reheater).

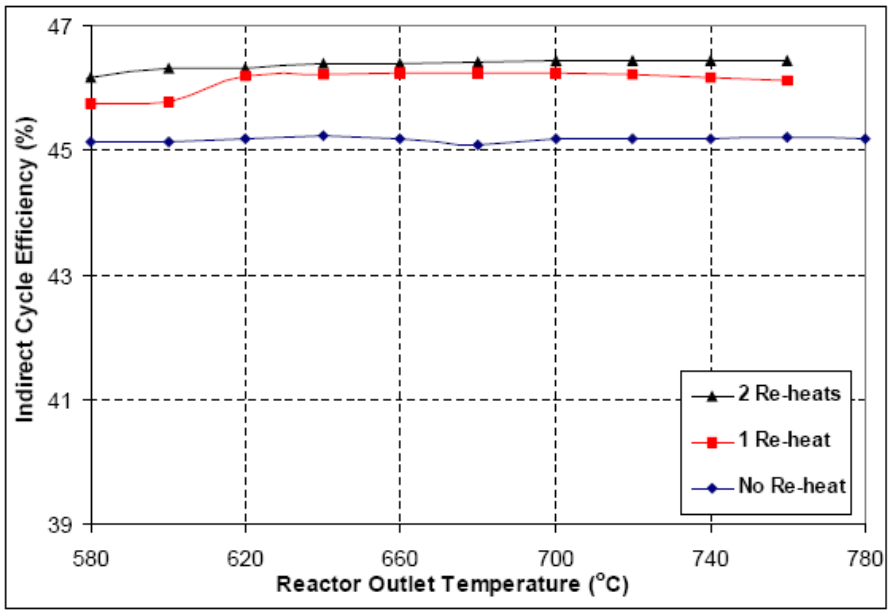


Figure 43 S-$CO_2$ cycle efficiency for different number of reheaters [49]

### *7.4 Power Control Scheme for Recompression Cycle*

The control of power output of the cycle is of major importance to the success of the cycle. Only control schemes relating to power level changes are considered in this project. Further studies need to be done on controls of the S-$CO_2$ in the events of accidents. In order for the cycle to remain as simple as possible, a single shaft is used. With a single shaft, the cycle is more capable of dealing with the loss of load transient. Further, the generator can be used as a start-up motor in the case of single shaft layout. However, the system is more constrained because the compressor can only run at speeds synchronized with the grid.

The goal of power control is to maintain high efficiencies over a wide range of power levels. An ideal approach to S-$CO_2$ cycle power controls can offer a lot of insight. Cycle efficiency is defined as

$$\eta = \frac{W_{net}}{Q_{in}}$$

where η is the cycle efficiency, $W_{net}$ is the net work (turbine work minus compressor work), and $Q_{in}$ is the thermal power. The net work $W_{net}$ can be defined as

$$W_{net} = \dot{m} c_p T_{cin} [(\eta_t \frac{T_{tin}}{T_{cin}} - \frac{r_p^{\frac{\gamma-1}{\gamma}}}{\eta_c})(1 - \frac{1}{r_p^{\frac{\gamma-1}{\gamma}}})]$$

The thermal power, $Q_{in}$ is defined as

$$Q_{in} = n_t \dot{m} c_p T_{tin} (1 - \frac{1}{r_p^{\frac{\gamma-1}{\gamma}}})$$

The recuperator is assumed to be 100% effective. From the second equation, the net work is dependent on the mass flow rate, turbomachinery efficiency, pressure ratio, inlet turbine temperature and inlet compressor temperature. The plant efficiency η depends on all of the mentioned parameters except the mass flow rate. This suggests that the control parameter for power control should be the mass flow rate because efficiency is independent of it while power is directly proportional to it. Thus, by varying the mass flow rate, the power can be adjusted while keeping the efficiency the same. Mass flow rate control is the most attractive form of control for closed gas turbine cycle, even for real systems like S-$CO_2$ [49].

One method to control the mass flow rate is by using by-pass control to adjust the mass flow rate across the turbine. Figure 44 offers possible locations of placing bypass and throttling valves. Discussion of throttling valves will be visited. The location of bypass valves must be made carefully to minimize the effect on the cycle operating temperature [50]. There are two possible locations in the cycle that can accomplish this requirement. One is to place the bypass valve after the recompressing compressor and merge it to the high temperature recuperator outlet (Valve A in Figure 44). The second option is to place the bypass valve before the reactor inlet and merge it with the turbine outlet (Valve B in Figure 44). It is easier to locate the bypass valve at point B from a plant design point of view, but this is more challenging from a materials viewpoint because it operates at higher temperature [49].

Bypass control works by forcing the turbine to operate away from its design point, which will affect its efficiency and pressure ratio. However, bypass controls create complications at the

compressor. There are two compressors operating in parallel in the cycle and their flow split must be constant to provide the required pressure ratio. The flow split is a function of high and low pressure. Real gas properties are different at different pressure, which means that there are different requirements for recompression. Normally, in an ideal situation, a throttling valve is placed on the inlet compressor (Valves C and D in Figure 44) to increase pressure ratio across the compressor through its pressure drop. However, for a realistic S-$CO_2$ cycle the throttling valve location does not work at Point C and D because of the need to keep the flow split constant. Another option is to place the throttling valve at the high temperature recuperator inlet and adjust the pressure to the original value (Valve E in Figure 44), which will make the flow split constant between the two compressors [50].

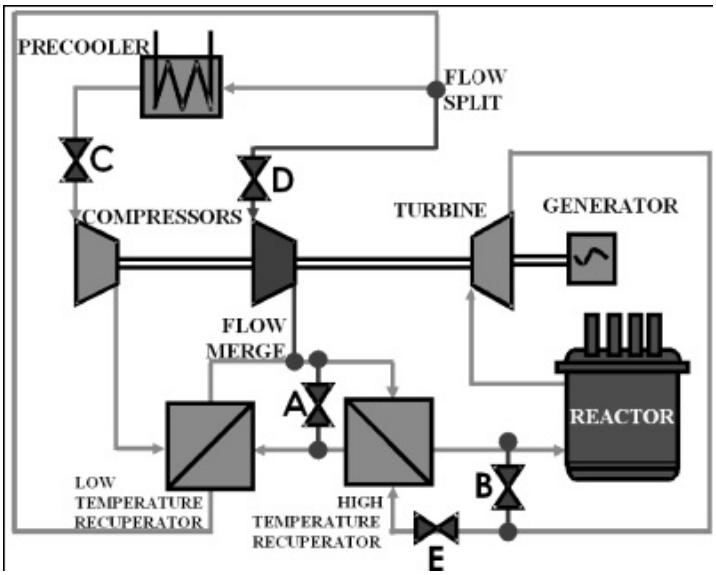


Figure 44 Possible locations of bypass and throttling valves [50]

Through the use of bypass control there is a decreasing linear relationship between efficiency and decreasing power. The S-$CO_2$ recompression cycle is best to use for base-load operation, which is the case for nuclear power plants. Figure 45 shows the relationship between cycle efficiency and decreasing power through the performance of bypass control [49]. Figure 46 shows the recompressed fraction for both cases of throttling and the bypass mass flow rate as a function of power level [49].

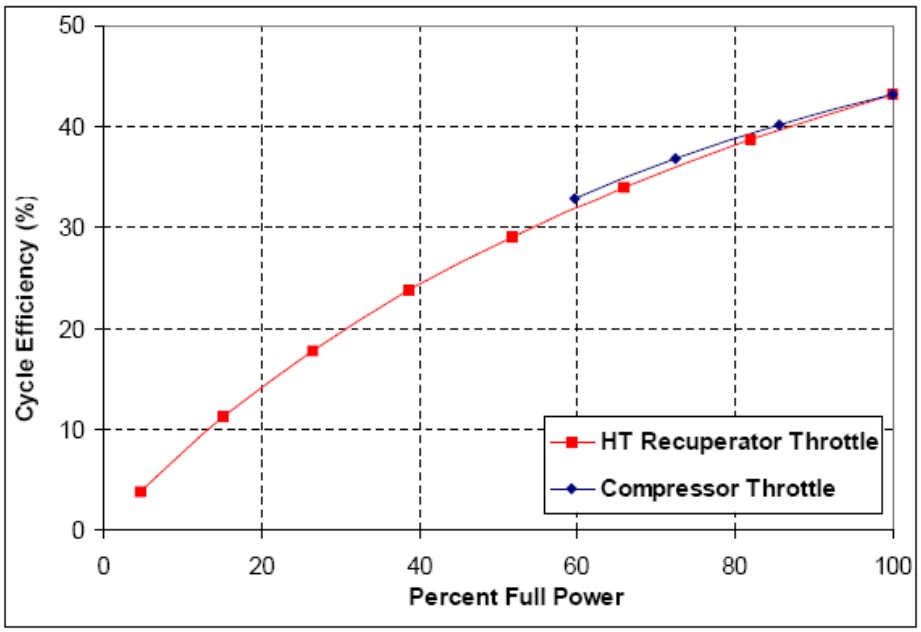


Figure 45 Bypass control performance [49]

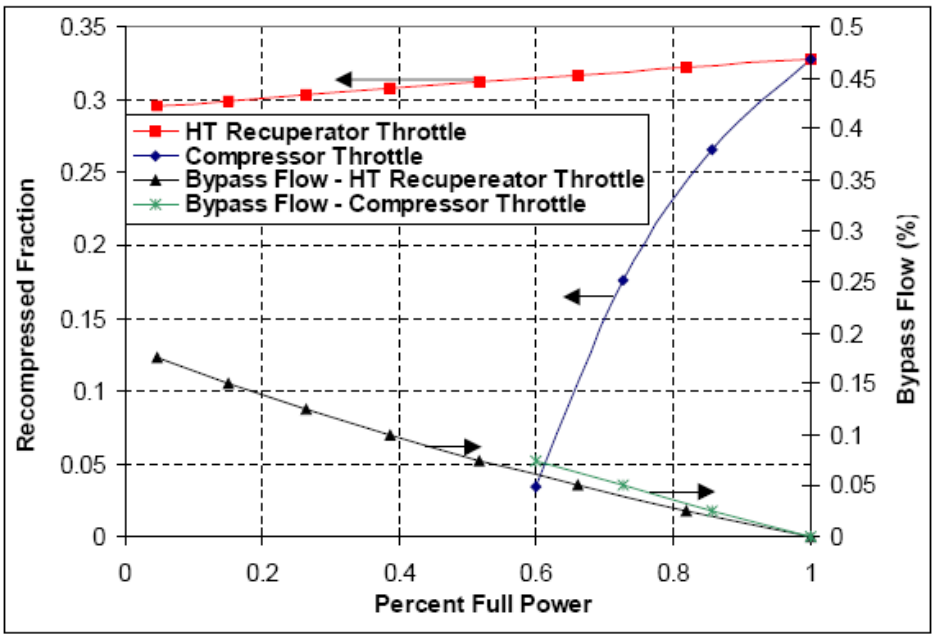


Figure 46 Recompress fraction and bypass flow [49]

### *7.5 Drawbacks of the S-$CO_2$ Cycle*

There are several disadvantages of the S-$CO_2$ cycle. In contrast to the helium Brayton cycle, increasing turbine inlet temperature does not increase efficiency. Attention must be given to the design of the precooler and heat sink. The S-$CO_2$ optimizes around a small difference in temperature between the small heat source inlet and outlet. Efficient recuperators are required because of the narrow operating temperature range. The emergence of the printed circuit heat exchangers (PCHE) from HEATRIC around 1990 made possible highly efficient and compact recuperators that can be used in the S-$CO_2$ cycle. If it were not for this particular technology, the compact design of the S-$CO_2$ would be cumbersome and uneconomical because of bulky heat exchanger technology [50].

Furthermore, $CO_2$ is more corrosive than inert helium, but less corrosive than steam and water. However, there is operating experience with $CO_2$ at the British AGR unit that indicates that the corrosion of $CO_2$ is not harmful to the development of $CO_2$ power conversion in the temperature range of 550 to 650 ºC [50]. However, more corrosion studies need to be conducted for supercritical operating conditions of the S-$CO_2$ cycle.

The S-$CO_2$ cycle was once criticized for its high pressure operating range, which exceeds 20MPa. However, utilities have had experience with high pressure systems in the form of supercritical steam units with pressure greater than 25MPa. High pressure does not represent a challenge to the design of turbomachinery seals, rather it is the high pressure differential across the turbine stages [50].

In addition, the recompression S-$CO_2$ cycle lacks a simple and effective implementation of a high-efficiency part-load operation. However, nuclear power plants are economical in base load operation, which makes this S-$CO_2$ cycle deficiency not as critical to its potential as a power conversion unit.

# 8. PRELIMINARY SAFETY ANALYSIS[3]

## *8.1 Introduction*

The preliminary safety analysis addresses the following issues: how does this reactor meet the advanced reactor policy of the NRC (Sec. 8.2), the design basis accidents (Sec. 8.3), severe accidents (Sec. 8.4), probabilistic risk assessment (Sec. 8.5), and seismic safety (Sec. 8.6). A specific objective is to assess the feasibility of licensing the HP-ENHS at the Diablo Canyon site in California.

## *8.2 Advanced Reactor Policy*

The NPC-issued "Regulation of advanced nuclear power plants; statement of policy" (59 FR 35261) [51] gives guidelines for all advanced nuclear reactors. The HP-ENHS will meet these guidelines in the following ways:

1. "Highly reliable and less complex shutdown and decay heat removal systems. The use of inherent or passive means to accomplish this objective is encouraged (negative temperature coefficient, natural circulation, etc)" [51]

The HP-ENHS shuts down by means of control slabs introduced at the center of the split solid core (Section 5.5). The control slabs have multiple actuation methods, one of which is gravity. As long as the control slabs are able to move, the system can shut down safely.

The primary and intermediate loops responsible for the cooling of the HP-ENHS are designed to function as solely passive systems, with any active systems supplementing the passive systems but not replacing them. The primary cooling system, which is the heat pipes, contains no moving parts except for the sodium flowing within them due to natural convection. The intermediate molten salt loop that transfers heat from the heat pipes to the energy conversion system also functions by natural convection. Decay heat is removed through these systems, which are both very reliable and incredibly simple when compared to current reactors.

[3] The work reported in this section was performed by an HP-ENHS design team consisting of Michael Levy, Steve Mullet, Thien-An Nguyen and David Simon as an NE-167 Nuclear Safety Project taught by Prof. Kastenberg. The team was co-advised by Prof. Greenspan.

In addition, if the power conversion unit is not active, the reactor vessel auxiliary cooling system (RVACS) will be able to act as an ultimate heat sink for the decay heat. RVACS has been proven to be able to remove the decay heat from a similar reactor size [52, 53].

2. "Longer time constants and sufficient instrumentation to allow for more diagnosis and management before reaching safety systems challenge and/or exposure of vital equipment to adverse conditions" [51]

The reactor has a negative temperature coefficient of reactivity that enables to shut the reactor down even if the primary heat sink is lost. In addition, the molten salt has a very high heat capacity of 0.57 cal/g and a density during operation of roughly twice that of water and is present in large quantities, which greatly slows the speed of the temperature gain. In the case of loss of the primary heat sink the reactor temperature and reactivity in the ENHS oscillated slowly and returned to a steady state value [52, 53]. Further testing will need to be done to see if the HP-ENHS behaves in the same manner, or if the addition of heat pipes interferes with this accident moderation ability.

3. "Simplified safety systems that, where possible, reduce required operator actions, equipment subjected to severe environmental conditions, and components needed for maintaining safe shutdown conditions. Such simplified systems should facilitate operator comprehension, reliable system function, and more straightforward engineering analysis" [51]

The moving parts in the HP-ENHS are confined to valves, fans, and control slab actuation. With the exception of the one-way pressure valves in the molten salt overflow area, all of these parts are supplementary to a passive system having the same function and operating by natural circulation. In addition, the intermediate molten salt loop is not pressurized, so equipment that is in containment will not be subject to harsh environmental conditions if the molten salt were to heat up. Also, the core is designed to maintain a nearly constant $k_{eff}$ breeding as much fissile fuel as is fissioned. This reduces the usage of the control slabs throughout the life of the reactor.

Heat pipes, control slabs, molten salt, and RVACS are the only systems needed for safe shutdown. The compressors for the circulation of the S-$CO_2$ could all fail to operate without hampering safe shutdown.

Since the reactor is designed to operate with very small burnup reactivity swing, operator actions are very limited. Operators are needed for the initial startup and final shutdown, but have little required actions between these times while the reactor is functioning correctly.

4. "Designs that minimize the potential for severe accidents and their consequences by providing sufficient inherent safety, reliability, redundancy, diversity, and independence in safety systems" [51]

The greatly simplified design of the HP-ENHS reduces potential types of severe accidents. The intermediate molten salt loop cannot have a LOCA except in the case of a reactor pressure vessel failure. The loss of the heat sink was discussed above as being handled by the passive systems. The control slabs can be operated in a number of different ways.

The HP-ENHS has a solid core design and has no positive void coefficient of reactivity. The solid core avoids reactivity increases due to fuel rod motion during earthquakes, and the negative temperature coefficients protect the core from going critical due to a failure of heat pipes .

5. "Designs that provide reliable equipment in the balance of plant (BOP) (or safety-system independence from the BOP) to reduce the number of challenges to the safety systems" [51]

Backup batteries are used to ensure power in the case of a loss of offsite power and plant generating capabilities. In addition, all of the passive safety systems are independent of the balance of plant and offsite power so a safe shutdown can occur should all forms of electricity fail.

6. "Designs that provide easily maintainable equipment and components" [51]

The HP-ENHS generator and core are separate entities. The core is not to be refueled; it is to be replaced as a whole after its twenty years of life. The feasibility of online maintenance is undetermined as of yet.

7. "Designs that reduce the potential radiation exposures to plant personnel" [51]

Plant personnel will not be handling fuel in the HP-ENHS. The fuel is to be loaded in the factory and the core is to be shipped as a whole in a sealed container. Likewise for the discharged core –

it will be shipped to a spent-fuel processing center in a sealed and shielded shipping cask. As there are no moving parts inside the reactor vessel, except for the control blades drive mechanism (that are located at the upper part of the vessel, well shielded from the core by several meters of liquid salt and structure), and as there are no safety systems (except for the control blades and their drive mechanism) to maintain, very little exposure to personnel is expected.

8. "Designs that incorporate defense-in-depth philosophy by maintaining multiple barriers against radiation release and by reducing the potential for and consequences of severe accidents" 51]

Radioactive materials must go through many barriers to get to the environment. First, they must leave the solid core and get into the secondary coolant. This is much less probable to happen in the solid core HP-ENHS than in conventional core designs in which the clad of each fuel rod is surrounded by the coolant. The HX and the reactor vessel provide additional barrier, as in many other reactor designs.

9. "Design features that can be proven by citation of existing technology or that can be satisfactorily established by commitment to a suitable technology development program" [51]

Heat pipes are used currently for a variety of applications related to the movement of thermal energy, including cooling computer components and transferring solar heat. Work still needs to be done on heat pipe performance in a reactor environment, but Los Alamos and Argonne National Laboratories both have heat pipe research programs. As of yet, no reactors exist that use LiF-$BeF_2$ as an intermediate loop. Like the heat pipes, the use of this molten salt is being explored in various labs around the world.

### *8.3 Containment/Confinement*

The HP-ENHS will use a confinement system in place of the traditional containment system. High temperature gas-cooled reactor designers have proposed a method of confinement called the vented lower-pressure containment (VLPC). The VLPC is at ambient pressure and is approximately two orders of magnitude worse at preventing dose release than a conventional containment structure. The HTGR designers claim that the construction of the pebble fuel greatly

decreases the ability of the fission products to escape into the containment structure. The multiple barriers to fission product release in the HP-ENHS along with the fact that the intermediate loop is not radioactive, lead us to believe that a confinement structure would be possible. Such a structure would reduce the cost of the reactor and make it a more viable competitor in the energy market.

The NRC has developed rough guidelines for dealing with confinement structures, which are contained in SECY-04-0103 attachment 2 [54]. These guidelines suggest a functional performance standard that requires that the entire plant system keep the dose under the limits for release. The functionality of the containment for a non-LWR system is measured by the following six measures:

1. "Reducing radioactive releases to the environment
2. Preventing or limiting potential core damage
3. Removing heat to mitigate accident conditions and prevent vital equipment from exceeding design and safety limits
4. Protecting vital equipment from internal and external events
5. Protecting onsite workers from radiation
6. Providing physical protection (i.e., security) for vital equipment" [54].

In addition, there are preliminary metrics in the form of a series of questions for deciding if a confinement building is acceptable:

- "Does the option adequately accommodate all containment building system functions (e.g., are there potential adverse effects on plant safety, event consequences, or other containment building system functions)?" [54]

Function 1: The main barriers to radioactive release are the solid fuel, fuel cladding, heat pipe cladding, and solid core structure. In addition to these, the molten salt is present in large quantities and acts as a barrier. The reactor vessel provides an additional barrier. A confinement structure would not impact these barriers.

Function 2: Neither containment nor confinement building will prevent or limit potential core damage.

Function 3: The heat removal capabilities of the RVACS will not be affected by the drop in internal pressure, as it relies on outside air.

Function 4: The HP-ENHS has much less vital equipment relative to LWRs and even most other GENERATION-IV reactor designs since its safety depends on passive safety features such as natural circulation. If needed, the vital equipment could be protected by an additional barrier.

Function 5: Onsite workers do not have to handle fuel and do not have to maintain activated equipment.

Function 6: Confinement provides complete coverage of the reactor site. The ability to monitor the personnel entering and leaving the site will not be diminished.

- "Would the option be expected to substantially improve plant safety by:
  - preventing certain types of accidents?
  - significantly reducing fission product release to the environment?
  - addressing known uncertainties?" [54]

The confinement option would improve plant safety in none of these things. However, confinement would also not worsen safety in any of these ways. Neither type of containment will prevent any accidents. The fission product release to the environment is handled by the HP-ENHS through barriers inherent to the fuel, heat pipes, intermediate loop and reactor vessel. The confinement has less ability to prevent fission products release, but the reactor is designed such that fission products are greatly reduced or eliminated before reaching this barrier. Unfortunately, the reactor is not developed enough to define the uncertainties. One goal for further research will be to develop a plant capable of using confinement.

- "Does the option account for plant risk (e.g., is it risk-informed, does it consider uncertainties)?"[54]

The plant will be designed with a confinement structure instead of a containment structure, so the plant risk should be factored into any dose release calculations.

- "Does the option provide flexibility to the designer in meeting the event consequence acceptance criteria (e.g., could it discourage innovation or accident prevention)?" [54]

A confinement structure provides the same or slightly lessened flexibility in meeting the event consequence acceptance criteria. Keeping dose below a certain limit can be accomplished with either the containment structure or the multiple fission product barriers. A confinement option requires that multiple fission barriers be present. However, the HP-ENHS design includes these barriers, leaving the net flexibility virtually unchanged.

### *8.4 Site Characterization*

The safety analysis is performed for the Diablo Canyon power plant site that is located on the southwestern part of the San Luis/Pismo structural block. The block is bounded by the San Simeon fault zone to the northeast, a diffuse zone of minor faults on the southwest, and by the Hosgri fault zone to the west-northwest. To the east of the site lies the San Andreas Fault. The site is equidistant from Los Angeles and San Francisco. The current minimum exclusion zone employed by the Diablo Canyon Power Plant is ½ mile in radius. There are no activities within the exclusion zone, nor public roads or railways. The Low Population Zone (LPZ) as described by 10 CFR 100 exists immediately surrounding the exclusion zone. The current LPZ used at the Diablo Canyon site is 6.2 miles. The LPZ has about 80 residents, with protective measures to be taken in the Emergency Plan in case of severe accidents [55]. The nearest population center is about 8.3 miles away. Figure 47 is a map showing the location of the Diablo Canyon site and the surrounding major faults.

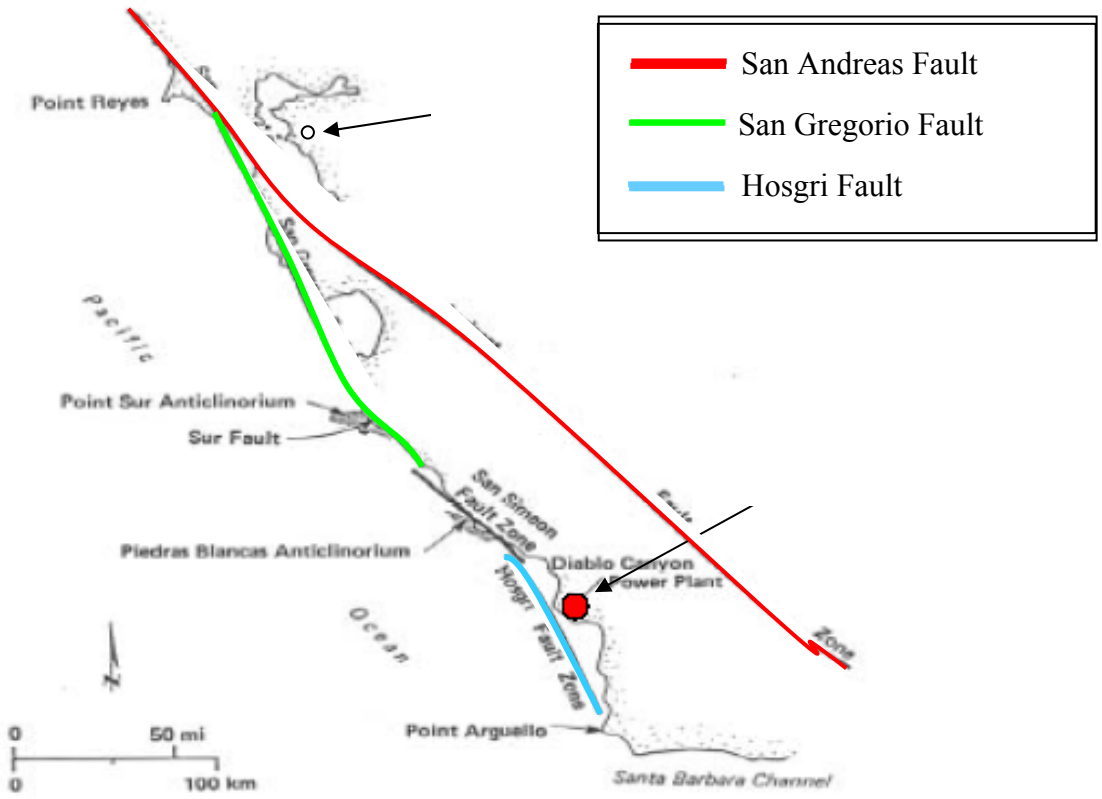


Figure 47 Diablo Canyon location and surrounding major faults

### *8.5 General design Criteria*

The design features of any nuclear plant must follow the general design criteria set forth in 10 CFR 50 Appendix A. These criteria are broken down into overall requirements, protection by multiple fission product barriers, protection and reactivity control systems, fluid systems, reactor containment, and fuel and radioactivity control. Before going into these requirements, a summary of the design features of the plant is provided in Table 8.

Table 8 Summary of Design Features of the HP-ENHS

| | |
|---|---|
| 1. Coolant Injection Systems | a. Reserve Flibe tank |
| 2. $CO_2$ Generator Heat Removal Systems | a. Power conversion systems |
| 3. Reactivity Control Systems | a. Control slabs |
| 4. Key Support Systems | a. DC power provided by 2-hour design basis station batteries. |
| 5. Containment Structure | a. Confinement building<br>b. Atmospheric pressure |
| 6. Containment Systems | a. RVACS air flow |

The HP-ENHS is still in the design phase. Many of the criteria in 10 CFR 50 Appendix A are for a fully designed reactor. As such, some general design criteria do not apply to the HP-ENHS reactor, and others do not apply to the scope of this report. Systems with applicable criteria are lacking in data to show compliance. This section will discuss the applicability of the criteria and what needs to be done to satisfy them. Each criterion mentioned will be in italics, and will be followed by its identifying number in the 10 CFR 50 Appendix A.

Criteria based around inspections and reports fall outside the scope of this report. This includes criteria *Quality Standards and Records* (1), *Inspection and Testing of Electrical Power Systems* (18), *Protection System Reliability and Testability* (21), *Inspection of Reactor Coolant Pressure Boundary* (32), *Inspection of Containment Heat Removal System* (36), *Testing of Emergency Core Cooling System* (37), *Inspection of Containment Heat Removal System* (39), *Testing Of Containment Heat Removal System* (40), *Inspection of Containment Atmosphere Cleanup Systems* (42), *Testing of Containment Atmosphere Cleanup Systems* (43), *Inspection of Cooling Water Systems* (45), *Testing of Cooling Water Systems* (46), *Capability for Containment Leakage Rate Testing* (52), *Provisions for Containment Testing and Inspection* (53), *Monitoring Fuel and Waste Storage* (63), and *Monitoring Radioactivity Releases* (64). In addition, only a single reactor is being licensed here, so *Sharing of Structures, Systems, and Components* (5) is not applicable. The control room and instrumentation for this reactor are not developed, so the following criteria cannot be shown to have been met: *Instrumentation and Control* (13) and *Control Room* (19). Criteria dealing with LWR systems that no longer exist in the HP-ENHS due

to the replacement of water with heat pipes at the primary coolant are: *Reactor Coolant Makeup* (33), *Emergency Core Cooling* (35), *Cooling Water* (44), *Systems Penetrating Containment* (54), and *Reactor Coolant Pressure Boundary Penetrating Containment* (55).

Criteria relating to the role of the containment and the containment spray pumps do not directly apply to the HP-ENHS as the coolants used are not pressurized so confinement will never be filled with vapors from the primary or intermediate loops. In addition the dose reduction from the core provides the necessary fission product release barriers, allowing for confinement instead of containment. The criteria that no longer apply due to the modified confinement are *Containment Design* (16) and *Containment Heat Removal* (38). The design criteria *Containment Atmospheric Cleanup* (41), *Containment Design Basis* (50), *Fracture Prevention of Containment Pressure Boundary* (51), *Primary Containment Isolation* (56), and *Closed Systems Isolation Valves* (57) are still valid and will be met in the final design.

Some criteria dealing with the reactor coolant system can be applied to the heat pipes. These are *Reactor Coolant Pressure Boundary* (14), *Reactor Coolant System Design* (15), *Quality of Reactor Coolant Pressure Boundary* (30), and *Fracture Prevention of Reactor Coolant Pressure Boundary* (31). Section 2.2 covers heat pipes and discuss the probability of heat pipes breaking. The heat pipes need further testing, but nothing in their design prevents them from achieving these criteria. *Reactor Design* (10), *Reactor Inherent Protection* (11), *Suppression of Reactor Power Oscillations* (12), *Control of Releases of Radioactive Materials to the Environment* (60), *Fuel Storage and Handling and Radioactivity Control* (61), and *Prevention of Critically in Fuel Storage and Handling* (62) are all related to the core design of the HP-ENHS. In particular, the modular construction of the core and the molten salt barrier should allow criteria 60 – 62 to be met, and the large heat capacity of the salt and the negative temperature coefficient of the core should allow 10-12 to be met.

The control slabs are the protection system in place to control reactivity. The control slabs will be designed to satisfy *Protection System Functions* (20), *Protection System Independence* (22), *Protection System Failure Modes* (23), *Separation of Protection and Control Systems* (24), *Protection System Requirements for Reactivity Control Malfunctions* (25), *Reactivity Limits* (28), *Protection Against Anticipated Operational Occurrences* (29). The control slabs are the only

system in place currently to shut down the reactor. This means that the HP-ENHS does not meet *Reactivity Control System Redundancy and Capability* (26), and thus cannot meet *Combined Reactivity Control Systems Capability* (27).

The remaining criteria are not as easily grouped by system, so they will be handled one by one. *Design Basis for Protection Against Natural Phenomena* (2) will be covered in the seismic analysis in chapter 6. *Fire Protection* (3) has not been addressed, as the physical plant layout has yet to be designed. *Environmental and Dynamic Effects Design Basis* (4) will be covered under design basis accidents in chapter 4 and beyond design basis accidents in chapter 5. *Electric Power Systems* (17) mandates backup power in case of a loss of offsite power. Station batteries will handle this power, as a diesel generator was deemed unnecessary. The last criterion is *Residual Heat Removal* (54). The heat pipes and the RVACS work together to provide this heat removal, even in the case of a loss of the ultimate heat sink.

## *8.6 Design Basis Accidents*

Design basis accidents are postulated accidents to which a nuclear plant, its systems, structures, and components must be designed and built to withstand without releasing a harmful amount of radioactive materials to the outside environment. Any design basis accident is controlled by the reactor safety systems with insignificant off-site consequences.

The following sections will cover the three main categories of design basis accidents. Class A DBAs have no probability of release and can occur multiple times a year. Class B DBAs have a small probability of release and occur infrequently. Class C DBAs can be severe, but have a very low probability of occurring.

### 8.6.1 Class A

Class A DBAs have a high frequency of occurrence and no release of dose. Due to the 20 year refueling cycle, many DBAs that can be handled by the reactor without dose release occur far less frequently than a comparable incident in a LWR. In addition, many common DBAs have been designed out of the HP-ENHS. This includes failures in pumps, valves, and other moving components, along with LOCAs in the intermediate loop. The remaining Class A accidents are

categorized as thus because they have no chance of dose release and not because of their frequency. This class includes loss of heat-sink accidents and heat pipe rupture.

A loss of the heat sink can result from a breach in the supercritical $CO_2$ cycle containment or failure of the turbo-generator. Failure of heat pipes may also cause a loss of heat sink. The feasibility of this to occur is discussed in the preceding section.

In any case the probability of radioactive release from the HP-ENHS is low even if they will get out from the fuel into the secondary coolant as a result of some incredible accident because the S-$CO_2$ loop is pressurized to 20MPa.

The loss of heat sink accident is self regulating. The negative temperature coefficients of reactivity cause the reactor to power down to a much lower steady state power and the Flibe will carry away excess heat. In addition to the negative temperature coefficient regulating the loss of heat sink accident, there is an overflow system in place in the HP-ENHS that provides extra cooling. During the loss of heat sink accident, the molten salt expands due to the excess heat that it is not able to transfer to the S-$CO_2$ loop. The density of the Flibe in the intermediate loop is very sensitive to temperature, which enables natural convection, but also implies that if the general temperature of the Flibe should go up, it would expand sufficiently to flow in the overfill (see Figure 48). There, the Flibe will bypass the $CO_2$ heat exchangers and be cooled down by the RVACS enough for its density to increase. The cold Flibe will then flow back into the main pool of intermediate coolant through a one-way pressure-dependant valve (see Figure 48). The Flibe is therefore able to evacuate heat through the RVACS in the case of the loss of the ultimate heat sink. Since the Flibe is hotter during the entire process, the heat pipes will evacuate a non-negligible part of their heat through the vessel to the RVACS. The effect on core temperature is small; thanks to the amount of heat that the heat pipes can remove to the RVACS.

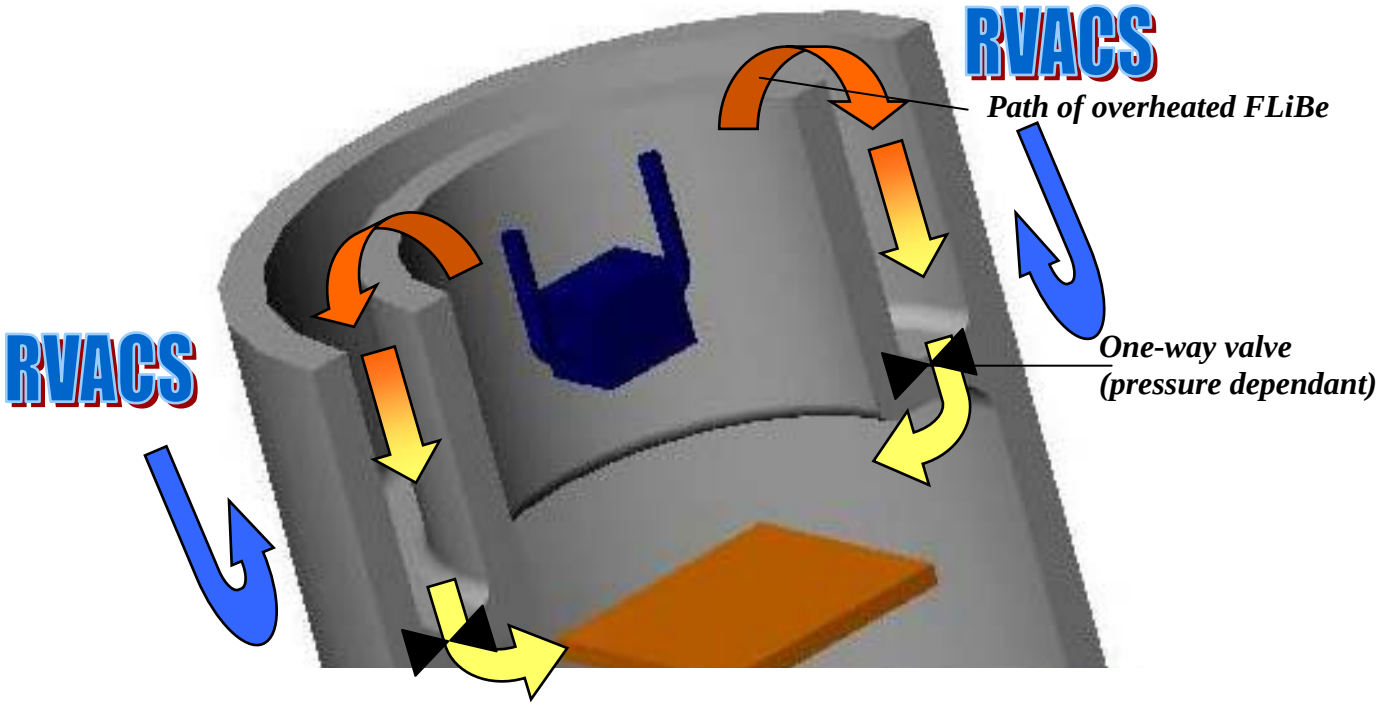


Figure 48 Overflow cooling of the Flibe

The heat pipe break assumes that the situation is stable and no other heat pipes have ruptured as a result of the ones currently inoperable. A heat pipe break or leakage has consequences on three major parameters of the reactor: core reactivity, core temperature, and secondary coolant temperature.

The reactivity coefficient of the fuel next to the coolant is linked to different parameters, such as whether Flibe enters and fills the broken heat pipe, the magnitude of the temperature changes around the fuel (inducing Doppler Effect) and the thermal expansion of materials. According to different sources, a reasonable postulate for this report is that the reactivity change is negligible.

The core is less efficiently cooled by heat pipes, so heat accumulates around the failing heat pipe region and lowers the reactivity of the reactor. As the system stabilizes, the surrounding heat pipes start to heat up until the temperature difference with the Flibe is sufficient to adjust the heat transfer and stabilize the system. The intermediate coolant has less heat pipes transferring heat and therefore can cool down slightly under the right conditions.

The way to regulate the accident itself is passive, as we have seen, the heat pipe heat flow adjusting to the temperature of the core to stabilize the system. Nonetheless, it is important to set counter-measures in case of repetitive heat pipe failure accidents. One active measure is to lower the control slabs in order to reduce power and lower the core temperature. This will affect the energy production of the reactor and should be used only if a significant number of broken heat pipes exist. In case too many heat pipes fail and the reactor comes too close to the threshold of two thirds of failing heat pipes, the reactor should be shutdown.

### 8.6.2 Class B

Class B accidents have the probability of a small release of radioactive material. Due to the large amount of barriers preventing radioactive material release, this class of accidents requires multiple failures. A heat pipe break in conjunction with a fuel cladding rupture must occur to allow radioactive material to pass into the intermediate loop. The molten salt acts as a barrier as well, as any radioactive material will be highly diluted. A break between the $CO_2$ heat exchanger is required to get the material into the generator building. From the generator, the radioactive material could escape into the atmosphere if there were a leak somewhere in the $CO_2$ system.

### 8.6.3 Class C

Class C accidents require many fuel cladding and many heat pipes break, in addition to a breach in the reactor vessel. This would cause radioactive Flibe to leak into the ground. However, being subjected to a nearly atmospheric pressure, a break in the vessel is improbable enough to be designed out of the possible outcomes. This will still be covered in the beyond design basis accidents section in Section 8.9.

A preliminary assessment of the consequences of a cascade failure of heat pipes is the subject of the following section.

## *8.7 Heat Pipes Failure*

Heat pipe failure is of critical importance to this reactor design since it is the most likely cause for any core damage. Among other problems, heat pipe failure could cause fuel swelling due to higher temperatures inside the core. The failure of heat pipes is similar to any other component in that they can be categorized by 3 main failure modes: juvenile failures, performance-related

failures, and age-related failures. In this respect one may visualize a typical component failure curve (sometimes referred to as a bathtub curve) as shown below in Figure 49.

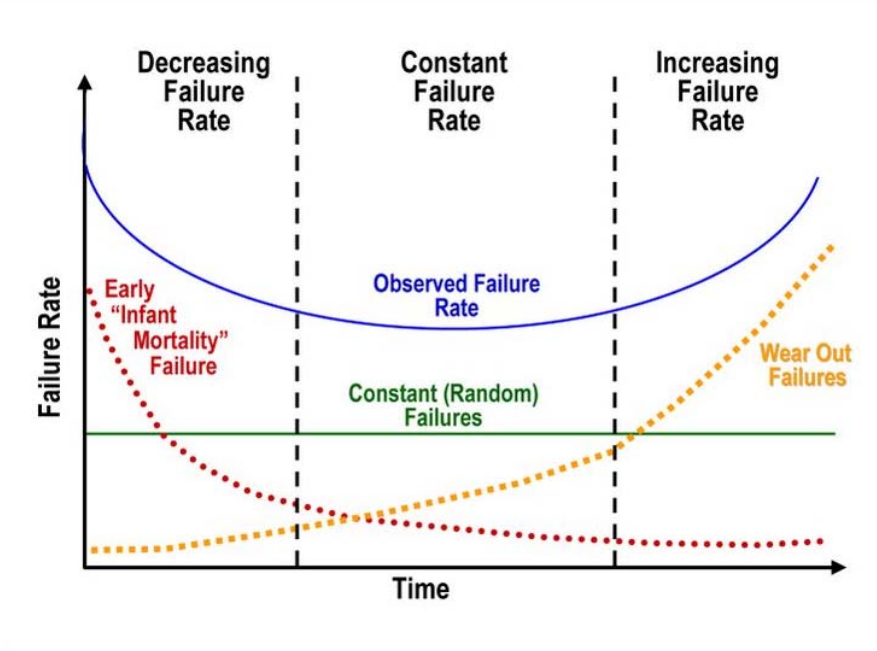


Figure 49 Component bathtub curve

The three failure modes are discussed below. The illustrations are taken from a LANL study [mmm]; they apply to the reference case defined in Table 9 and in Figure 50 below.

Table 9 Reference Heat Pipe Specifications

| Parameter | Values |
|---|---|
| Wick Shape | Annular |
| Evaporator Length | 0.50 m |
| Adiabatic Length | 0.50 m |
| Condenser Length | 1.00 m |
| Container Inside Radius | 0.584 cm |
| Channel Dimension | ~0.056 cm |
| Wick Pore Radius | 15 μm |
| Nucleation Site Radius | 3 μm |
| Solid Thermal Conductivity | 60 $W \cdot m^{-1} \cdot K^{-1}$ |
| Working Fluid | Na |
| Temperature | 1250 K |
| Design HP Power | 8.0 |
| Design Axial Heat Flux | 5.123 $kW \cdot cm^{-2}$ |
| Evaporator Radial Heat Flux | 36.14 $W \cdot cm^{-2}$ |

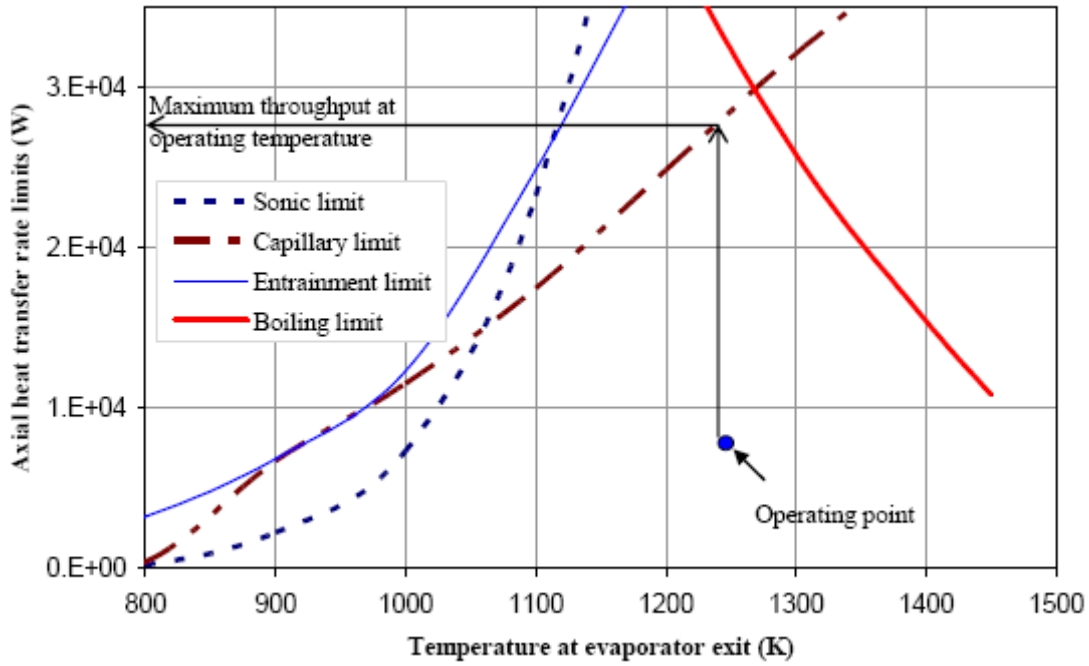


Figure 50 Performance limit curves for the reference case in Table 9

Figure 50 shows curves of the various heat pipes limits and the deduced operating point; this HP can deliver 8 kW at ~1240K. This operating power level is more than a factor of 3 smaller than the maximum possible axial heat transport rate – shown by the horizontal arrow. That is, a safety margin of more than 3 is used in this application.

*Juvenile Failures* Juvenile failures could be caused by a number of factors including improper design, manufacturing errors, welding errors, heat pipe filling errors, mechanistic failures, etc. These failures may occur early in a cycle, and can possibly be mitigated through slow startup procedures.

*Performance-Related Failures* Performance-related failures occur during the mid-life of a component and are typically caused by events external to the heat pipe. For example, a neighboring heat pipe failure will put more of a load on a heat pipe. Such a case is illustrated in Figure 51 below.

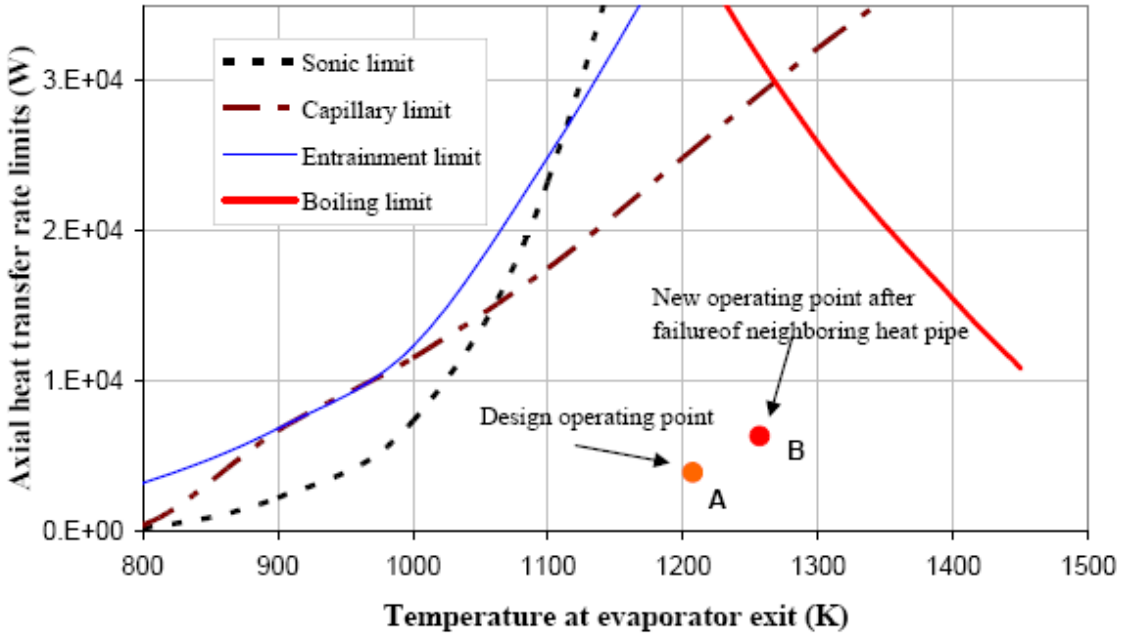


Figure 51 New operating point caused by neighboring heat pipe failure

*Age-Related Failures* A number of age-related failures could occur and are usually due to the gradual degradation in performance of a heat pipe during its design life. The loss of heat pipe tube integrity caused by the corrosion of the wall due to nonmetallic impurities is a concern. Similarly, the loss of wick functionality due to corrosion or dissolution poses another problem. The effective pore radius could also change with time, lowering some of the performance limits.

*Cascading Heat Pipe Failure* The most important safety issue involved with the HP-ENHS is a cascading heat pipe failure. The failure of one or more heat pipes would increase the thermal load on adjacent heat pipes, which increases their likelihood to fail. Several analyses had been done on a small 1MW heat pipe reactor design. The increase in temperatures and heat load on a heat pipe based on the failure of its neighbors is listed in Table 10 below.

Table 10 Temperature and Heat Load Increases Due to Heat Pipe Failure

| | Number of Failed Adj. Heat Pipes | | |
|---|---|---|---|
| | 1 | 2 | 3 |
| Max Increase in T-vapor (K) | 28 | 60 | 82 |
| Max Increase in P-heat pipe (%) | 7.4 | 16.0 | 22.6 |

This data gives a relative idea of a heat pipe cascading failure for the HP-ENHS. Figure 52 below gives a similar picture as was provided previously, except here multiple heat pipe failures are assumed raising the operating point to an even more dangerous level.

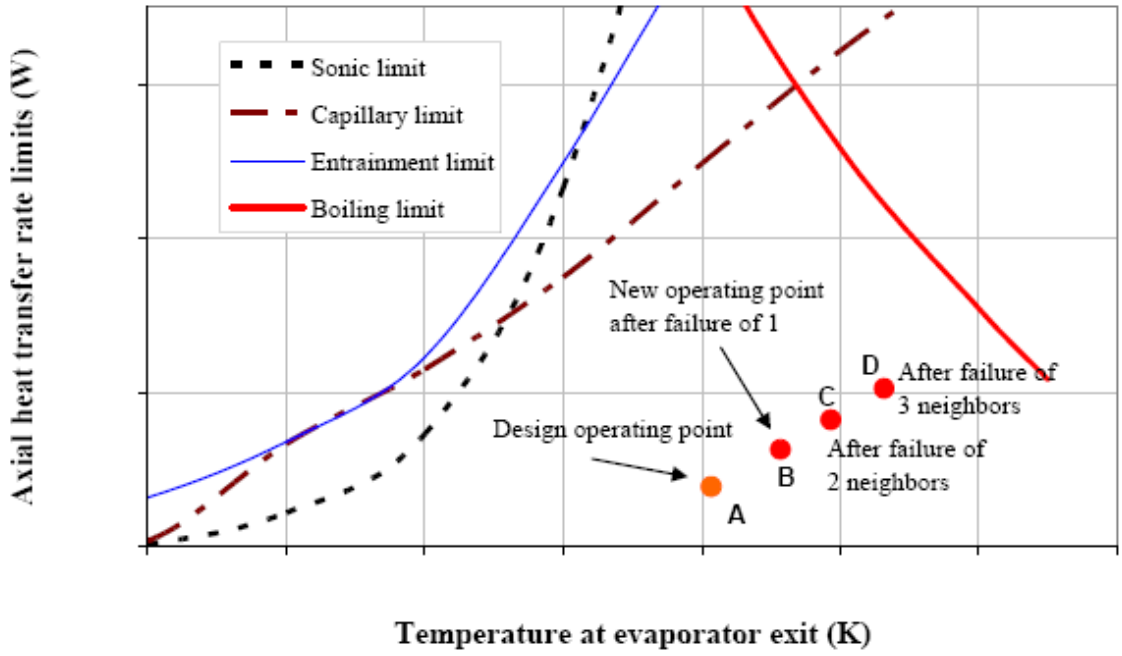


Figure 52 New operating points caused by cascading heat pipe failure

The LANL study assumed a single heat-pipe reliability of 99.5%. Applying the DIPREL Monte Carlo tool at LANL to account for cascading heat-pipe failure resulted in a probability of success estimation of 0.99842.

### *8.8 Reactor Site Criteria*

When calculating the suitability of a site to house a reactor, 10 CFR 100 [56] must be followed to minimize exposure in the case of a DBA. 10 CFR 100 says:

- "(1) An exclusion area of such size that an individual located at any point on its boundary for two hours immediately following onset of the postulated fission product release would not receive a total radiation dose to the whole body in excess of 25 rem or a total radiation dose in excess of 300 rem to the thyroid from iodine exposure." [56]

- "(2) A low population zone of such size that an individual located at any point on its outer boundary who is exposed to the radioactive cloud resulting from the postulated fission product release (during the entire period of its passage) would not receive a total radiation dose to the whole body in excess of 25 rem or a total radiation dose in excess of 300 rem to the thyroid from iodine exposure." [56]

- "(3) A population center distance of at least one and one-third times the distance from the reactor to the outer boundary of the low population zone. In applying this guide, the boundary of the population center shall be determined upon consideration of population distribution. Political boundaries are not controlling in the application of this guide. Where very large cities are involved, a greater distance may be necessary because of total integrated population dose consideration." [56]

The Exclusion Zone of the HP-ENHS will be much smaller compared to the current boundary of ½ miles employed by PG&E at Diablo Canyon. This is because the solid core of the HP-ENHS reactor provides a more effective fission product barrier than in other reactor concepts and because of the highly passive safety feature along with nearly zero burnup reactivity swing of the HP-ENHS. Thus it is likely that the HP-ENHS will have the same or smaller dose release probabilities when compared to the ENHS. Using this assumption, the Exclusion Zone can be set as the reactor plant boundary and the Low Population Zone can be set as the site boundary [57].

### *8.9 Severe Accidents*

The NRC has four requirements contained in the "Policy Statement on Severe Reactor Accidents Regarding Future Designs and Existing Plants" that new reactors must fulfill (50 FR 32138) [58]. These criteria are:

- "Demonstration of compliance with the procedural requirements and criteria of the current Commission regulations, including the Three Mile Island requirements for new plants as reflected in the CP [Construction permit] rule [10 CFR 50.34(f)]" [58]

- "Demonstration of the technical resolution of all applicable Unresolved Safety Issues and the medium- and high-priority Generic Safety Issues, including a special focus on assuring the

reliability of decay heat removal systems and the reliability of both AC and DC electrical supply systems" [58]

- "Completion of a Probabilistic Risk Assessment (PRA) and consideration of the severe accident vulnerabilities the PRA exposes along with the insights that it may add to the assurance of no undue risk to public health and safety" [58]
- "Completion of a staff review of the design with a conclusion of safety acceptability using an approach that stresses deterministic engineering analysis and judgment complemented by the PRA" [58]

This report can only show completion of the first three requirements, as a staff review is not possible at this time. The first requirement, that the Three Mile Island conditions be met is satisfied to the best of the plant's abilities. As this reactor is not a light water reactor, many of the criteria outlined in CP rule 10 CRF 50.34(f) are not applicable. Subsection 1 requires a PRA, which will be provided in chapter 5. The remainder of subsection 1 is LWR-specific and pertains to core cooling, containment spray, and other features that are not needed in the HP-ENHS. Subsection 2 deals with the control room and the ability of the containment to hold. The control room has yet to be finalized; however, a simulation control room can be completed when the design is ready. The containment will be designed to prevent the leakage of radioactive materials and to monitor the conditions inside containment in accordance with this subsection, although certain sections are not applicable to our reactor due to the nature of the molten salt loop. Subsection 3 requires compliance with procedures and adherence to building codes. This subsection will be followed in the final design.

### *8.10 Beyond Design Basis Accidents*

Beyond design basis accidents are accidents that could lead to core melt. The HP-ENHS core is postulated to have two conditions that might lead to core melt. One is a failure of 2/3 of the heat pipes without a scram, and the other is a reactor vessel break resulting in loss of the intermediate coolant. The heat pipe condition will be covered in Section 8.11.2. The loss of Flibe accident is discussed below.

An important safety issue in the case of a Loss of Coolant Accident is the handling of the decay heat of the fuel. Upon a LOCA, the control slabs will immediately be scrammed in order to shut

the reactor down. Therefore, only the decay heat of the core would need to be evacuated to a heat sink without the help of the Flibe.

The heat from the core is carried by the heat pipes to the wall of the reactor vessel that will heat up. This heating will increase the heat flux from the outer surface of the reactor vessel to the air flowing in the RVACS by natural circulation. Figures 53 and 54 schematically illustrate this process – heat from the core (Point 1) is transferred to the heat pipes (Point 2) which deliver this heat to the vessel wall (Point 3).

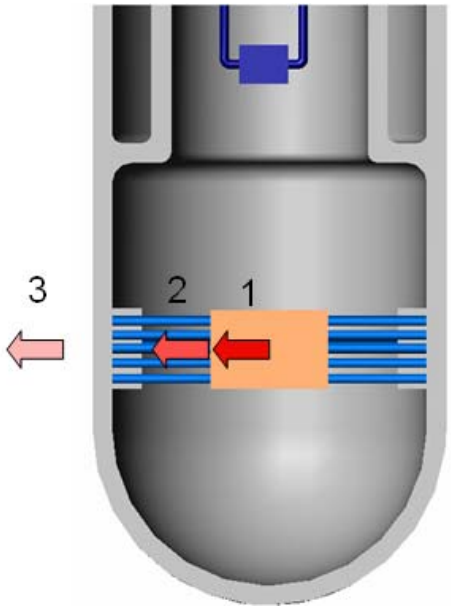


Figure 53 Heat transfer in LOCA

The following is a preliminary estimation of the velocity of air needed in the RVACS and the temperature profile in the vessel. Although a 2D or 3D model is required for accurate analysis of this heat transfer problem, a simplified model is used to obtain a preliminary assessment of the feasibility of this cooling system in case of LOCA in the intermediate loop.

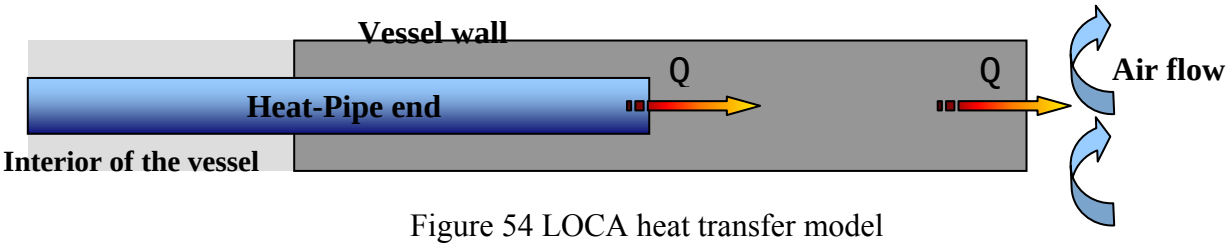


Figure 54 LOCA heat transfer model

It is assumed that all of the decay heat generated by the core, Q, is evacuated to the heat sink (air), in a steady-state scenario. The decay heat level is assumed to be 10% of the nominal power of the core. It is also assumed that the air flow of the RVACS has a laminar boundary layer. These assumptions are conservative. Finally, it is postulated that the heat coming out of the heat pipes is spread uniformly over a large band of the vessel wall, corresponding to a section of half of the height of the vessel (see Figure 53).

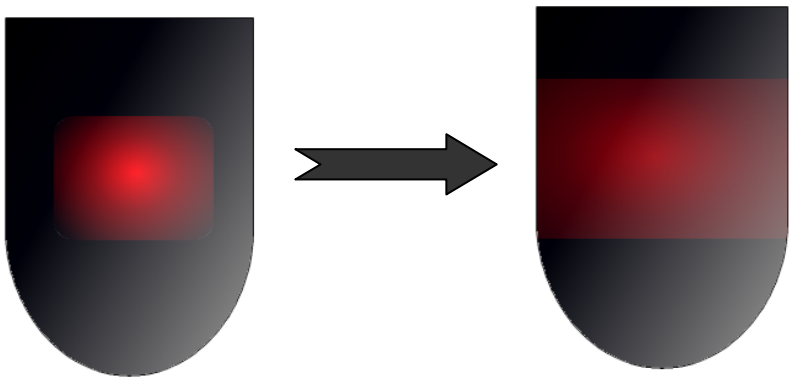

Figure 55 Heat distribution on reactor pressure vessel

In order to obtain the velocity of air necessary to cool down the vessel and take away Q=12.5 MW of heat, we make use of the Prandtl, Reynolds, and Nusselt numbers of the flow.

$$Nu = \frac{hL}{k} \qquad Re = \frac{\rho V L}{\eta}$$

Pr (air) = 0.7

K (Hastelloy N , 1000K) = 30 W/m-K

The Laminar Boundary Layer relation gives : $Nu = 0.332 \times Pr^{0.3} \times Re^{0.5}$

It is therefore possible to estimate V, postulating a linear temperature profile in the vessel wall (the left side being considered adiabatic since the heat exchanges with the interior of the vessel are assumed to be negligible)

This model gives an external wall temperature of 1084K and an air velocity of 2.71 m/s.

According to this study, the RVACS is sufficient with a slight forced convection, and the temperature of the vessel wall does not exceed the maximum temperature for Hastelloy N. The reactor can safely accept the decay heat of the core without damage in case of a LOCA accident. Thus, no confinement modes are needed.

### *8.11 Risk Assessment, Risk Management and Safety Goals*

The NRC policy for the safety goals are stated in 51 FR 30028 [59]. The quantitative goals are:

- "The risk to an average individual in the vicinity of a nuclear power plant of prompt fatalities that might result from reactor accidents should not exceed one-tenth of one percent (0.1 percent) of the sum of prompt fatality risks resulting from other accidents to which members of the US population are generally exposed." [59]
- "The risk to the population in the area near a nuclear reactor of cancer fatalities that might result from nuclear power plant operation should not exceed one-tenth of one percent (0.1 percent) of the sum of cancer fatality risks resulting from all other causes." [59]

The number of deaths in the United States from in 2004 from prompt deaths (accidents, murder, and suicide) was 52.8 people per 100,000 leading to a limit of 5.28E-7 prompt nuclear fatalities per year. The rate of deaths due to cancer was 187.4 people per 100,000 for an upper limit of 1.87E-6 latent nuclear fatalities per year [60].

#### 8.11.1 Risk Assessment of Inherently Safe Features

The HP-ENHS employ passive safety features to avoid core damage and radioactive isotopic release. The passive safety systems include the sodium heat pipes, natural convection of the intermediate Flibe loop, and the Reactor Vessel Air Cooling System (RVACS). Because the system is inherently safe, is there a way to characterize risk?

Upon initial inspection, it is expected that inherent safe reactors carry no probability of causing core damage or isotopic release. However, these reactors are dependent on features whose failure can lead to severe accidents. Thus, to quantify the risk associated with inherently safe reactors, assessment of the probability of failure of the underlying safety structures that could affect the assumptions of the passive safety characteristics need to be made [61].

The structures critical to the inherent safety of the HP-ENHS are the RVACS, reactor vessel, and heat pipes. The HP-ENHS reactor is small and compact such that decay heat can be removed by natural convective air flow over the reactor vessel. The decay heat is transferred to the wall of the vessel by heat pipes. Two potential weaknesses are identified in this passive safety system. The first weakness is the failure of heat pipes that can lead to a cascade of failure which will increase core temperature. The second weakness is a failure of structural components inside the reactor vessel that may reduce the Flibe natural circulation sufficient to cause core damage.

In order to quantify risk associated with passive safety in a reactor, the probability of failure of critical structures must be determined. However, it is a challenge to quantify the probability of failure of a structure because it is necessary to have data on the probability distributions for both load and material strength. If the distributions were normal, then in order to demonstrate that the probability of failure is of the order $10^{-7}$, the distributions would need to be known accurately out to 5 or 6 standard deviations [61]. In reality, it is very difficult to predict the probability distributions for either load or strength to this degree of accuracy. Another challenge is that different assumptions of the type of distribution can lead to varying values on the probability of failure [61]. In the case of the HP-ENHS, the operating temperature of the structure is high, which can lead to creep and fatigue damage. Available data on the probability distribution in these regimes are only estimates.

Because of the lack of adequate data on materials, detailed information on the vibration and temperature distribution exposed to critical structures, it is difficult to quantify the probability of structural failure in inherently safe systems. Even though more information concerning materials will become available over time as research continues, it is still unlikely possible that low probability of failure of critical structures in inherently safe systems can be demonstrated. Thus, the assessment of risk associated with the HP-ENHS will be performed for heat pipes failure.

### 8.11.2 Probabilistic Risk Assessment of Heat Pipes

From the Beyond Design Basis Accident, it is shown that the greatest threat to core damage is the loss of heat pipes. Loss of intermediary coolant, Flibe, is highly unlikely since it would entail the reactor vessel to fail; reactor vessel has low probability of failure. One mode of failure of heat pipes in the same area can cause more heat pipes to fail in the same vicinity, causing a

cascade of failing heat pipes. This failure mode of the heat pipe is taken as an initiating condition that could lead to core melt. A Monte Carlo type simulation was used to predict failure of heat pipes due to cascading effect. It was found after 100,000,000 runs that the maximum limit on the probability of a fatal cascade, where over 2/3$^{rd}$ of the heat pipes fail, was 1.0E-5. The probability that a heat pipe will fail is 5.0E-3 [7]. Using this probability, the probability of three adjacent heat pipe failing was 1.3E-7. If heat pipes start to fail because of the cascading effect, then control slabs are used to scram the reactor. Using these events, a simple event tree was constructed to determine the core damage frequency (CDF), which can be seen in Figure 56. The component failure rates were taken from sample failure rates given in IAEA general reliability data [62]. The CDF due to an initial three heat pipes failing is 1.3E-18 per year. This value is lower than the federal regulation of 1E-4 per year in Regulatory Guideline DG-1145. The event tree used to calculate the CDF is very crude and does not factor in other possible scenarios that can lead to core damage. To further reduce uncertainties related to the CDF, further studies need to be done on the behavior of heat pipe cascade and other scenarios that might lead to core damage.

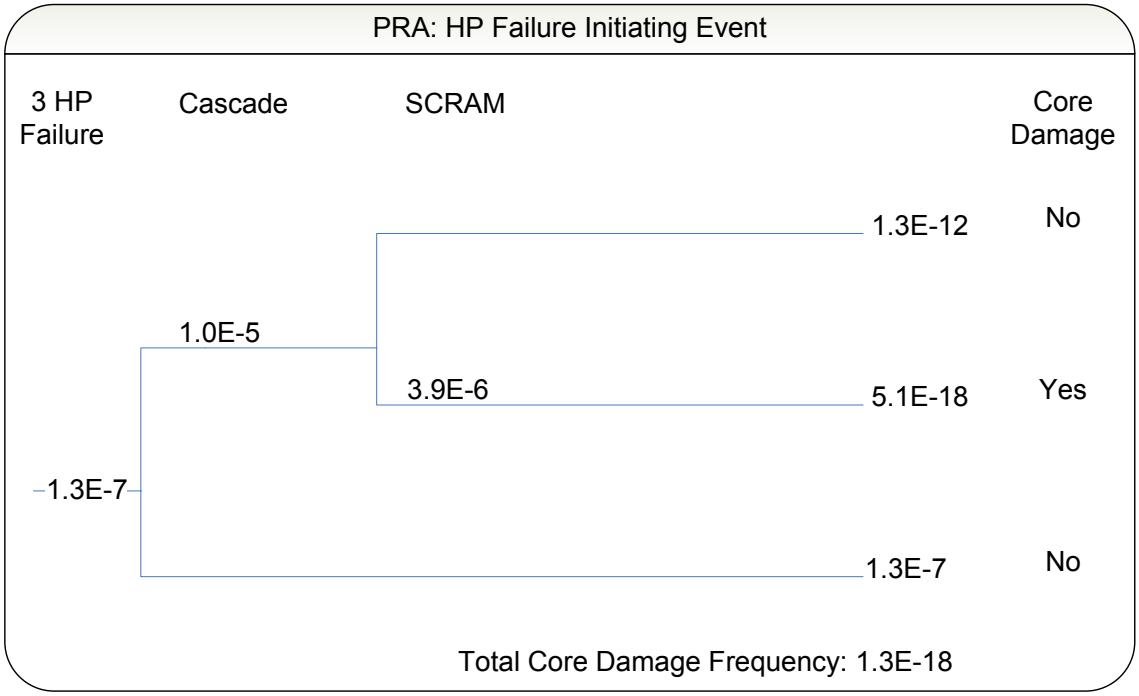


Figure 56 Heat pipe failure event tree

In the event of numerous heat pipes breaking, the control slabs will be engaged to scram the reactor and shut it down. There are two control slabs in the scram system and only one slab needs to be dropped onto the core to shut it down. The control slabs employ neutron flux sensors to trigger the actuators to drop the slabs. Three sensors are used and two out of three positive signals from the sensors are needed to trigger the actuator. The sensors can either use on/offsite or station battery power. The value of the failure probability of the sensors, battery, on/offsite power are taken from industry data. From the probability tree in figure 24, the control slab's probability of failure to deploy is 4.5E-10/hr or 3.9E-6/year. The probability of failure determined is crude and more precise methods will be employed in the future.

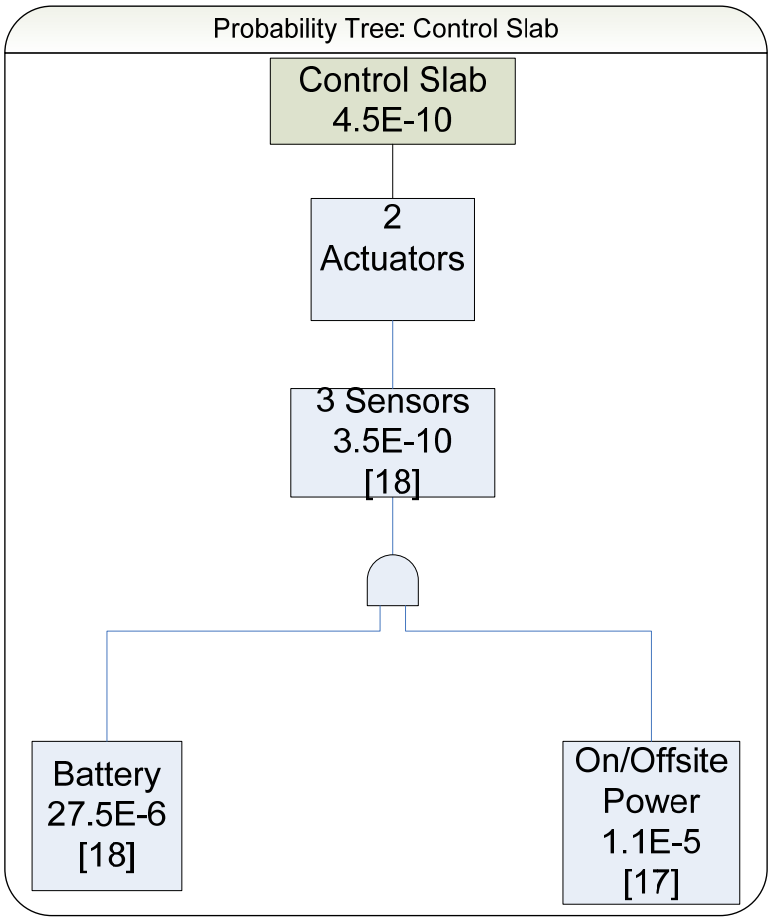


Figure 57 Probability tree of control slab (per hour)

### 8.11.3 Loss Of Offsite Power (LOOP)

The loss-of-offsite-power (LOOP) initiating event is investigated to determine whether this will lead to core damage. LOOP will lead to loosing the tertiary loop, which includes the S-$CO_2$ power conversion unit that serves as the HP-ENHS ultimate heat sink. Loosing the tertiary loop will not lead to failure of the heat pipes, which is the main reason for causing core damage. Loosing the tertiary loop will cause temperature in the intermediate loop to rise because the heat taken to power the conversion units will remain in the Flibe. However, the Flibe and the heat pipes are capable of transferring the excess heat to the RVACS to cool down. Thus, LOOP will not lead to core damage because the probability of heat pipes failing is low.

## *8.12 Seismic Safety*

The Nuclear Regulatory Commission (NRC) set forth requirements for proposed sites for nuclear reactors in "Reactor Site Criteria", 10 CFR 100 [56]. The HP-ENHS will meet NRC criteria at the Diablo Canyon site in the following way:

"The geologic, seismic and engineering characteristics of a site and its environs shall be investigated in sufficient scope and detail to provide reasonable assurance that they are sufficiently well understood to permit an adequate evaluation of the proposed site, and to provide sufficient information to support the determinations required by these criteria and to permit adequate engineering solutions to actual or potential geologic and seismic effects at the proposed site [56]."

Even though the Diablo Canyon site is surrounded by major faults, the Hosgri Fault zone dominates seismic hazard because it is the closest fault to the site. The Los Osos and San Luis Bay faults taken together contribute 3-5% of the total hazard. Other fault contributions are insignificant. Thus, analysis of seismic study will focus primarily on the Hosgri fault. The majority of information regarding the Diablo Canyon site is found in Pacific Gas & Electric Long Term Seismic Program [55].

The Hosgri fault zone is the southernmost part of the San Gregorio/Hosgri fault system, which is a complex system of faults that is subparallel to the central California coast [55]. To the north of the Hosgri fault zone are two other major fault zones, namely the San Gregorio and San Simeon.

The San Gregorio/Hosgri fault zone splits from the San Andreas system to the north, near Bolinas. The system seems to die out near Point Pedernales, 410 kilometers to the southeast. The Hosgri fault zone lies offshore throughout its length and is about 110 kilometers long [55]. The determination of the characterization of the Hosgri fault zone is best determined by using logic trees.

The characterization of seismic source often carries uncertainty because there is usually no specific data or recorded history of earthquake activity. Thus, indirect methods are employed to evaluate the seismic potential of faults by using indirect measurement of size, frequency and location of earthquakes that the fault may generate. Logic trees can aid in the process of fault evaluation by incorporating alternative interpretation of data as a measure of uncertainty. Using logic tree has advantages since it gives complete enumeration of possible states of nature and ensures all hypothetical situations have been accounted for properly with appropriate weights to each. Logic trees are made of branches and nodes, with the nodes representing a choice between different values of a variable. The branches are the particular value leading off particular nodes. To arrive at the final magnitude distribution, the logic tree goes through different nodes in the tree that are associated with particular characteristics of the fault.

The maximum quake magnitude for the Hosgri fault zone is estimated using empirical relations between magnitudes and source characteristics in logic trees. Paths taken through the logic tree define scenarios that are each associated with a maximum magnitude. By repeating the calculation for all branches of the trees, a probability distribution for maximum magnitude quake is developed. The distribution of the maximum magnitude has a mean value of 6.96 and a standard deviation of 0.27 magnitude units [55]. Figure 60 shows the distribution of the maximum magnitude earthquake.

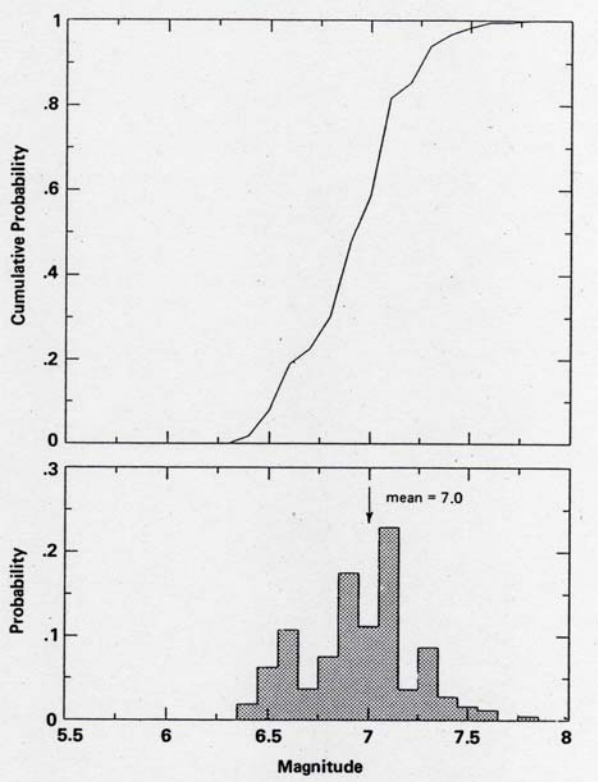


Figure 58 Maximum magnitude distribution for Hosgri fault zone

Figure 59 describes the magnitude distribution for the Hosgri fault zone obtained conditional on the sense of slip. Sense of slip models modes of deformation. The ratio of horizontal to vertical components of slip defines the mode of deformation. For strike-slip, the ratio is greater than 2:1; oblique is less than 2:1; and thrust slip is greater than 1:2 and less than 2:1. The distributions are similar for each style of slip and the resulting mean estimates are 6.98, 6.93, and 6.98 for strike-slip, oblique, and thrust faulting, respectively. The total probability of the entire different slip style is one.

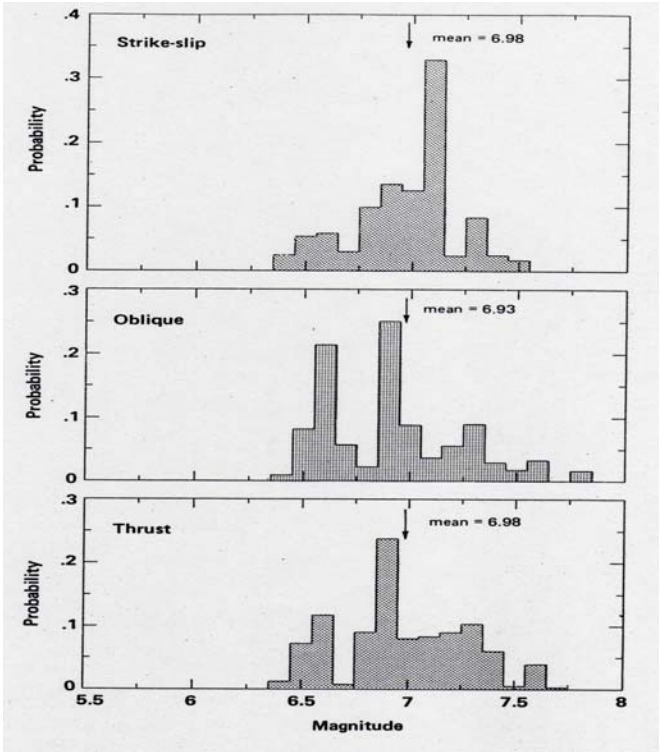


Figure 59 Maximum magnitude distribution for Hosgri fault zone for several sense of slip

8.12.1 Seismic Isolators

"Where unfavorable physical characteristics of the site exist, the proposed site may nevertheless be found to be acceptable if the design of the facility includes appropriate and adequate compensating engineering safeguards [56]."

Seismic isolators are used as added protection for the plant during an earthquake. Isolators work by preventing the full amount of motion from being transferred to the object being isolated. This is done by creating a discontinuity in the form of a different material with low motion transfer properties between the object and the ground [63]. The HP-ENHS will be placed in the ground with room around the vessel for the RVACS to function. The reactor will be supported at its top, which is where the seismic isolators will be placed. Figure 60 is a diagram of the placement of the seismic isolators on an ENHS. The HP-ENHS has the same shape, although the dimensions differ.

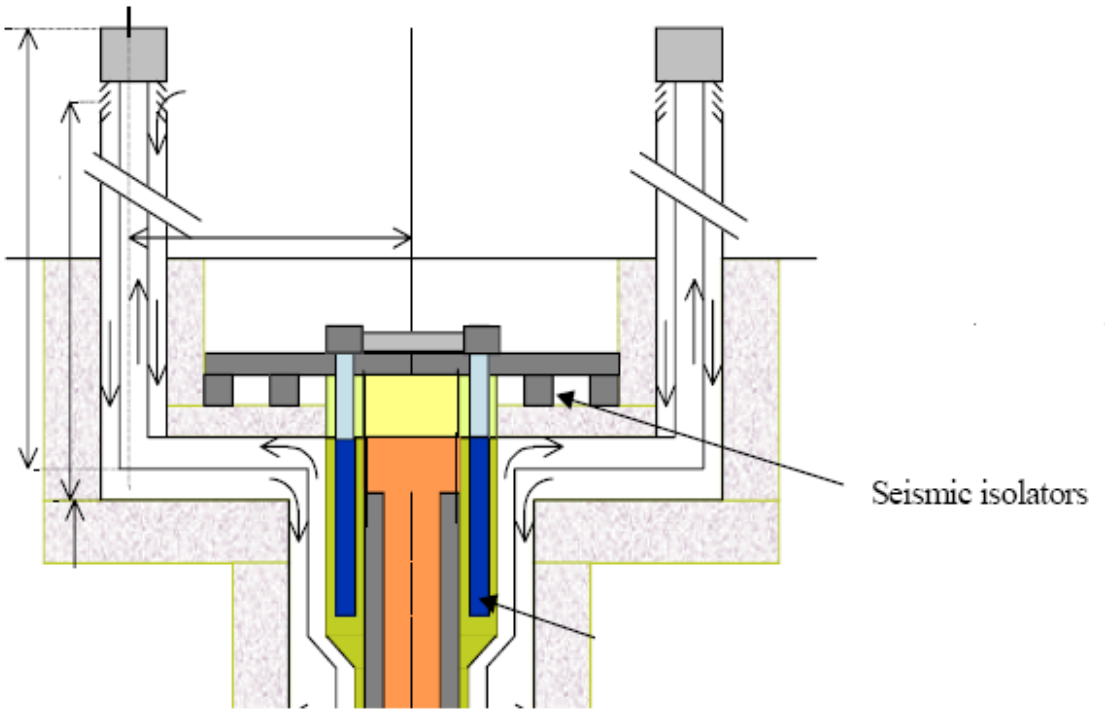


Figure 60 Location of seismic isolators, represented on an ENHS [57]

Lead rubber isolators were chosen for this purpose, as they have proved successful in preventing structural damage to the University Hospital in the 1994 Los Angeles earthquake. Lead rubber isolators also dampen vibrations, making them well suited to this application. Figure 61 shows a diagram of a lead rubber isolator.

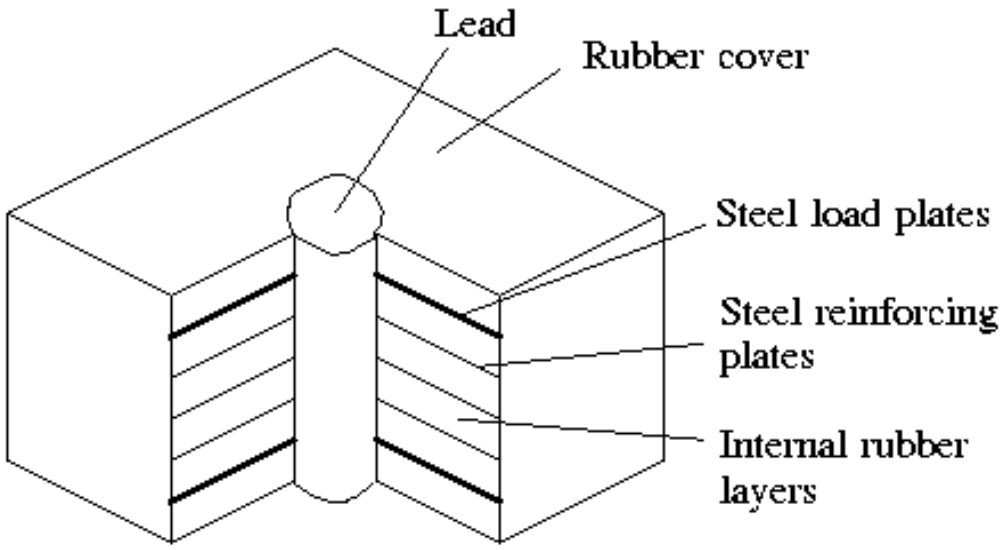


Figure 61 Lead rubber isolator diagram [64]

8.12.2 Seismically Induced Component Failure

The mean failure frequency of key components at discrete acceleration in Table 11 is taken from the LTSP. These key systems are similar to the ones employed in the HP-ENHS. The loss-of-offsite-power has the highest probability of failure, while the station batteries and reactor vessel has low failure fraction. The failure fraction obviously increases as the discrete acceleration of the ground increases.

Table 11 Failure Fraction of Key Structures (LTSP)

| Conditional Mean Failure Fractions of Key Structures or Components | | | | | | |
|---|---|---|---|---|---|---|
| Component/Structure | Discrete Acceleration Range (g) | | | | | |
| | 0.750 | 1.500 | 1.875 | 2.250 | 2.750 | 3.500 |
| Batteries | 6.10E-08 | 4.11E-05 | 4.14E-04 | 2.19E-03 | 1.11E-02 | 4.13E-02 |
| Battery Charger | 1.36E-06 | 1.53E-04 | 7.44E-04 | 2.14E-03 | 6.64E-03 | 1.75E-02 |
| Offsite Power, 230 kV | 8.37E-03 | 3.19E-01 | 6.23E-01 | 7.93E-01 | 9.29E-01 | 9.80E-01 |
| Offsite Power, 500 kV | 1.61E-01 | 9.63E-01 | 9.96E-01 | 9.99E-01 | 1.00E+00 | 1.00E+00 |
| Reactor Vessel | 2.50E-08 | 1.21E-05 | 1.05E-04 | 4.88E-04 | 2.43E-03 | 9.50E-03 |

The risk assessment regarding seismically induced component failures leading to core damage is examined. The behavior of heat pipes under seismic conditions has yet to be studied. Fragility and seismic hazard analysis needs to be determined for heat pipes in order to answer the question

of whether the HP-ENHS is safe in the event of earthquakes. One concern for heat pipe behavior is that they can break during earthquakes because the oscillatory motion of the reactor causes the heat pipes to impact the reactor vessel wall. Furthermore, the behavior of the S-$CO_2$ power conversion unit under seismic events is an important area of research in the future. The issue of seismic safety for the HP-ENHS is still uncertain since the reactor has major areas that need to be studied, including the heat pipes and power generation system. However, we know from the heat pipe analysis that the total failure rate of the heat pipes should be under 35% in order for the reactor to experience safe shutdown.

### *8.13 Summary*

The HP-ENHS is a concept reactor that is highly dependent on passive safety to prevent and mitigate accidents. The system employs supercritical carbon dioxide in the tertiary loop to convert heat to power using the recompression cycle. An indirect cycle is used, where heat is transferred by the intermediate Flibe coolant to the S-$CO_2$ through heat exchangers. The reheat in the indirect loop was found uneconomical. Heat pipes are used to transport heat from the core to the intermediate loop. Heat pipes have a 99.5% reliability, with a conservative success probability of 99.8%. Under normal operation, the Flibe flow rate was found to be .25 $m^3/s$ and ITS average outlet temperature IS 1040 K or 767 ºC. Corrosion of the vessel wall due to interaction with high temperature Flibe is not a concerning issue as long as compatible alloy such as Hastelloy N is used as the Flibe container material.

The severe accident event of loss-of-intermediate-coolant, Flibe, was investigated. The Flibe intermediate coolant was assumed lost. In this event, it was postulated that all the heat from the core is removed by the heat pipes and transferred to the reactor vessel wall to be cooled by RVACS. It was found that with an air velocity of 2.71 m/s that the vessel wall reached 1084 K or 811 ºC. Thus, RVACS alone is sufficient to cool the reactor to temperatures below the maximum temperature of Hastelloy N. The reactor's passive safety system is adequate to remove the decay heat of the core in the event of an intermediate loop LOCA.

Heat pipe failure remains the major concern for core damage. To prevent further nuclear reactions in the core once the threshold of $2/3^{rd}$ of the heat pipes failed is reached, the active

safety system of control slabs are employed. The frequency of failure of the reactor to scram was found to be 3.9E-6 failure per year.

Probabilistic risk assessment of inherently safe reactors is challenging since it would require determining the probability of failure distribution of the critical structure underlying the passive safety systems. Thus it is highly unlikely that the low probability of failure of the critical structures underlying the inherently safe systems can be verified.

The operating site for the HP-ENHS was chosen to be Diablo Canyon in California, one of the more stringent site criteria since it is located next to a major fault system, the Hosgri fault. From the LTSP, the distribution of the maximum magnitude earthquake at the site was found to have a mean value of 6.96 and a standard deviation of 0.27 magnitude units. Seismic isolators are used in the HP-ENHS design as added protection for earthquakes. Lead rubbers isolators were chosen because they can dampen vibrations, which is well-suited for this reactor. The lead rubbers isolators were also proven to successfully prevent structural damage to the University Hospital in the 1994 Los Angeles earthquake. Nevertheless, seismic related accidents are still of much concern. Little is known about how the components of the reactor, including the reactor vessel, will handle an earthquake.

Although a good deal of research has gone into the HP-ENHS already, more work needs to be done before it can be licensed at DCPP. Earthquakes are a major danger at Diablo Canyon, and more tests need to be run on alkali-metal heat pipes before they can be placed into commercial reactors. A core melt accident due to heat pipe cascading failure is a very real problem in this design due to the great amount of uncertainty involved.

More types of design basis accidents must be identified. These new types along with the current DBAs must be characterized with greater certainty than done in this report.. In addition, the dose release from all of the DBAs must be found. Heat pipe failure and cascading are two of the more important areas for research since multiple heat pipe failures are the main cause of core damage. Beyond design basis accidents also require more analysis in the identification of such accidents and making design modifications to mitigate the consequence of such accidents.

The HP-ENHS has the potential to be the safest reactor yet. With a high number of fission product barriers and the ability to operate fully in a passive manner, the HP-ENHS greatly reduces the dose to plant workers. In addition, decay heat removal through the heat pipes could one day provide unparalleled core melt protection.

## 9. CONCLUSIONS

The feasibility assessment performed during the first year of the project found that it is feasible to design an ENHS-type reactor to have a solid core, to use liquid-metal heat-pipes for the primary coolant system and to use a naturally circulating intermediate coolant system. The 125 $MW_{th}$ core is designed to provide the intermediate coolant average outlet temperature of ~ 1040K; significantly higher than the ~750K average outlet temperature of the reference ENHS intermediate coolant. This could be translated into approximately 25% increase in the energy conversion efficiency – from ~40% of the reference ENHS to over ~50% for the HP-ENHS.

Alternatively, the higher average intermediate coolant outlet temperature can be used to minimize the HP-ENHS reactor dimensions and weight. For the reference ENHS reactor energy conversion efficiency, the HP-ENHS vessel height needs be only 9 m versus nearly 20 m of the reference ENHS. Its vessel diameter is approximately 4 m versus ~ 3.5 m of the reference ENHS reactor module and versus 4 m to 5m of the reference ENHS reactor pool. No such pool is required for the HP-ENHS reactor. Not only can the HP-ENHS reactor be significantly smaller than the reference ENHS reactor of comparable power, but it could also be significantly lighter, making it easier to transport fueled from the factory. Whereas the reference ENHS module has to have the fuel embedded in solidified Pb-Bi for safe transportation, the HP-ENHS fuel is permanently supported by a solid structure.

The preferred design of the HP-ENHS core uses nitride fuel, Mo TZM alloy structure and Na-filled HPs. The solid core is oriented horizontally to efficiently transfer heat from the core to the natural circulation intermediate coolant system via the HPs extending from both ends of the core. The preferred intermediate coolant is LiF-$BeF_2$ and preferred reactor vessel and heat-exchanger structural material is Hastelloy.

The HP-ENHS offers sustainable energy (CR~1.05) along with fission energy at a very high temperature (>1000K). In addition it features

- High proliferation resistance
- Very low probability for reactivity insertion accidents

Relative to the reference ENHS reactor design [1, 57], the HP-ENHS design concept offers a number of advantages including the following:

- higher coolant outlet temperature, potentially offering higher efficiency and hydrogen production capability;
- significantly enhanced passive decay heat removal capability;
- no positive void reactivity coefficient;
- smaller and lighter reactor;
- more robust core for safe transportation.

A disadvantage of the HP-ENHS is that its core averaged specific power is ~10% lower than that of the reference ENHS core. However, the increased energy conversion efficiency and/or reduced size and weight of the HP-ENHS are likely to make the HP-ENHS more economically viable. Optimization of the fuel rod and heat pipe diameters and of the core length and diameter could possibly result in increased specific power.

## Acknowledgement

This work was funded by the US DOE NEER program under Award # DE-FG07-05ID14706

## REFERENCES


1. E. Greenspan and the ENHS project team, "The Long-Life Core Encapsulated Nuclear Heat Source Generation IV Reactor," ICAPP'02, Hollywood, FL, June 9-13, 2002.
2. D.I. Poston, "Nuclear design of the SAFE-400 space fission reactor", Nuclear News, December 2002.
3. S.J. Zinkle and N. M. Ghoniem, *Operating Temperature Windows for Fusion Reactor Structural Materials,* Fusion Engineering and Design, 51-52, 2000.
4. S. J. Zinkle et al., *Overview of Materials Technologies for Space Nuclear Power and Propulsion*, Space Technology and Applications International Forum-STAIF 2002
5. *Multimegawatt Space Nuclear Power Program Structural materials Data Sheet*, Oak Ridge National laboratory, Aug 12 1988.
6. Carmak and Hartless, *Biaxial creep of Re lined biaxial tubing*, ANS Transactions, 89, 2003, 903-904.
7. R. L. Klueh, *Oxide Dispersion Strengthen Steels: A Comparison of Some Commercial and Experimental Alloys*, Journal of Nuclear Materials 341, 2005, 103-114.
8. T. R. Allen, University of Winsconsin, private communications.
9. S. J. Zinkle and F. W. Wiffen, *Radiation effects in Refractory Alloys*, Space Technology and Applications International Forum-STAIF 2004
10. Vendor catalog, Special Metals, www.specialmetals.com
11. Handbook of Chemistry and Physics, CRC press, Cleveland 55$^{th}$ edition, 1974-1975
12. ASM Handbooks, Binary Alloy Phase Diagram
13. T. Kaito et al. *High Temperature Oxidation Behavior of ODS Steels*, Journal of Nuclear Materials 329, 2004, 1388-1392.
14. J. J. Park et al., *Review of Liquid Metal Corrosion Issues for Potential Containment Materials for Liquid Lead and Lead-Bismuth Eutectic Targets as a Neutron Source*, Journal of Nuclear Materials 196, 2000, 315-325.
15. E. Yoshida et al., *Sodium Compatibility of ODS Steels at Elevated Temperature*, Journal of Nuclear Materials, 329, 2004, 1393-1397
16. J. Saito et al., *Alloying Effects on the Corrosion Behavior of Binary Nb-based and Mo-based alloys in Liquid Metal*, Journal of Nuclear Materials 264, 1999, 216-227.
17. *Nuclear Design of the SAFE 400 Space Fission Reactor*, Nuclear News, Dec. 2004
18. V. Ignatev et al., Experience with Alloys Compatibility with Fuel and Coolant Salts and their Application to Molten Salt Actinide Recycler and Transmuter, Proceedings of ICAPP 2006, Reno NV, June 2006.
19. P. Hejzlar, M.J. Driscoll, M.S. Kazimi. *"Conceptual Reactor Physics Design of A Lead-Bismuth-Cooled Critical Actinide Burner"*. Nuclear Engineering Department, MIT. Technical Report MIT-ANP-TR-069. February 2000.

20. P. Losonen, *Modelling Intragranular Fission Gas Release in Irradiation of Sintered LWR UO2 Fuel*, Journal of Nuclear Materials 304, 2002, 29-49.

21. Y. Koo et al., *Analysis of Fission Gas Release and Gaseous Swelling in UO2 Fuel under the Effect of External Restraint*, Journal of Nuclear Materials 280, 2000, 86-98.

22. E. K. Storms, *An Equation which Describes the Fission Gas Release from UN Reactor Fuels*, Journal of Nuclear Materials 158, 1988, 119-129.

23. K. Tanaka et al., *Fission Gas Release and Swelling in Uranium-Plutonium Mixed Nitride Fuels*, Journal of Nuclear Materials 327, 2004, 77-87.

24. J. Choi et at., Lawrence Livermore National Laboratory, private communications.

25. R. G. Pahl et al., *Irradiation Behavior of Metallic Fast Reactor Fuels*, Journal of Nuclear Materials, 188, 1992, 3-9

26. B. D. Wirth and D. Olander, 2006 NE120 Lecture Notes, Nuclear Engineering Department, University of California at Berkeley.

27. D. Harries, *Irradiation Creep in Non-fissile Metals and Alloys*, Journal of Nuclear Materials 65, 1977, 157-173

28. L. K. Mansur, *Theory and Experimental Background on Dimensional Changes in Irradiated Alloys*, Journal of Nuclear Materials 261, 1994, 97-123.

29. D. J. Michel, *Transient Irradiation Induced Creep of Nickel During Deuteron Bombardment*, Journal of Nuclear materials 75, 1978, 1-6.

30. M. B. Toloczko, Journal of Nuclear Materials, 2004.

31. M. Fratoni, private communications.

32. E. Greenspan, *Fusion Reactor Blanket Nucleons*, Progress in Nuclear Energy Vol. 17, n. 1, 1986, 53-139

33. E. Greenspan, private communications.

34. B. Ross and S. El Genk, *UN Fuel Swelling Correlation*, Journal of Nuclear Materials 170, 1990.

35. Y. Kurata et al., *Creep Properties of 20% Cold-Worked Hastelloy XR*, Journal of Nuclear Materials 228, 1996, 176-183.

36. Haynes Vendor online catalog, www.haynesintl.com.

37. Los Alamos National Laboratory document

38. D. Barnes et al. *Particle Fuel Reactor Thermal Hydraulic Design,* NE265 Final Report. 15 Dec. 2003.

39. C. C. Silverstein, *Design and Technology of Heat Pipes for Cooling and Heat Exchange,* Taylor & Francis. 1992.

40. R. S. Reid, E-mail to Lance Kim. May 4, 2006.

41. R. S. Reid, *Alkali Metal Heat Pipe Life Issues,* Proceedings of ICAPP 2004. Pittsburgh, PA, June 13-17, 2004.

42. Incropera & Dewitt, *Fund. of Heat and Mass Transfer*, 5th Ed.

43. Munson, *Fundamentals of Fluid Mechanics*, 2nd ed.

44. El-Wakil, *Nuclear Heat Transport*, International ed. 1971

45. A. Susplugas and E. Greenspan*, Implementation of the ENHS Thermal Hydraulic Optimization Code for Recent ENHS Design Improvements,* UCBNE Internal Report UCB-NE-5104, December 2005.

46. E. Greenspan, *ENHS Final report,* NERI Project No. 99-154, Grant No. DE-FG03-99SF21889

47. Fink, Liebowitz, *Thermodynamic and Transport Properties of Sodium Liquid and Vapor*, ANL 1995

48. D. Williams et. al., *Assessment of Properties of Candidate Liquid Salt Coolants for the Advanced High Temperature Reactor (AHTR)*, ORNL 2005

49. V. Dostal, *A Supercritical Carbon Dioxide Cycle for Next Generation Nuclear Reactors,* Massachusetts Institute of Technology Internal Report (2004)

50. V. Dostal, P. Hejzlar, and M.J. Driscoll, *High Performance Supercritical Carbon Dioxide Cycle for Next-generation Nuclear Reactors,* Nuclear Technology 154 (2006) 265-282.

51. Nuclear Regulatory Commission, *10 CFR 50 Regulation of Advanced Nuclear Power Plants; Statement of Policy,* (July 12, 1994) 59 FR 35461 last accessed May 13, 2007 http://www.nrc.gov/reading-rm/doc-collections/commission/policy/59fr35461.pdf.

52. D. Saphier, E. Greenspan, D. C. Wade, M. Dzodzo, L. Conway and N.W. Brown, *Some Safety Aspects of the Encapsulated Nuclear Heat Source LMR Plant*, Proc. 9th Int. Conf. On Nuclear Engineering, ICONE-9, Nice, France, April 8-12, 2001.

53. D. Saphier, D. C. Wade, N.W. Brown, L. Conway, M. Dzodzo, E. Greenspan, *An Inherently Safe Modular LMR Plant - the Encapsulated Nuclear Heat Source*, Trans. American Nuclear Society, 85, 78-80, Reno, NV, Nov. 2001.

54. L. A. Rayes, *Non-LWR Containment Functional Performance Requirements,* Attachment 2 of SECY-04-0103 last accessed May 13, 2007 (June 23, 2004).

55. PG&E Final Report of the Diablo Canyon Long Term Seismic Program, July 1988.

56. Nuclear Regulatory Commission, *10 CFR 100 Reactor Site Criteria,* last accessed May 13, 2007 http://www.nrc.gov/reading-rm/doc-collections/cfr/part100/full-text.html

57. E. Greenspan, *ENHS General Information, Technical Features, and Operating Characteristics*, IAEA Status Report on Innovative Small and Medium-Sized Reactors (SMRs), International Atomic Energy Agency Report Number IAEA-TECDOC-1536, 2007, ANNEX XX, pp. 551-586.

58. Nuclear Regulatory Commision, *10 CFR 50 Policy Statement on Severe Reactor Accidents Regarding Future Designs and Existing Plants*, 50 FR 32138 last accessed May 13, 2007 (November 8, 1985) http://www.nrc.gov/reading-rm/doc-collections/commission/policy/50fr32138.pdf

59. Nuclear Regulatory Commission, *10 CFR 50 Safety Goals of the Operation of Nuclear Power Plants; Policy Statement; Republication,* 51 FR 30028 (August 21, 1986) http://www.nrc.gov/reading-rm/doc-collections/commission/policy/51fr30028.pdf

60. Center for Disease Control and Prevention, *Deaths: Preliminary Data for 2004,* National Vital Statistics Report volume 54, number 19 (June 28, 2006) http://www.cdc.gov/nchs/data/nvsr/nvsr54/nvsr54_19.pdf

61. L. Cave, W.E. Kastenberg, *On the Application of Probabilistic Risk Assessment to Reactors With Inherently Safe Features,* Nuclear Engineering and Design 128 (1991) 339-347 North-Holland

62. International Atomic Energy Agency, *Generic component reliability data for research reactor PSA,* last accessed May 13, 2007 (February 1197) http://www-pub.iaea.org/MTCD/publications/PDF/te_0930_scr.pdf

63. The Hartford, *Understanding Seismic Isolators,* Loss Control TIPS last accessed May 13, 2007 (2002) http://www.thehartford.com/corporate/losscontrol/TIPS/140-008.pdf

64. Wane-Jang Lin, and M. Austin, *Behavior of Lead-Rubber Isolators under Cyclic Shear Loadings,* last accessed May 13, 2007 (March 22, 1998).